

NATIONAL ADVISORY COMMITTEE FOR AERONAUTICS

TECHNICAL NOTE 3626

EXPERIMENTAL INVESTIGATION OF THE FLOW AROUND LIFTING
SYMMETRICAL DOUBLE-WEDGE AIRFOILS AT MACH
NUMBERS OF 1.30 AND 1.41

By Paul B. Gooderum and George P. Wood

Langley Aeronautical Laboratory
Langley Field, Va.



Washington

March 1956

TECHNICAL NOTE 3626

EXPERIMENTAL INVESTIGATION OF THE FLOW AROUND LIFTING

SYMMETRICAL DOUBLE-WEDGE AIRFOILS AT MACH

NUMBERS OF 1.30 AND 1.41

By Paul B. Gooderum and George P. Wood

SUMMARY

Measurements were made of the flow around a 10-percent-thick, double-symmetrical, two-dimensional wedge at a Mach number of 1.30 and of a 14.2-percent-thick wedge at Mach numbers of 1.30 and 1.41 for various angles of attack up to 5° . Results were thus obtained in the vicinity of the theoretically interesting region between shock attachment and the lower limit for completely supersonic flow over the surface of the airfoil. Pressure and Mach number distributions, lift and drag coefficients, center of lift, and pitching moment are presented for the angles of attack used. By means of the transonic similarity laws, the results are compared with each other, with small-disturbance theory, and with shock-expansion theory wherever possible. The data show that pressure distributions on wedges of different thickness and Mach number are similar at the same values of transonic similarity parameter and reduced angle of attack for angles of attack as large as the thickness ratio; that the lift-curve slope is approximately independent of the angle of attack for an angle-of-attack range from -2° to 2° ; and that, for the airfoils tested at Mach numbers greater than the attachment value, the center-of-pressure location is nearly independent of the angle of attack, the variation being ± 3 percent chord for the angles of attack used in this investigation. For the airfoil tested at a Mach number slightly less than the shock-attachment value, the center-of-pressure location was only roughly independent of the angle of attack, the variation of this location being ± 6 percent chord.

INTRODUCTION

One of the transonic flow problems currently receiving attention is that of a double-wedge airfoil in slightly supersonic flow. Previous experimental work has provided a detailed description of the flow characteristics for nonlifting wedges. The available data for lifting wedges, however, are far less complete. Aside from the research of Vincenti,

Dugan, and Phelps (ref. 1), which was unpublished at the start of the present investigation, the only experimental data available are two papers (refs. 2 and 3) concerning wedges at values of the transonic similarity parameter ξ_0 which are much above the shock-attachment value.

From a theoretical standpoint, an experimental study of a lifting wedge is of interest because of theoretical findings in references 4 and 5 which show an irregular behavior of the lift characteristics in the neighborhood of shock attachment. In addition, the theoretical findings are typical of all small-disturbance theories in that they can presumably be expected to apply only for a range of angle of attack and thickness ratio close to zero. So, in addition to providing information about the flow around a wedge in areas where the theory may not hold, an experimental investigation might also answer the questions regarding the range of angle of attack and airfoil thickness ratio over which the theory would be applicable.

For this purpose, doubly symmetrical wedge-airfoil models of 10-percent thickness at a Mach number of 1.30 and 14.2-percent thickness at Mach numbers of 1.30 and 1.41 are investigated in this paper, since for these models the values of the similarity parameter ξ_0 lie close to the interesting region near shock attachment. Also, by means of the transonic-similarity laws, as developed in references 6 to 9, which state that the flow around airfoils of different thickness is similar at the same values of ξ_0 and reduced angle of attack $\tilde{\alpha}$, the 14.2-percent-thick wedge at a Mach number of 1.30 ($\xi_0 = 1.00$) can be compared with the theoretical results of references 4 and 10 ($\xi_0 = 1.058$), and the 14.2-percent-thick wedge at a Mach number of 1.41 ($\xi_0 = 1.28$) can be compared with the 10-percent-thick wedge at a Mach number of 1.30 ($\xi_0 = 1.26$).

SYMBOLS

c	chord
c_d	section pressure-drag coefficient
$c_{d,0}$	section pressure drag for zero angle of attack
c_l	section lift coefficient
$\tilde{c}_{l\alpha}$	generalized lift-curve slope, $\left[(\gamma + 1) M_0^2 \frac{t}{c} \right]^{1/3} \frac{dc_l}{d\alpha}$

- c_m section pitching-moment coefficient about quarter-chord point
- C_p pressure coefficient, $\frac{p - p_0}{q_0}$
- \tilde{C}_p generalized pressure coefficient, $\frac{[(\gamma + 1)M_0^2]^{1/3}}{\left(\frac{t}{c}\right)^{2/3}} C_p$
- d section drag
- l section lift
- M Mach number
- p static pressure
- q dynamic pressure
- R Reynolds number
- t maximum thickness of airfoil
- x coordinate in chordwise direction with origin at leading edge
- α angle of attack, deg
- $\tilde{\alpha}$ generalized angle of attack, $\frac{\alpha}{t/c}$
- γ ratio of specific heats
- $\left(\frac{x_{cp}}{c}\right)_{\alpha \rightarrow 0}$ position of center of pressure for small angles of attack
- ρ density
- ξ_0 transonic similarity parameter, $\frac{M_0^2 - 1}{[(\gamma + 1)M_0^2 \frac{t}{c}]^{2/3}}$

Subscripts:

- o free-stream conditions
cp center of pressure

PRELIMINARY CONSIDERATIONS

In figure 1, the values of thickness ratio, Mach number, and similarity parameter used in the present investigation are compared with the available theoretical and experimental data (refs. 1 to 5, and 10 to 14). Figure 1(a) pertains to nonlifting wedges ($\alpha = 0$) whereas figure 1(b) deals with lifting wedges.

In figure 1(a), all possible airfoil and Mach number combinations included between $\xi_0 = 0$ and the nearly horizontal line which intersects $t/c = 0$ at $\xi_0 = 1.191$ are characterized by a detached bow wave followed by a region of mixed subsonic-supersonic flow. This is true for all angles of attack. Airfoil and Mach number combinations above the line which intersects $t/c = 0$ at $\xi_0 = 1.26$ are characterized by an attached-bow-wave configuration followed by a completely supersonic flow field. This is true only for a variable range of angles of attack about zero which depend on the free-stream Mach number and the thickness ratio. In figure 1(b), the location of the upper limit for a detached shock wave and the lower limit for sonic velocity over the front wedge are shown for a representative value of $\tilde{\alpha}$. Between these two lines is a region of mixed flow characteristics; and it is the region in the vicinity of this narrow band, especially at zero angle of attack, that is of interest in the present investigation.

APPARATUS AND PROCEDURE

Wind Tunnel

The tests of the airfoils were made at Mach numbers of 1.30 and 1.41 in a blowdown tunnel of the Langley gas dynamics laboratory. Dry compressed air from a storage-tank field was passed through an automatic pressure-regulating system, a 24-inch-diameter settling chamber, and a supersonic nozzle, and then exhausted to the atmosphere. The test section was 3 inches wide and 4 inches high. The nozzle side walls were extended past the ends of the nozzle blocks, and thereby the bottom and top edges of the test section were open to the atmosphere and the sides were bounded by glass windows.

The free-stream Mach numbers given herein were obtained from previous nozzle calibrations which were performed as carefully as was practical. The nozzle-wall static pressure was measured at a point in the nozzle block 1/4 inch upstream of the end of the nozzle block by means of an alcohol manometer. The total pressure in the settling chamber was measured by means of a mercury manometer. While the total pressure was varied slowly past the design pressure, interferometric records of the nozzle rim shock were taken. At the point where the interferograms indicated that there was no density change across the rim shock, the Mach number was calculated from the ratio of stagnation pressure to atmospheric pressure under the assumption that the free-stream pressure was the same as atmospheric pressure. The uncertainty in determining the free-stream Mach number in this manner was estimated to be not more than 0.01 for the Mach numbers used in this investigation. The nozzle was then operated at the nozzle-wall pressure measured at the time the rim shock was of zero strength.

The Reynolds number for all tests was approximately 1.2×10^6 per inch.

Models

The models were a 10-percent-thick symmetrical double wedge with a 1-inch chord and a 14.2-percent-thick symmetrical double wedge with a 0.7-inch chord and were constructed of a chrome-molybdenum steel of good machinability and stability. After manufacture, the semiwedge angles were measured and found to be $5^\circ 43'$ ($t/c = 10$ percent) and $8^\circ 05'$ ($t/c = 14.2$ percent) with an accuracy of $\pm 2'$. The span of both models was 2.9 inches; this left an end gap of 0.05 inch between the model and the tunnel windows. Both models were held in the airstream by two struts attached to the rear half of the upper surface. A view of the 10-percent-thick model mounted in the angle-of-attack changer is shown in figure 2.

Eight static-pressure orifices of 0.020-inch diameter were located on the lower surface of the 10-percent-thick airfoil. Four were spaced 0.4 inch apart in a spanwise direction beginning 0.2 inch from the center line on the front surface at about 0.2 chord. The other four were similarly placed on the rear surface at about 0.7 chord, with the exception that the first orifice was located on the center line. All orifices were connected by internal galleries to tubes soldered to the upper rear half of the model. The 14-percent-thick model had two static-pressure orifices in the lower surface, one located 0.25 inch from the center line on the front half of the model at about 0.3 chord and the other located 0.25 inch away from the opposite side of the center line on the rear half of the model at about 0.7 chord. These orifices were connected to tubes in a manner similar to that used with the 10-percent-thick airfoil.

Interferometer

Observations were made with a Mach-Zehnder interferometer that had 4-inch-square plates and has been previously described (ref. 13). It was used to take both interferograms and shadowgraphs. The light source consisted of a 15,000-volt magnesium spark of approximately 3 microseconds' duration and a monochromator to isolate the lines at 5,170 angstroms.

Installed in the light beam which bypassed the test section at the focal point of the camera was a reference wire which was used to determine the true angle of attack in case there was any deflection of the model due to bending of the supporting struts. Two small pointers were placed in the back of the camera in such a manner as to throw a shadow on the image of the test section, which could be used to give a check on the scale of the enlargement during processing of the interferograms. Both the reference wire and the pointers are visible in the original interferograms.

Experimental Procedure

Tests of the various combinations of thickness ratio and Mach number were made in the following manner. After the angle of attack was set, several no-flow interferograms and a picture showing the reference wire in relation to a straightedge placed parallel to the center line of the nozzle were recorded. The tunnel was started and allowed to come up to operating conditions. The pressure regulator was adjusted until the static pressure measured at an orifice located just upstream of the end of the nozzle reached a pressure determined in the original calibration of the nozzle. This was necessary to minimize the disturbances from the nozzle rim on the open sides of the jet. No data were taken until the flow over the model became steady. After recording several interferograms of the flow, the monochromator slits were opened and a white-light interferogram and a shadowgram of the flow were also taken.

Because the model was supported by two struts on the upper rear surface, orifices were present in only the lower surface and tests at both positive and negative angles of attack were necessary to provide data for the complete profile. (In this case, positive is taken in the sense that an upward movement of the leading edge results when the angle of attack is changed in a positive direction.) The angular setting for the no-flow condition was measured by a precision level applied to a flat surface on the model holder.

Data were taken at 13 angles of attack from 5° to -5° for $\xi_0 = 1.28$ and 1.26 and at 11 angles of attack from 4° to -4° for $\xi_0 = 1.00$. The angle-of-attack range for $\xi_0 = 1.00$ was restricted because of the

intersection of the jet boundary by the sonic line between 4° and 5° . The angular settings were made in $\frac{1}{2}^\circ$ increments near zero angle of attack.

Reduction of Data

The interferograms were analyzed to obtain density contours in the flow fields by the method of superposing with-flow and no-flow interferograms. The method has been previously described (refs. 12, 14, and 15). Pressure and Mach number distributions along the surface of the model were also obtained from the interferograms by measuring the fringe positions along the surface. The fringe positions were then related to the density by the use of a reference density which was obtained from the measurement of the static pressure at an orifice in the model surface at about $0.2c$ near the center line of the tunnel. The estimated uncertainty in the reference density is ± 0.5 percent. From the density distributions, the pressures were obtained and were converted to pressure coefficients. In order to compute the distribution of C_p from the pressure, the free-stream static pressure was assumed to be the same as the measured value of atmospheric pressure.

In the calculation of the densities from the fringe shifts as obtained in this manner, two corrections were applied. One correction was made to account for the effect of the side-wall boundary layer on the optical path through the tunnel. Static pressures were measured at two chordwise positions near the jet center line. From the pressures, the densities were calculated by taking into account the change in reservoir conditions through the bow shock and by making the assumption that the surface streamline of the airfoil passed through a normal shock for all detached shock-wave angles of attack. (At negative angles, the lip shock was proved to be quite weak by a total-pressure survey and for that reason the change in total pressure across it was ignored.) From the observed fringe shift between these two locations and from the calculated densities, the effective width of the test section was calculated. The rest of the flow field behind the bow wave was then evaluated by making the assumption that the effective width was constant over the whole field. The other correction was made to account for slight changes in the "undisturbed" fringe spacing caused by vibration of the interferometer during a run. The correction was accomplished by making the spacing and direction of the fringes on the enlargement of the no-flow interferogram coincide with the spacing and direction of the fringes in the regions of uniform flow on the with-flow interferogram.

Because the flow in the boundary layer is nonisentropic, the density at the surface cannot be converted to pressure on portions of the model surface where the airfoil boundary layer is thick enough to be visible.

Where the boundary layer is visible, the fringes bend sharply because of the high density gradient. The procedure in these cases was to extrapolate the fringes through the boundary layer to the surface to obtain what would have been the fringe positions if there had been no entropy gradient.

In the evaluation of the interferograms, it was necessary to assume that the model possessed two-dimensional flow over all its span. Actually, this was not entirely the case, as was evidenced on the interferograms by the bending of the free-stream fringes just ahead of the bow wave. This bending indicates a sharp rise in free-stream density as the bow wave is approached. Obviously, this is a spurious effect that is restricted to the neighborhood of the side walls and is due to the action of the pressure increase across the shock wave on the boundary layer on the side walls. Another three-dimensional effect of this boundary-layer-shock-wave interaction occurs on models with supersonic flow behind the bow shock and is usually undetected by optical methods. A disturbance which originates at the shock-wave-boundary-layer intersection is propagated obliquely across the model in a spanwise direction.

Although the method of evaluation requires two-dimensional flow throughout the flow field under consideration, it was possible to investigate the magnitude of the end effects only at the model surface, and for this purpose the 10-percent-thick wedge had eight orifices installed on its lower front surface. Subsequently, when it was desired to observe the end effects on the rear surface, four of these orifices were moved to the back. This investigation of end effects was done preparatory to obtaining the data reported herein.

An exhaustive examination of the effects of end gap on the spanwise pressure distribution of a lifting wedge was not considered to be within the scope of the present investigation. The brief study that was conducted, however, gave some interesting results that are as follows: The 10-percent-thick wedge at a Mach number of 1.3 and at an angle of attack such that a detached bow wave was produced was found to have the sharpest appearing bow wave (at the nose) with an end gap of 0.05 inch. At an angle of attack of approximately 4° , it was found that even though an end gap was used that made the bow wave appear sharp, the spanwise pressure distribution for the lower surface was not two-dimensional as was expected. Varying the end gap from 0 to 0.09 inch caused only a minor variation in the spanwise pressure distribution on this surface. (See fig. 3.) It was found that the use of a side-wall boundary-layer scoop did make the pressure distributions over the wedge two-dimensional and this fact is shown in figure 3 for the 10-percent-thick wedge at an angle of attack of approximately 2° . Because of the fact that a side-wall boundary-layer scoop would require extensive modification of the test equipment, it was not used in obtaining any of the data reported in this paper. The upper-surface end effects were found to be much reduced by

the use of an end gap (see fig. 3, $\alpha \approx -4^\circ$), the improvement being enough to warrant the use of an end gap at all angles of attack.

Further argument in favor of the use of an end gap is due to the interaction of the previously discussed tip disturbances. At a Mach number of 1.30, the flow over the front of the 10-percent-thick wedge at an angle of attack of approximately zero is slightly supersonic. Under these conditions, the disturbances from the tips of the airfoil are strong enough to interact with each other at the center of the span to form a Mach reflection type of shock wave. The center portion of this configuration is visible on the interferograms as a normal shock in the flow behind the attached oblique bow wave (fig. 4(a)), and it is distinguishable from a regular normal shock in that there is not sufficient fringe shift across it for it to have much spanwise extent. The density jump was not strong enough to be observed in a shadowgram (fig. 4(b)). Apparently, the use of end gap weakened the tip disturbances since in the interferograms, a similar interaction was observed to be much weaker. (For example, see fig. 5(a).)

Four of the intermediate orifices on the front surface were then closed and new ones drilled on the rear. For an end gap of 0.05 inch, it was found that the end effects on the rear surface were practically zero for all the angles of attack used.

By means of the reference wire, the deflection of the model caused by the elastic deformation of the supporting struts was measured on the interferogram and all angles of attack were corrected to the true angle. The uncertainty in these measurements is estimated to be not more than 0.1° . For the 10-percent-thick wedge at $M = 1.3$ where the angle of attack could be checked by means of the pressures measured at the orifices on the front surface for a small range of angles of attack about zero, the inaccuracy was determined to be $\pm 0.03^\circ$.

RESULTS AND DISCUSSION

Flow Fields

The interferograms of the flow about a 10-percent-thick double wedge at a Mach number of 1.30 ($\xi_0 = 1.26$) for thirteen angles of attack from 5.00° to -5.50° are presented in figure 5, together with contours of constant density ratio. The sonic line is sketched in its approximate location and is represented by a dashed line on the figures. An interferogram of the flow taken with white-light is shown in figure 6 for comparison with figure 5(a) taken with monochromatic light under otherwise identical circumstances. The series of interferograms in figure 5

shows the phenomena that take place as the angle of attack of the wedge is changed from zero for the case when the free-stream Mach number is greater than the value required for completely supersonic flow over the surface of the wedge at zero angle of attack ($\xi_0 \geq 1.18$).

The most prominent features of these phenomena are as follows. At some positive value of α , the flow behind the shock wave on the lower front surface becomes subsonic while the top remains supersonic. At a slightly larger angle, the shock wave becomes detached from the leading edge. When detachment occurs (fig. 5(c)), the central streamline in the subsonic region of the flow behind the bow wave becomes curved and approaches the leading edge from below, the flow decreasing in velocity until the stagnation point is reached. At this point the flow branches and part continues rearward with increasing velocity toward the shoulder where it reaches sonic speed. The other part flows up and forward, the velocity increasing until it reaches the sonic value at or near the leading edge (fig. 5(j)). The behavior of the flow in the immediate vicinity of the leading edge when the previously mentioned sonic lines appear will not be described beyond making the statement that, whatever occurs, it is generally agreed that on reaching the upper surface, the flow separates and immediately thereafter becomes reattached.

The flow, in becoming attached to the upper surface of the leading edge, is caused to turn and flow along the upper surface by a shock wave which is propagated outward. As was mentioned previously, this shock wave was weak for the Mach number and angles used herein. The total-pressure loss of the flow that traverses the shock wave at the model could not be detected by any total-pressure measurements. Incoming compressions, which are reflections from the outgoing sonic line of supersonic expansions from the leading edge, strike the solid surface behind the shock wave and are reflected as compressions, effecting a drop in Mach number along the surface and combining with the outgoing shock wave so that it curves forward.

It can be demonstrated that the sonic line that occurs at the shoulder of the wedge should leave the shoulder normal to the forward surface of the profile. Inspection of the interferograms of figures 5(b) to 5(f) shows that in actuality this phenomenon does not occur and that the angle between the tangent to the sonic line at the wedge surface and the front surface is noticeably different from 90° . It is possible that this deviation is due to lack of resolution; however, it is more likely due to curvature of the effective profile inasmuch as a boundary layer would have the effect of rounding off the surface at the corner.

When the stream Mach number is less than the minimum needed for completely supersonic flow over the wedge surface ($\xi_0 < 1.18$, $M = 1.3$), the sequence of events that occurs as the angle of attack is varied

from 0° is slightly different. Since the region behind the shock wave is subsonic at zero angle of attack, a small increase in α results in the flow expanding around the leading edge in a manner similar to the foregoing case of $\xi_0 = 1.26$ with the angle of attack great enough for detachment. In the beginning, however, the supersonic region that develops at the leading edge is completely surrounded by subsonic flow and, as a consequence, the supersonic flow must be terminated by a normal shock wave. Although it might seem, at least at small angles of attack, that this normal shock would tend to dominate the flow pattern and cause a large change in the pressure distribution as compared with the case of the wedge at a slightly higher Mach number, the fact that such is not the case will be shown. It might seem that, as the angle of attack was further increased and the dimensions of the imbedded supersonic region increased, the flow would eventually appear similar to the flow for $\xi_0 = 1.26$ at a large angle of attack. This is shown to be true by the interferograms in figure 7.

The interferograms of the flow about a 14.2-percent-thick double-wedge airfoil at a Mach number of 1.30 ($\xi_0 = 1.00$) are presented in figure 7 for eleven angles of attack from 4.25° to -4.80° . No density contours are plotted in the figures. The changes in the flow phenomena do not appear to be as severe as might be imagined. The imbedded supersonic regions at the leading edge are microscopic. For values of ξ_0 near the attachment value and small angles of attack, the effects of this supersonic region on the surface pressure distributions can safely be ignored - as was done in the theoretical analyses of the problem in references 4 and 5.

Interferograms of the flow about a 14.2-percent-thick double-wedge airfoil at a Mach number of 1.41 ($\xi_0 = 1.28$) are presented in figure 8 for comparison with the interferograms in figure 5 ($\xi_0 = 1.26$). The phenomena exhibited in both figures are similar.

Surface Pressure and Mach Number Distributions

Surface pressure and Mach number distributions are presented in figures 9 and 10, respectively, for the lower front and rear surfaces of the airfoils at positive and negative angles of attack. Between values of x/c of approximately 0.42 and 0.55, the data points of some of the curves lie so close together as to overlap. These points have been omitted from the figures so that the curves can be more easily followed. As a check on the reproducibility of the results, three or more interferograms were evaluated for each angle of attack of the wedge at $\xi_0 = 1.26$. Only negligibly small variations in the pressure distributions measured on a given wedge at the same angle of attack were found;

these small variations showed that the results were reproducible and contained no random errors.

A check on the applicability of small-disturbance theory lies in the use of the transonic similarity laws to compare the characteristics of different wedges at different Mach numbers with each other and with the theoretical results (refs. 4, 5, and 10). Since the similarity rules are based on the equations of small-disturbance theory, they are therefore of the same order of approximation and any correlation of the results of experiments by means of the similarity rules would also infer the validity of the basic equations. The present data are presented in the form prescribed by the similarity laws for comparison with each other and with other available data, except where deviations from the rule seem prudent. The reasons for such deviations will be discussed whenever they occur.

Chordwise pressure distributions written in generalized form are compared in figure 11 for nearly identical values of α for some of the interferograms of figure 5 ($\xi_0 = 1.26$) and figure 8 ($\xi_0 = 1.28$). Reasonable agreement, particularly for these thick airfoils, is seen to exist between the pressure distributions for conditions where the similarity theory predicts that the pressure distributions should agree.

In figure 12 a comparison of the theoretical pressure distributions due to small-disturbance theory for a lifting wedge as obtained from references 4 and 10 ($\xi_0 = 1.058$) is made with the present data ($\xi_0 = 1.00$). Although this comparison is not an exact application of the similarity laws, that it is a reasonable one is based on the following argument. The value of ξ_0 given by the small-disturbance theory for the shock-attachment condition is 1.191. However, the precise value of ξ_0 for shock attachment for a 14.2-percent-thick wedge at a Mach number of 1.31 is 1.135. Since the theoretical results for $\xi_0 = 1.058$ are for thin airfoils, it was thought that for a thick airfoil a more nearly correct value of ξ_0 for comparison with the small-disturbance theory might be proportionately smaller than 1.058 by the ratio of 1.135:1.191, or $\xi_0 = 1.01$. In the present results shown in figure 12, the data points have been omitted for the sake of clarity.

The agreement between the pressure distributions of experiment and theory shown in figure 12 is poor. The greatest disagreement occurs on the lower front surface at zero angle of attack, but there is considerable improvement as the angle is increased. At angles of attack near zero, the experimental pressures on the lower front surface for both positive and negative angles of attack are higher than theory predicts. Part of this difference can be attributed to the displacement effect of the boundary layer as has been discussed in references 1 and 12. At

an angle of attack of 2.05° , the theory predicts accurately the measured pressure distribution over the front surface, the measured pressures on the upper surface remaining high as compared with theory. At 4.25° , however, the theoretical pressures become larger than the measured values. At -2.50° , for the region of the airfoil surface immediately behind the leading edge, it appears that the theory does not take adequate account of the supersonic expansion around the leading edge; at -4.80° , the reverse is true, and the theory appears to indicate that there should be more compressions incident on the surface than are actually measured. Actually, the theory neglects this expansion completely and what is shown in figure 12 is the magnitude of the error caused by this omission.

Over the rear portion of the front surface (discounting the corner effect which is in evidence at all angles of attack), the theoretical solution is again at variance with the experimental data, the discrepancy being reversed in sign between -2.50° and -4.80° . This discrepancy is due to the requirement of the theory that the flow go to sonic velocity at the shoulder at all angles of attack. Actually, the flow does not go to sonic velocity at large negative angles since, because of the supersonic expansion at the leading edge, the Mach number on the front surface is well above 1.0.

Over the rear half of the model the measured pressures were higher than the theoretical pressures, with the possible exception of the -4.80° angle of attack; this indicates that the boundary layer over the rear surface has a tendency to decrease the amount of turning of the flow at the corner as compared with the actual surface angle available for an expansion. The overall range of variation is quite small, however, when compared with the poor agreement of the pressures on the front wedge with theory. Viscous effects also appear on the rear surface but these, like the corner effect, are quite consistent and their net effect on the lift is believed to be of minor importance at small angles of attack.

Figure 12 shows that the flow violates an assumption used in extending the small-disturbance theory to the range of angles of attack shown in figure 12; this assumption is that the value of $dC_p/d\alpha$ is constant at the value computed for $\alpha \rightarrow 0$. From a theoretical standpoint, as has been shown in reference 16, difficulty such as this may be anticipated whenever the airfoil is at a Mach number such that local regions of near sonic velocity occur on its surface. Local regions of near sonic flow on an airfoil are very sensitive to small disturbances; this sensitivity gives rise to nonlinear pressure variations.

In order that these data might be compared with some of the wealth of experimental and theoretical data available concerning double-wedge airfoils under conditions of zero lift, the pressure distributions for

$\xi_0 = 1.00$ were interpolated to zero angle of attack and plotted in generalized form in figure 13, along with data obtained from references 1, 10, and 12. In general, there seems to be better agreement between the present data and other experimental data than between the present data and the small-disturbance theory of reference 10. This disagreement with theory is probably due to boundary-layer effects, as has already been suggested. The effects of the boundary layer rounding off the shoulder and the pressure rise at the trailing edge due to the proximity of the terminal shock are readily apparent. However, the effect of the terminal shock on the pressure distribution is variable and seems to be influenced by the Reynolds number. This fact is borne out by figure 13 where the shock-wave—boundary-layer effect at the trailing edge is less for the present data ($R = 840,000$) than for the data of reference 1 ($R = 540,000$).

Lift, Drag, and Pitching Moment

Lift and drag coefficients were obtained by integration of the pressure distributions, and the results are plotted against angle of attack in figure 14. These plots indicate that the lift coefficient, with the exception of minor deviations, is a roughly linear function of angle of attack for the range from -2° to 2° . The ratio of lift to drag is plotted against angle of attack in figure 15.

In reference 8, it is shown theoretically that for the angle-of-attack range in which the lift coefficient varies linearly with angle of attack, the drag due to lift should be proportional to the square of the lift coefficient. The square of the lift coefficient is plotted against drag due to lift in figure 16 and these curves show good agreement with the theory of reference 8 with the exception of the data for the wedge at $\xi_0 = 1.00$ which shows substantial divergence from a linear variation. However, after consideration of the data and discussion of figure 12, this divergence is not surprising.

The generalized lift-curve slope \tilde{c}_l/α for small angles of attack is plotted as a function of transonic similarity parameter ξ_0 in figure 17 and compared with the results of small-disturbance theory (refs. 4, 5, and 17), the results of shock-expansion theory for the case of completely supersonic flow over the surface of a relatively thick wedge ($\xi_0 \geq 1.186$), and the experimental results of reference 1. The most conspicuous feature of figure 17 is as follows: For values of ξ_0 larger than 1.186, there is good agreement between the present data, previous experimental results, and shock-expansion theory. None of these results appear to agree very well with small-disturbance theory, however, and this is believed to be due to the failure of the similarity rules to correlate satisfactorily both thick and thin airfoils at values of ξ_0

near shock attachment. By referring to figure 1, where the detached-shock condition has been plotted for different values of ξ_0 and M_0 , and by using the detachment condition as a criterion for similarity of flow, it can be seen that thick airfoils are better compared with each other by means of similarity laws than with airfoils of vanishingly small thickness ratios, at least for values of ξ_0 in the neighborhood of shock detachment. Provided the same adjustment is made in the values of ξ_0 for small-disturbance theory as was made for the data of figure 12, it can then be said that fair agreement exists between theory and experiment at $\xi_0 = 1.26$ and 1.28 . In contrast with this is the poor agreement between theory and experiment at $\xi_0 = 1.00$ where the present results are below both the other experimental data and the small-disturbance theory.

The curves obtained by small-disturbance theory in figure 17 show two maximums in the lift-curve slope. The higher one occurs in the region of shock detachment ($\xi_0 = 1.191$) and the other occurs in the region of sonic velocity on the front wedge ($\xi_0 = 1.26$). The question has arisen as to whether these maximums or less severe variations actually occur because of viscous effects or for other reasons. The data from reference 1 indicate that there is a possibility that the variations are not as severe and that the magnitude of the rise is much less than indicated by theory. However, the present data as plotted in figure 17 show that, for values of ξ_0 as low as 1.26 , both the thick-airfoil theory and the adjusted small-disturbance theory predict the lift-curve slope reasonably well.

In addition to these results for zero angle of attack, figure 17 also shows the lift-curve slope at an angle of attack of 4.5° for the present data. These data are below those shown for zero angle of attack because the curve of c_l against α is nonlinear at the higher angles of attack.

Another interesting quantity is the location of the center of pressure at small angles of attack. This quantity was obtained by plotting the location of the center of pressure for the lower surface against angle of attack and determining its positions as $\alpha \rightarrow 0$. The center-of-pressure location for the lower surface was a much steadier quantity than the location of the center of pressure for the complete profile. Figure 18 presents the variation of both of these quantities with angle of attack. If the chordwise lift-distribution variation with angle of attack is linear, so are the lift coefficient and the moment. The center of pressure of the complete profile is thus independent of angle of attack. Theoretically, when the flow over the front wedge is just sonic (and $\alpha \rightarrow 0$), the lift contributed by the rear wedge is zero (ref. 4) and therefore the center of pressure is at the quarter-chord point.

Actually, because of the interaction of the trailing-edge shock with the boundary layer and because of the rounding off of the shoulder by the boundary layer, the position might be farther back. For the range of Reynolds numbers used, the true position appears to be in the neighborhood of $0.3c$ and appears to be nearly independent of angle of attack. The variation of this position is not more than ± 3 percent chord for $\xi_0 = 1.28$ and 1.26 , and ± 6 percent chord for $\xi_0 = 1.00$.

The location of the center of pressure for small angles of attack is plotted as a function of the transonic similarity parameter ξ_0 in figure 19 and compared with the theoretical results of references 4, 5, and 17, and with the experimental results of reference 1. If the same adjustment is made in values of ξ_0 for small-disturbance theory as was done for figure 12, it could be said that much better agreement exists between these data at $\xi_0 = 1.26$ and 1.28 and small-disturbance theory than between these data and the results of reference 1. At $\xi_0 = 1.00$ the present results are above both the other experimental data and the results indicated by the small-disturbance theory.

A plot of the variation of the moment coefficient about the quarter-chord point with angle of attack is presented in figure 20 for both airfoils.

CONCLUDING REMARKS

The flow fields around two-dimensional symmetrical double-wedge airfoils of 10- and 14.2-percent thickness have been observed at angles of attack up to 5° with an interferometer for Mach numbers of 1.30 and 1.41. Pressure distributions for the wedges tested at Mach numbers above the detachment Mach number showed good correlation, within the framework of the similarity laws, with each other and with experimental data for the range of angles of attack used in this investigation. Poor correlation was found between these data and small-disturbance theory for these same Mach numbers. It was found that the difference between the results for small-disturbance theory and airfoils of substantial thickness is due principally to the variation of the transonic similarity-parameter ξ_0 with thickness ratio for similar airflows. By a slight adjustment of ξ_0 , these differences can be substantially reduced. Comparisons were also made of the lift-curve slope and position of center of pressure, for small angles of attack, with the data of other investigations, with shock-expansion theory for thick airfoils, and with the adjusted small-disturbance theory. These comparisons showed satisfactory agreement.

Comparisons made between the pressure distributions of this experiment at Mach numbers below the detachment Mach number and other theoretical and experimental investigations were not so satisfactory. In general, the agreement between these data and other experimental data is better than between these data and small-disturbance theory. These differences were reflected in the poor agreement exhibited by the section lift-curve slopes and the center-of-pressure positions.

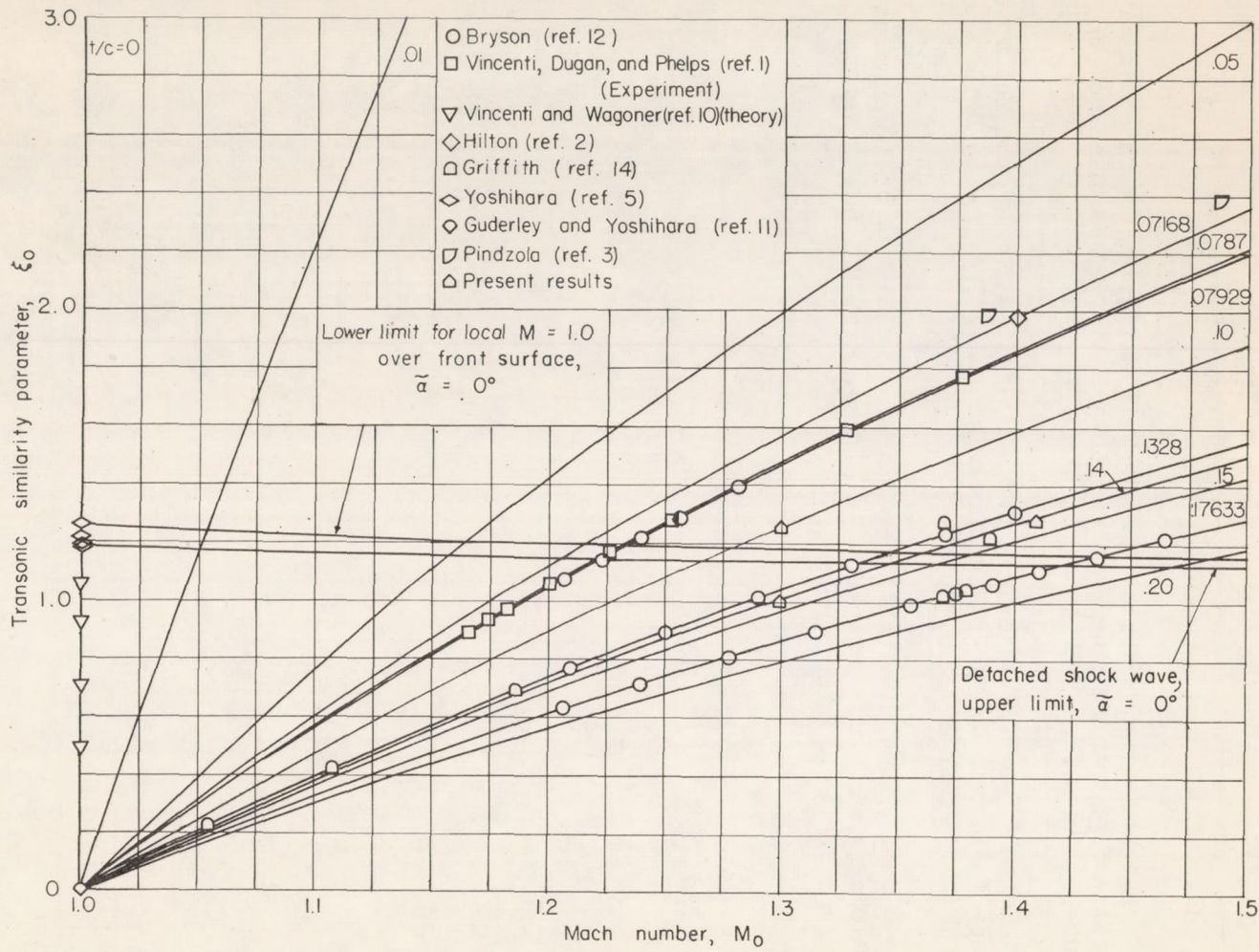
It was found that the lift coefficient is proportional to the angle of attack for a range of angles of attack from -2° to 2° for all combinations of airfoil and Mach number. The center-of-pressure position was found to be nearly independent of angle of attack for two of the combinations tested ($\xi_0 = 1.28$ and 1.26), not varying more than ± 3 percent chord from its position at small angles of attack. For the third combination ($\xi_0 = 1.00$), the center-of-pressure position was found to be only roughly independent of the angle of attack, the variation being ± 6 percent chord.

Langley Aeronautical Laboratory,
National Advisory Committee for Aeronautics,
Langley Field, Va., December 9, 1955.

REFERENCES

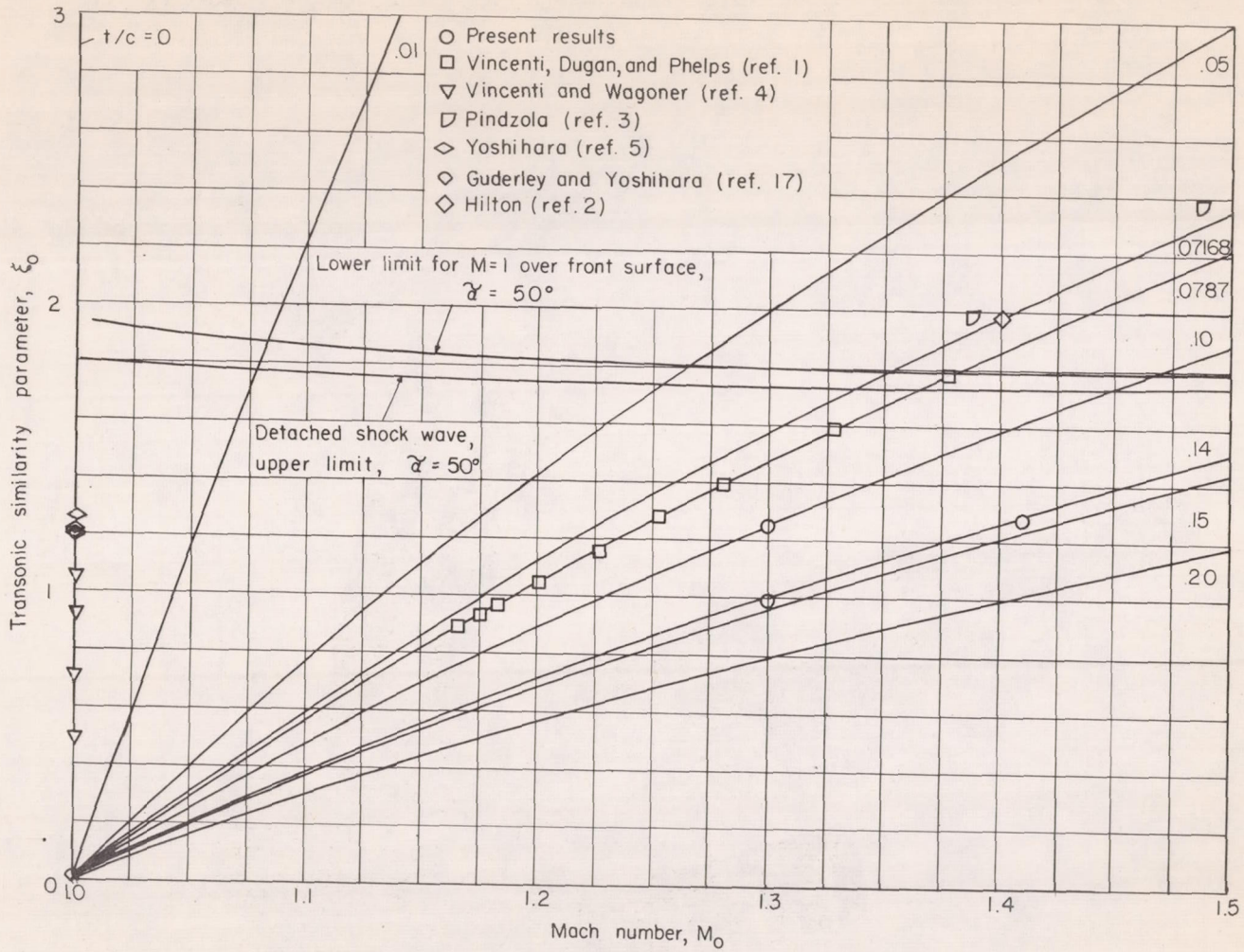
1. Vincenti, Walter G., Dugan, Duane W., and Phelps, E. Ray: An Experimental Study of the Lift and Pressure Distribution on a Double-Wedge Profile at Mach Numbers Near Shock Attachment. NACA TN 3225, 1954.
2. Hilton, John H., Jr.: Flow Characteristics Over a Lifting Wedge of Finite Aspect Ratio With Attached and Detached Shock Waves at a Mach Number of 1.40. NACA TN 2712, 1952.
3. Pindzola, Michael: Supersonic Tests of Conventional Control Surfaces on a Double-Wedge Airfoil. Jour. Aero. Sci., vol. 17, no. 4, Apr. 1950, pp. 204-210.
4. Vincenti, Walter G., and Wagoner, Cleo B.: Theoretical Study of the Transonic Lift of a Double-Wedge Profile With Detached Bow Wave. NACA Rep. 1180, 1954. (Supersedes NACA TN 2832.)
5. Yoshihara, Hideo: On the Flow Over a Wedge in the Upper Transonic Region. WADC Tech. Rep. No. 53-478, Wright Air Dev. Center, U. S. Air Force, Nov. 1953.
6. Spreiter, John R.: Similarity Laws for Transonic Flow About Wings of Finite Span. NACA TN 2273, 1951.
7. Busemann, Adolf: Application of Transonic Similarity. NACA TN 2687, 1952.
8. Harder, Keith C.: Transonic Similarity Rules for Lifting Wings. NACA TN 2724, 1952.
9. Spreiter, John R.: On the Application of Transonic Similarity Rules to Wings of Finite Span. NACA Rep. 1153, 1953. (Supersedes NACA TN 2726.)
10. Vincenti, Walter G., and Wagoner, Cleo B.: Transonic Flow Past a Wedge Profile With Detached Bow Wave. NACA Rep. 1095, 1952. (Supersedes NACA TN's 2339 and 2588.)
11. Guderley, Gottfried, and Yoshihara, Hideo: The Flow Over a Wedge Profile at Mach Number One. AF Tech. Rep. No. 5783 (ATI No. 57842), Air Materiel Command, U. S. Air Force, July 1949.
12. Bryson, Arthur Earl, Jr.: An Experimental Investigation of Transonic Flow Past Two-Dimensional Wedge and Circular-Arc Sections Using a Mach-Zehnder Interferometer. NACA Rep. 1094, 1952. (Supersedes NACA TN 2560.)

13. Gooderum, Paul B., Wood, George P., and Brevoort, Maurice J.: Investigation With an Interferometer of the Turbulent Mixing of a Free Supersonic Jet. NACA Rep. 963, 1950. (Supersedes NACA TN 1857.)
14. Griffith, Wayland: Shock-Tube Studies of Transonic Flow Over Wedge Profiles. Jour. Aero. Sci., vol. 19, no. 4, Apr. 1952, pp. 249-257, 264.
15. Wood, George P., and Gooderum, Paul B.: Investigation With an Interferometer of the Flow Around a Circular-Arc Airfoil at Mach Numbers Between 0.6 and 0.9. NACA TN 2801, 1952.
16. Harder, Keith C., and Klunker, E. B.: An Application of the Method of Characteristics to Two-Dimensional Transonic Flows With Detached Shock Waves. NACA TN 2910, 1953.
17. Guderley, Gottfried, and Yoshihara, Hideo: Two-Dimensional Unsymmetric Flow Patterns at Mach Number One. AF Tech. Rep. No. 6683, Wright Air Dev. Center, U. S. Air Force, Jan. 1952.



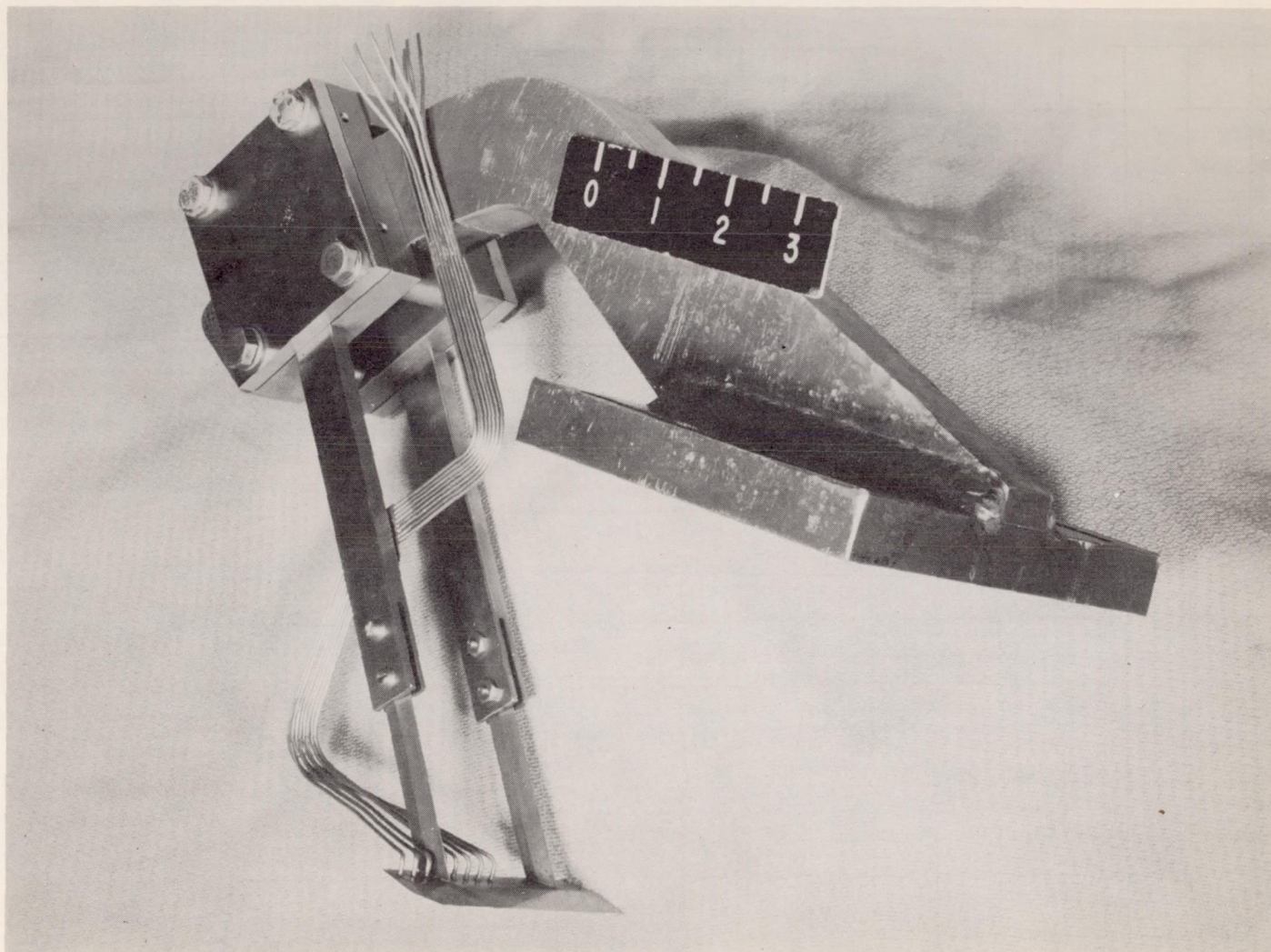
(a) Available data on nonlifting wedges.

Figure 1.- Variation of t/c with ξ_0 and M_0 .



(b) Available data on lifting wedges.

Figure 1.- Concluded.



L-87618

Figure 2.- Photograph of 10-percent-thick double-wedge airfoil mounted in angle-of-attack changer.

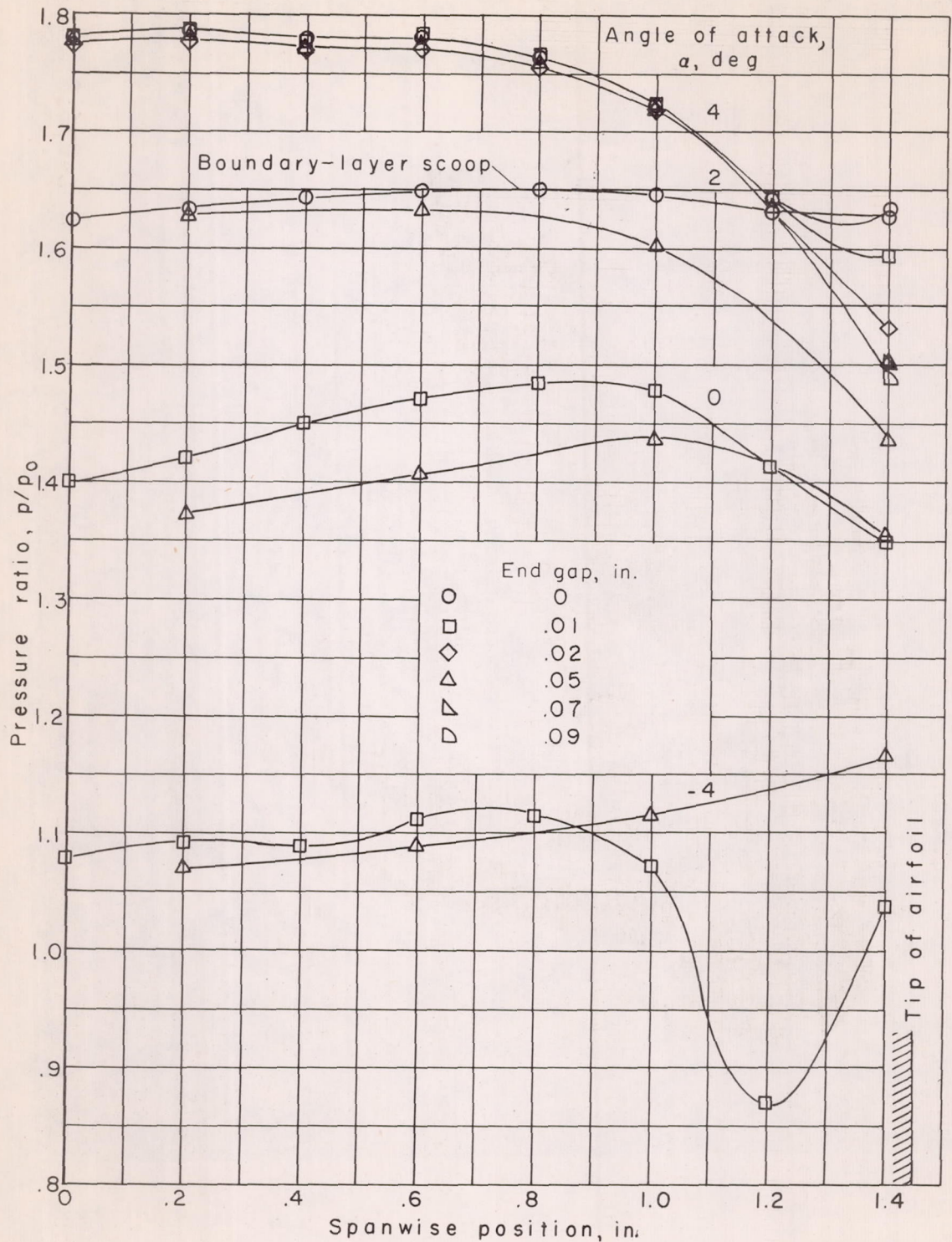


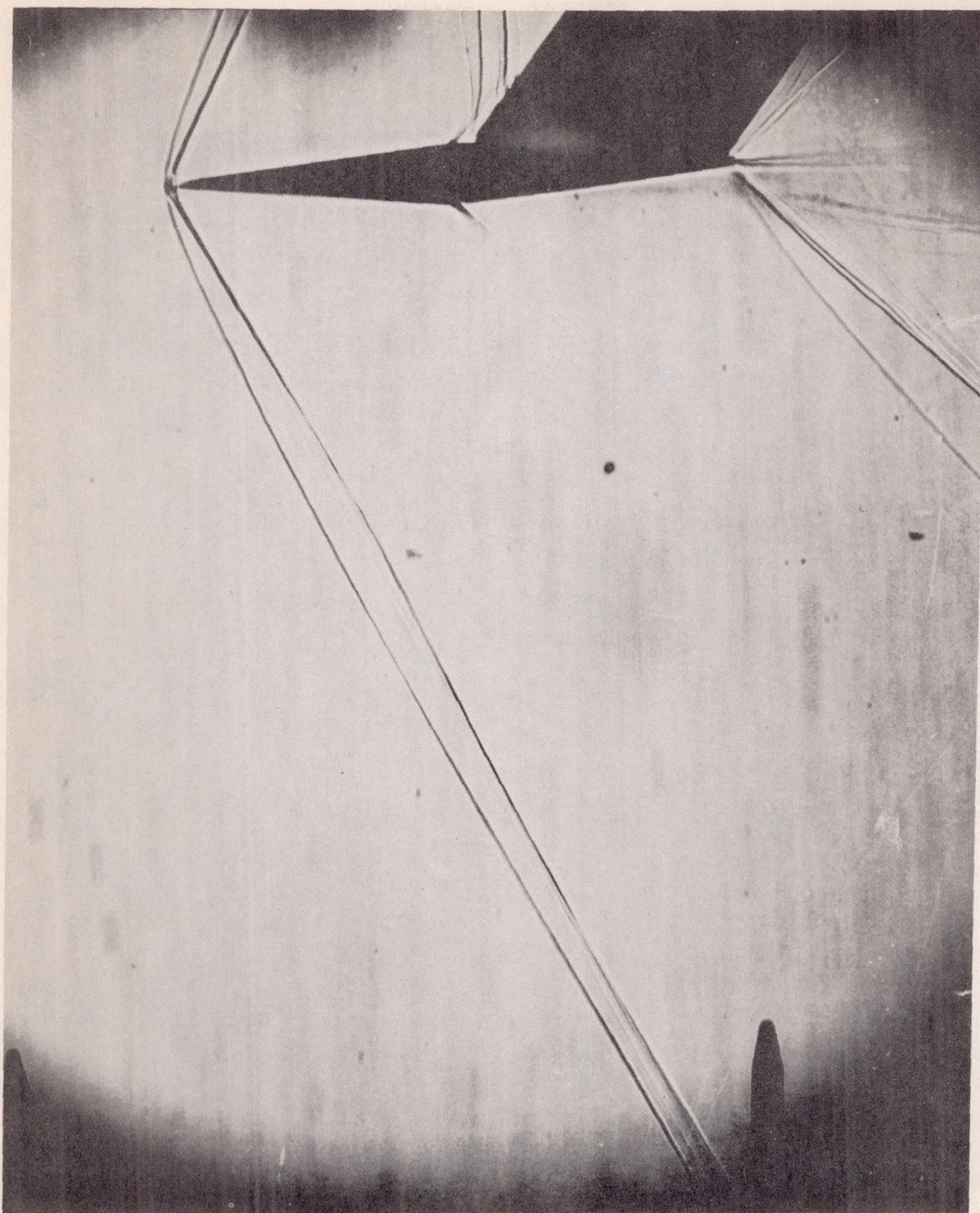
Figure 3.- Typical spanwise pressure distributions (measured from center line) at $x/c = 0.20$ for $t/c = 0.10$ at $M = 1.30$ for various end gaps and angles of attack.



(a) Interferogram. $\alpha \approx 0^\circ$.

L-91712

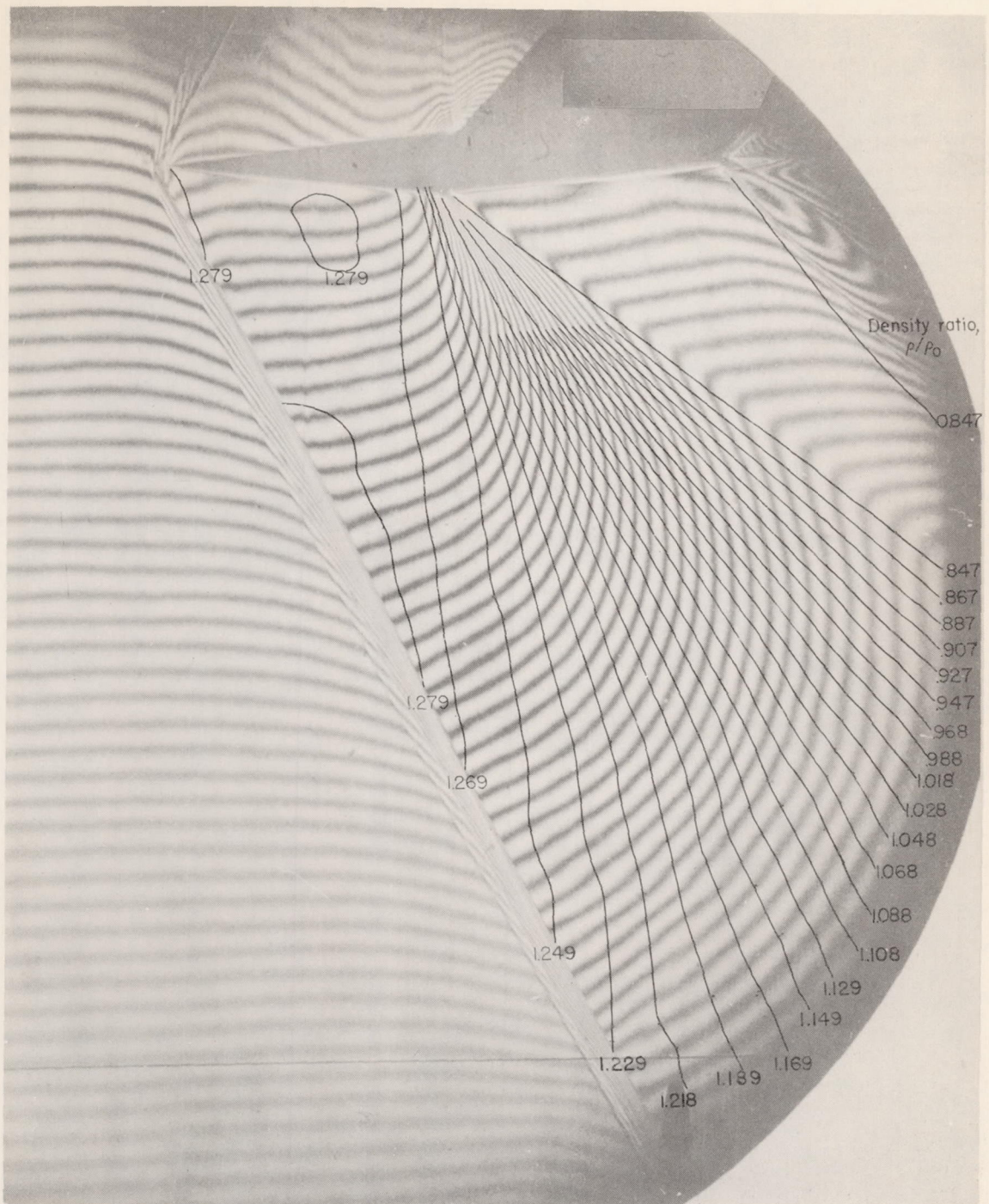
Figure 4.- Interferogram and shadowgram of flow about 10-percent-thick double wedge at $M = 1.30$ for shock wave caused by interference of tip disturbances.



(b) Shadowgram. $\alpha \approx 0^\circ$.

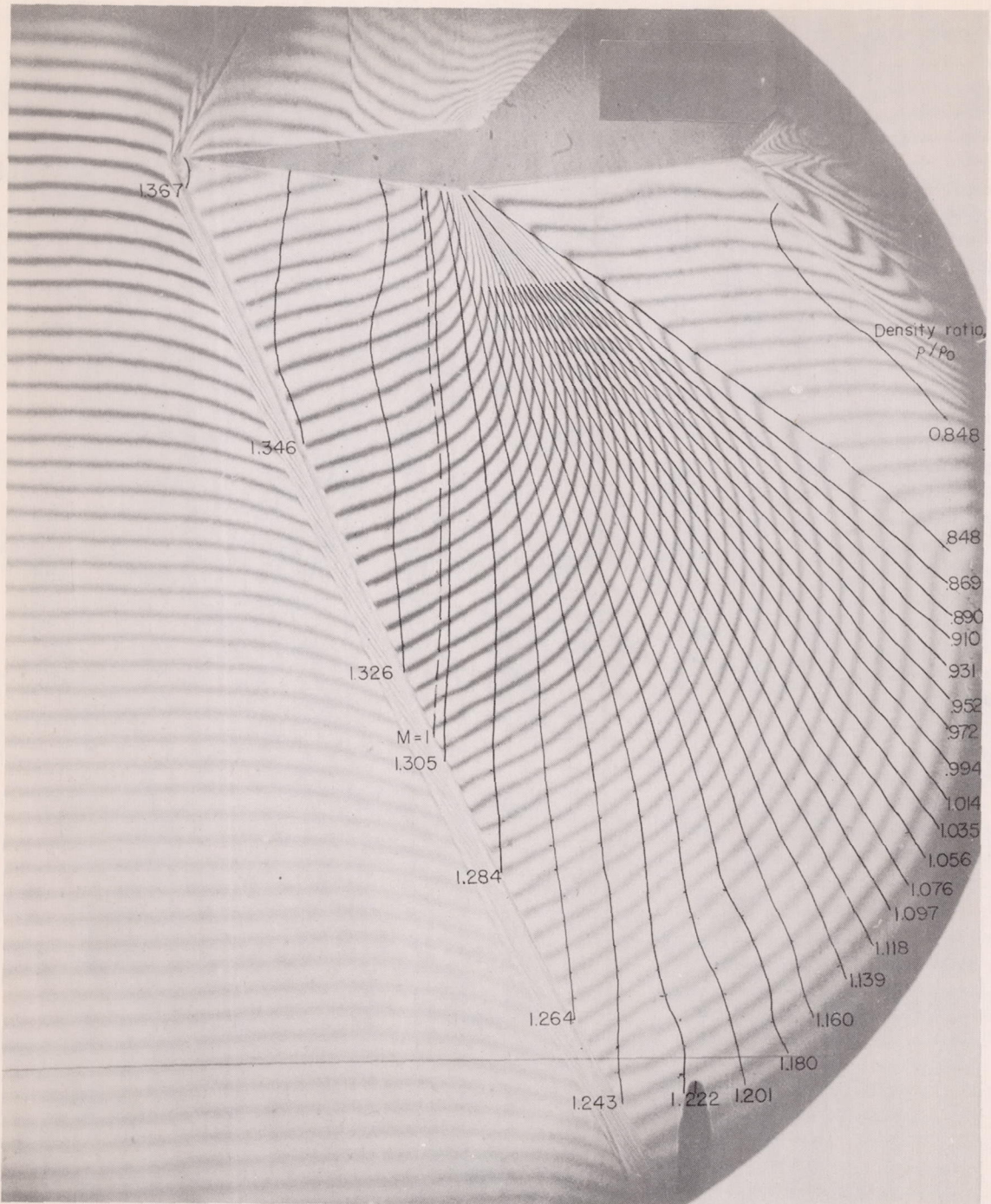
L-91713

Figure 4.- Concluded.

(a) $\alpha = 0.28^\circ$.

L-91714

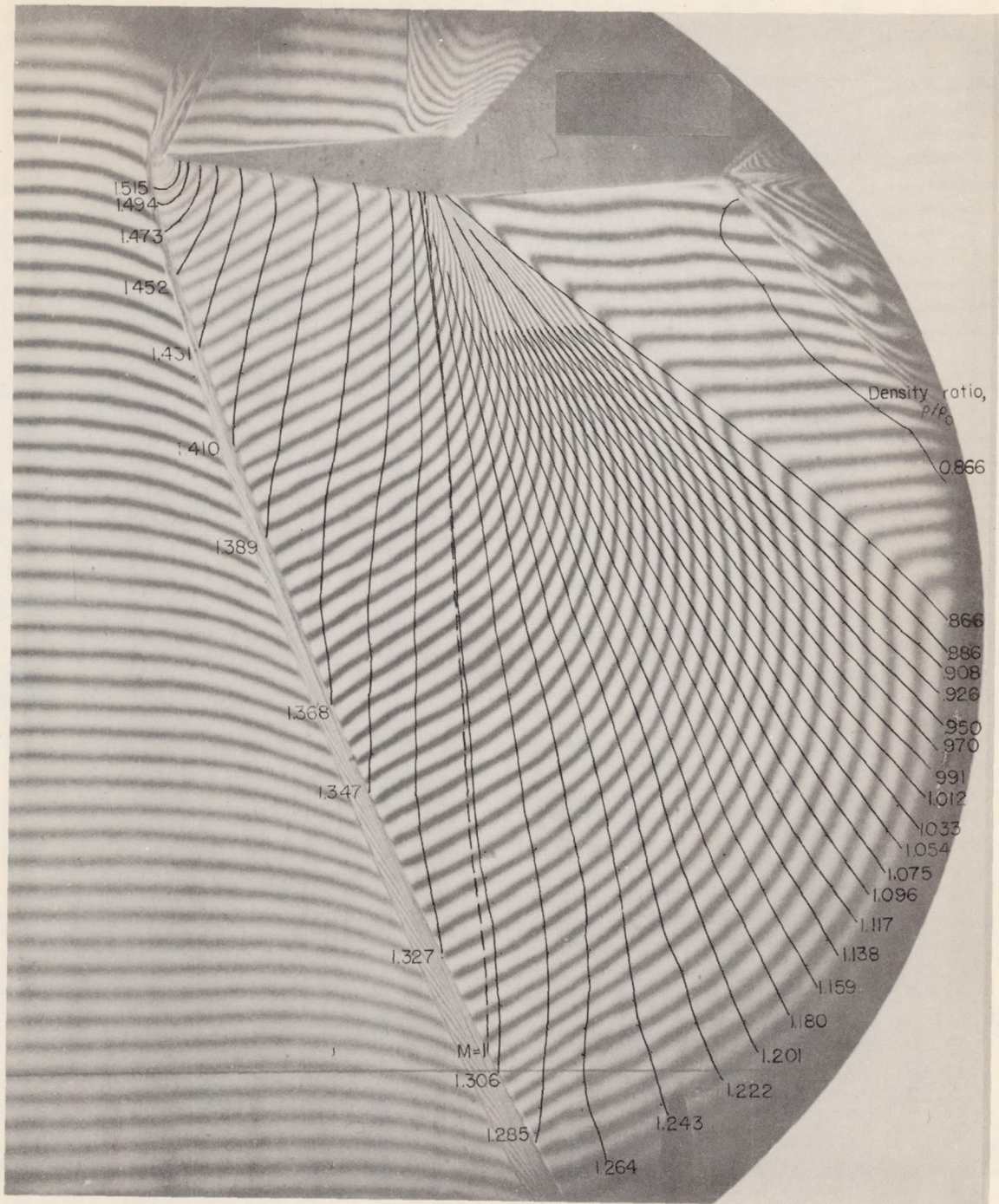
Figure 5.- Interferograms of flow past 10-percent-thick double wedge at $M = 1.30$ ($\xi_0 = 1.26$).



(b) $\alpha = 0.80^\circ$.

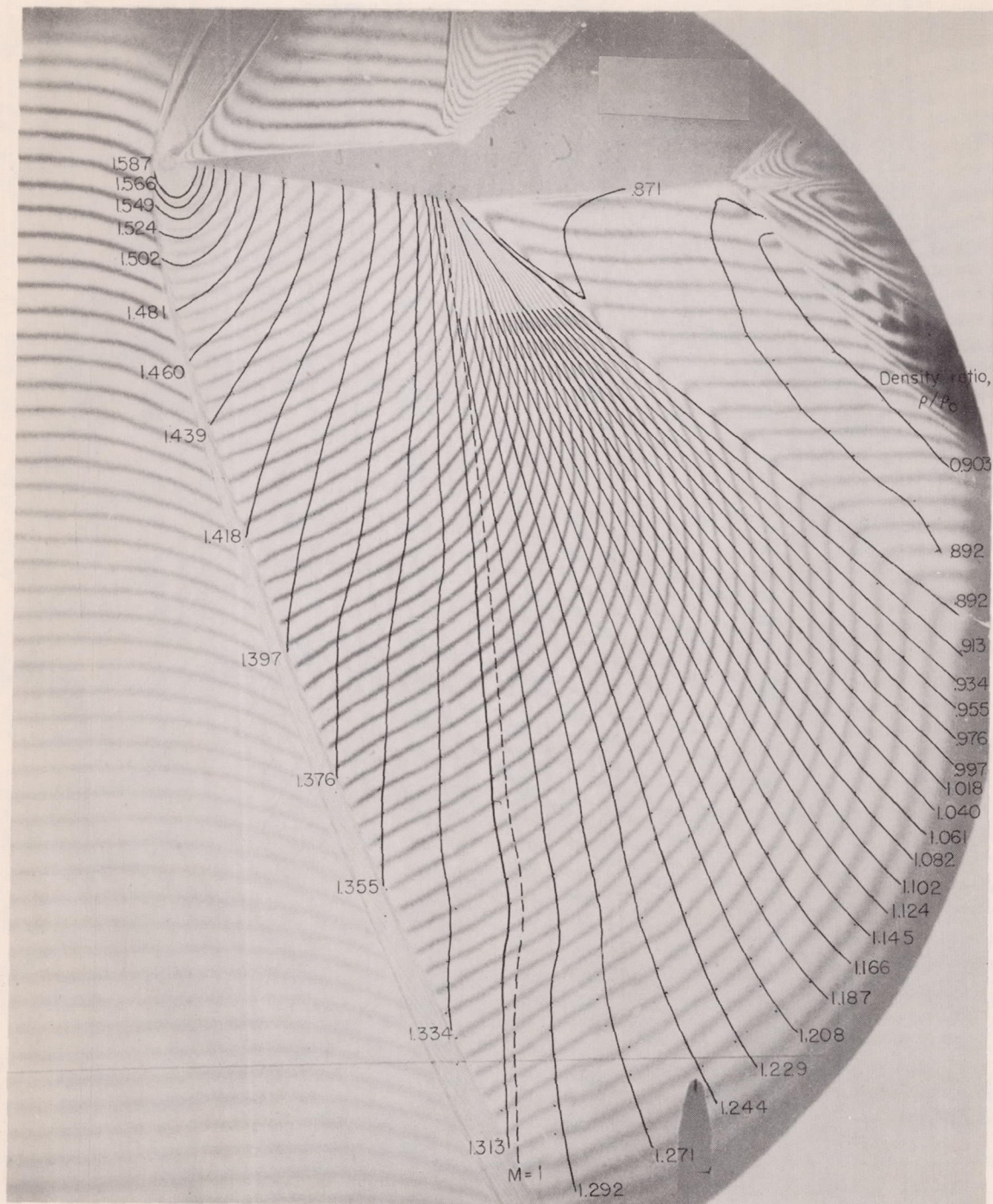
L-91715

Figure 5.- Continued.

(c) $\alpha = 1.85^\circ$.

L-91716

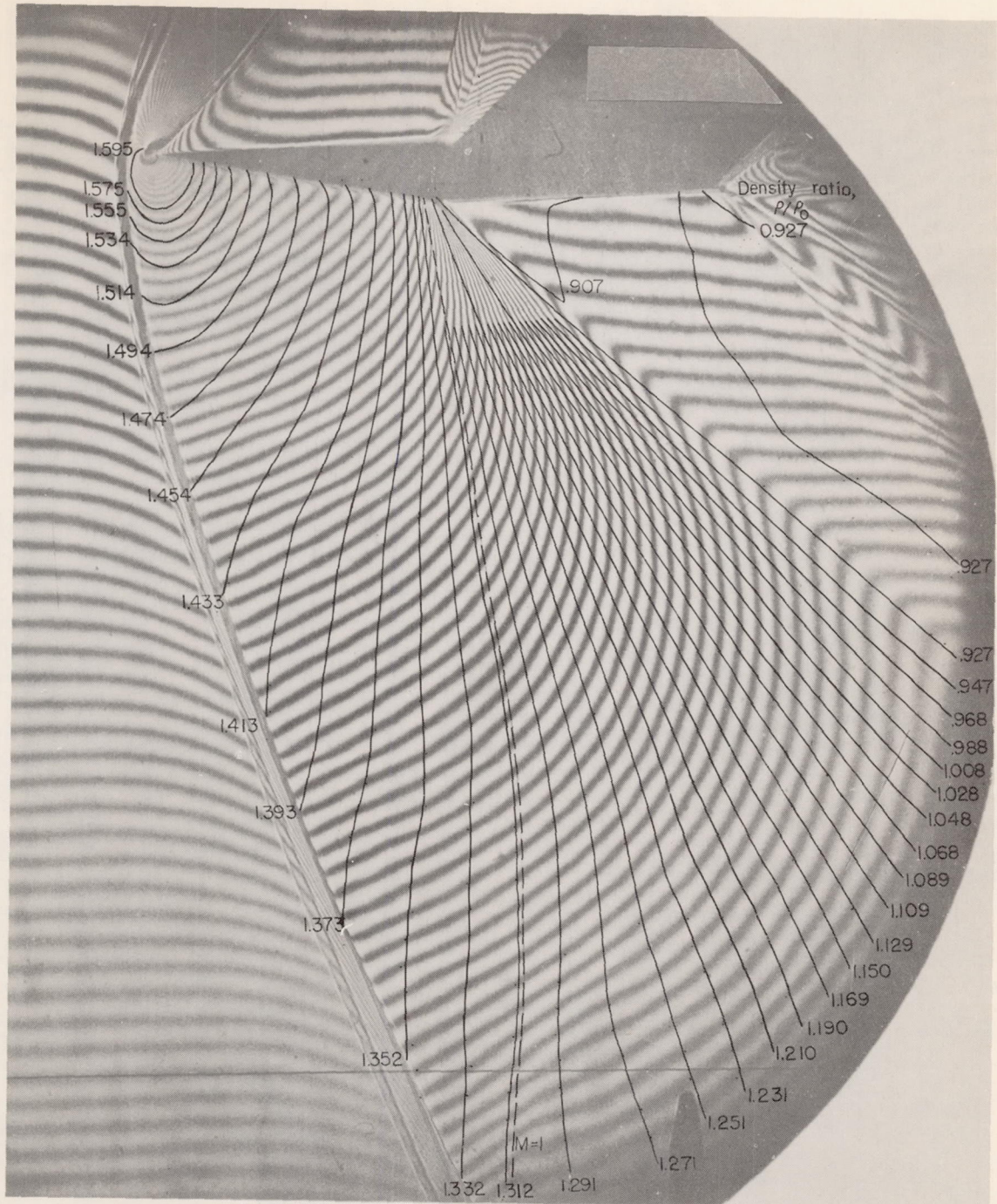
Figure 5.- Continued.



(d) $\alpha = 2.90^\circ$.

L-91717

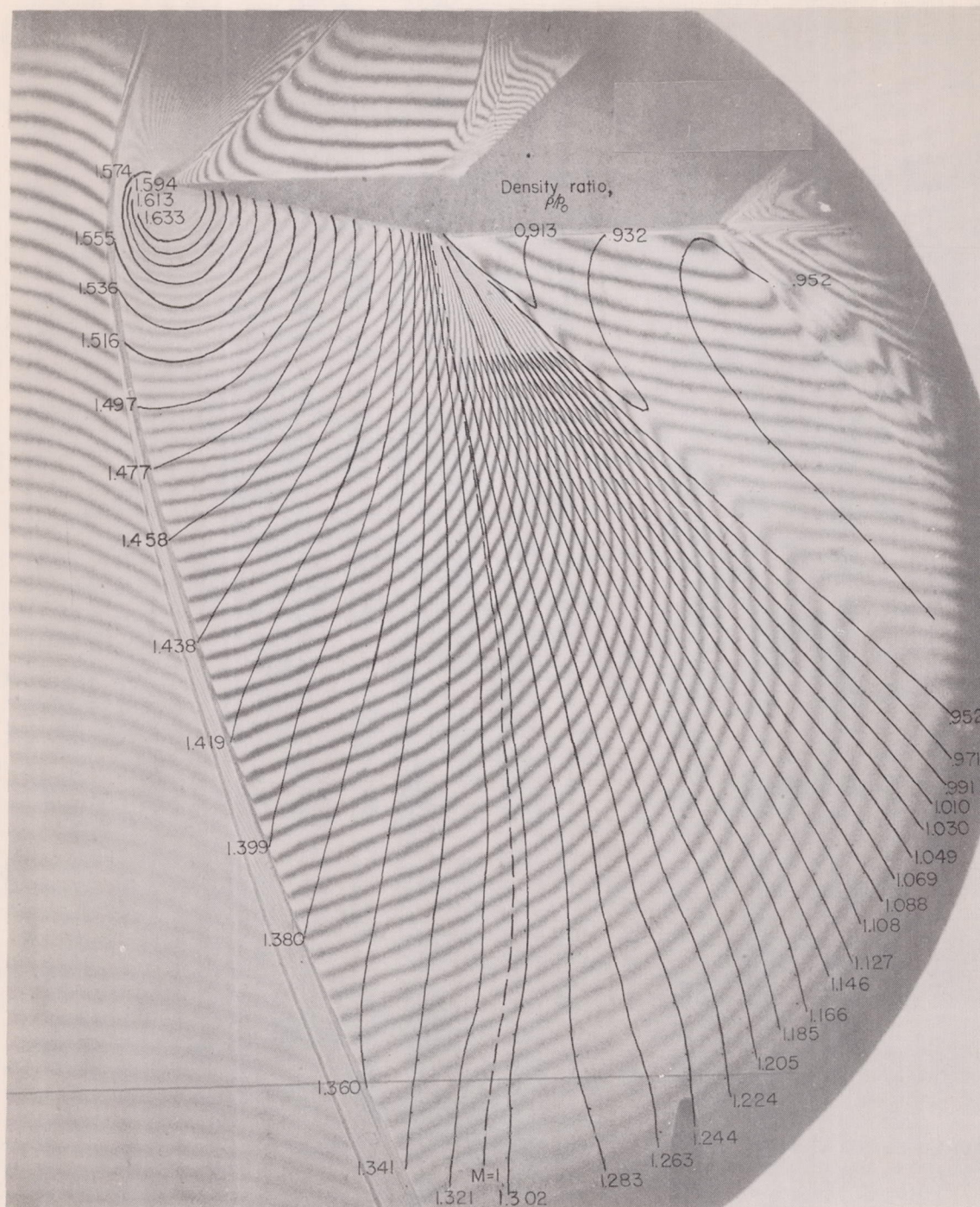
Figure 5.- Continued.



(e) $\alpha = 3.95^\circ$.

L-91718

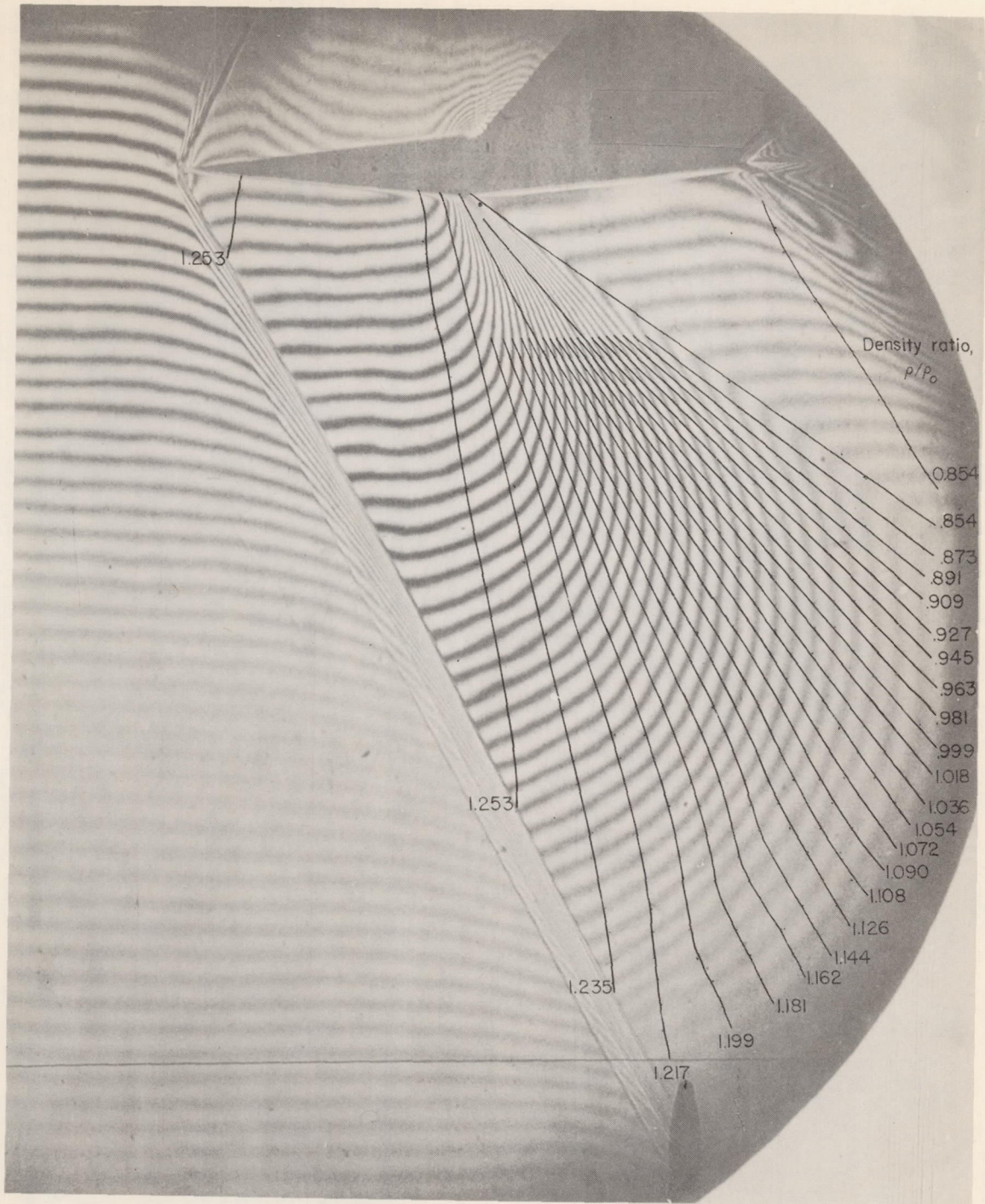
Figure 5.- Continued.



(f) $\alpha = 5.00^\circ$.

L-91719

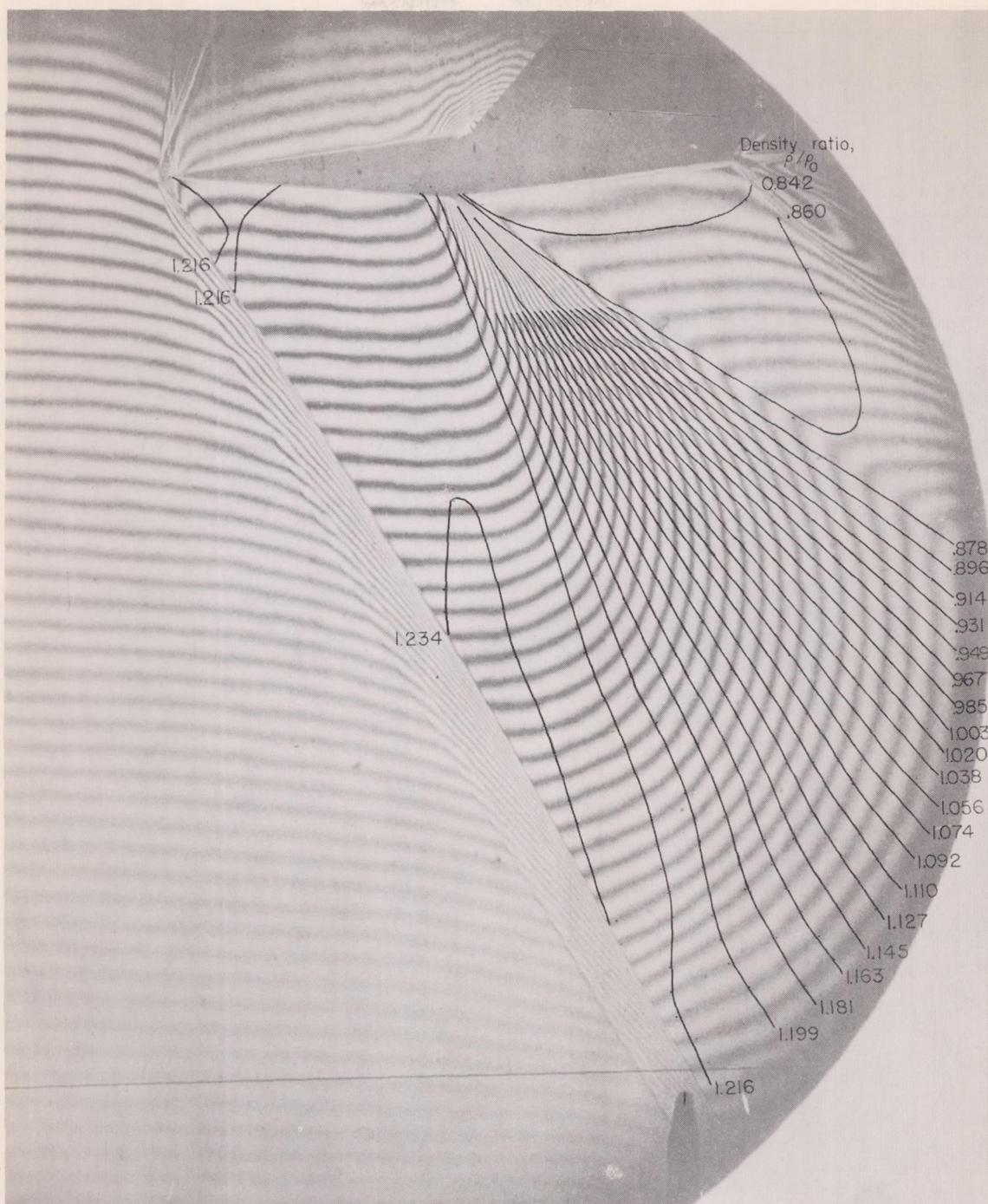
Figure 5.- Continued.



(g) $\alpha = -0.25^\circ$.

L-91720

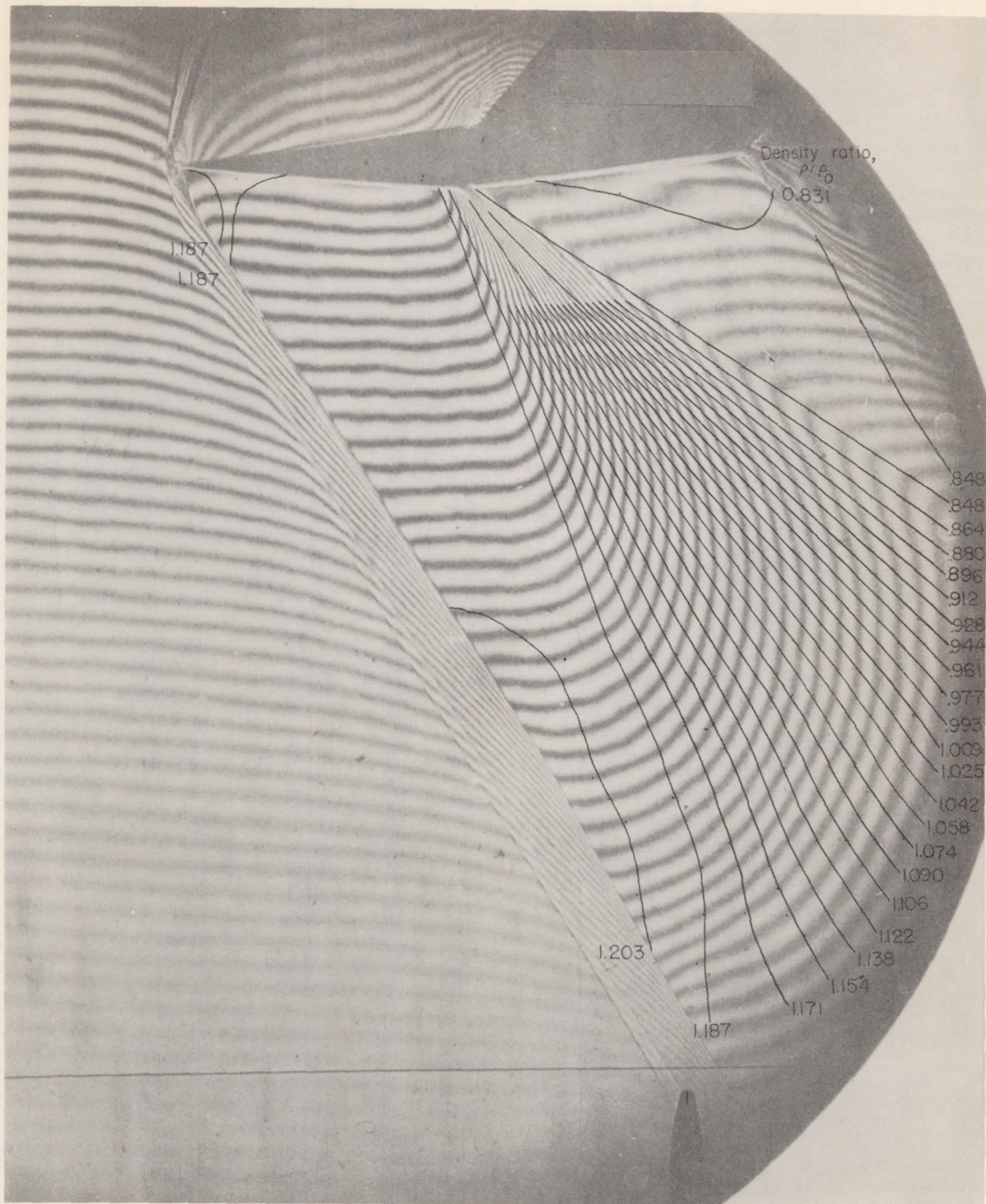
Figure 5.- Continued.



(h) $\alpha = -0.78^\circ$.

L-91721

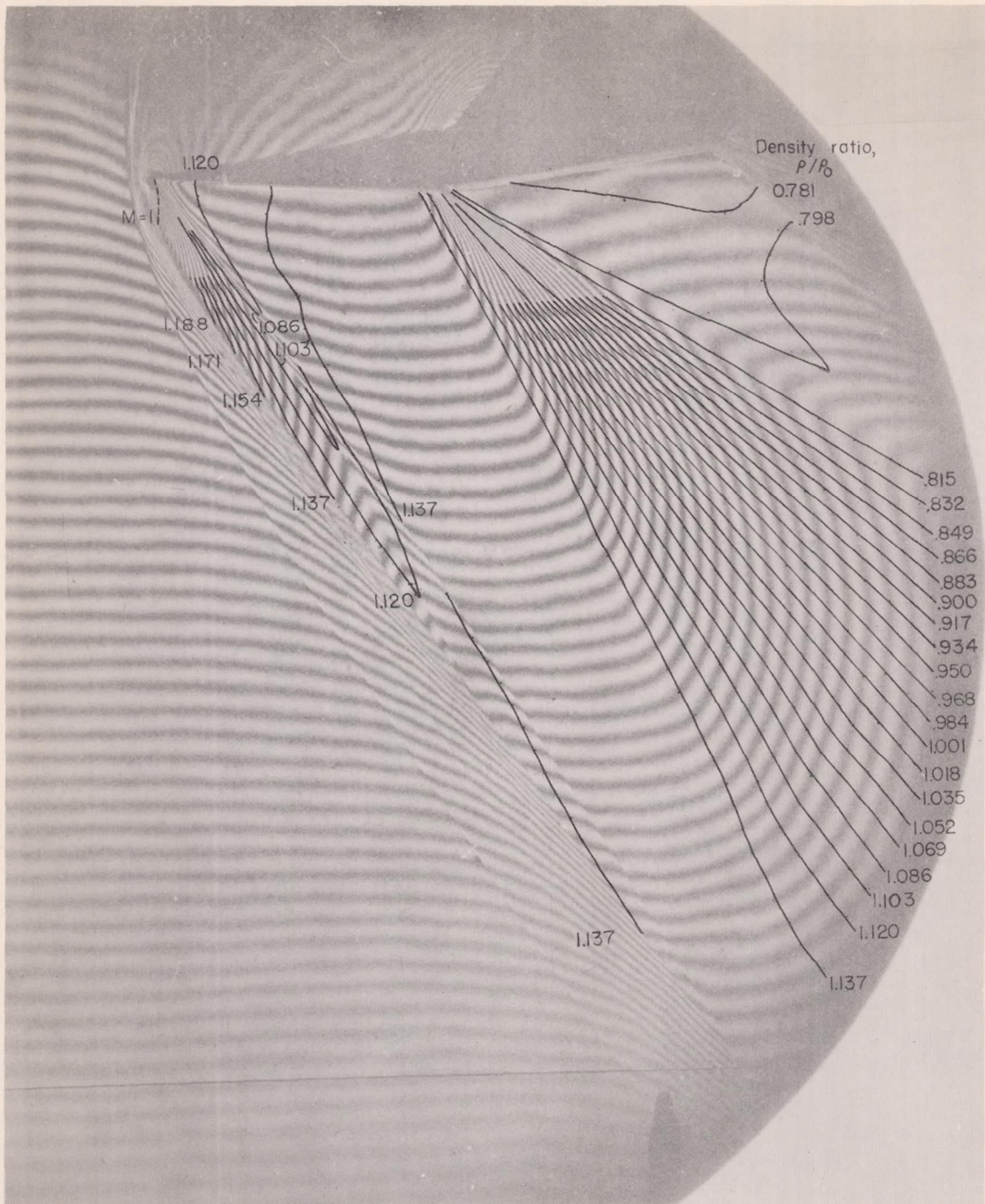
Figure 5.- Continued.



(i) $\alpha = -1.30^\circ$.

L-91722

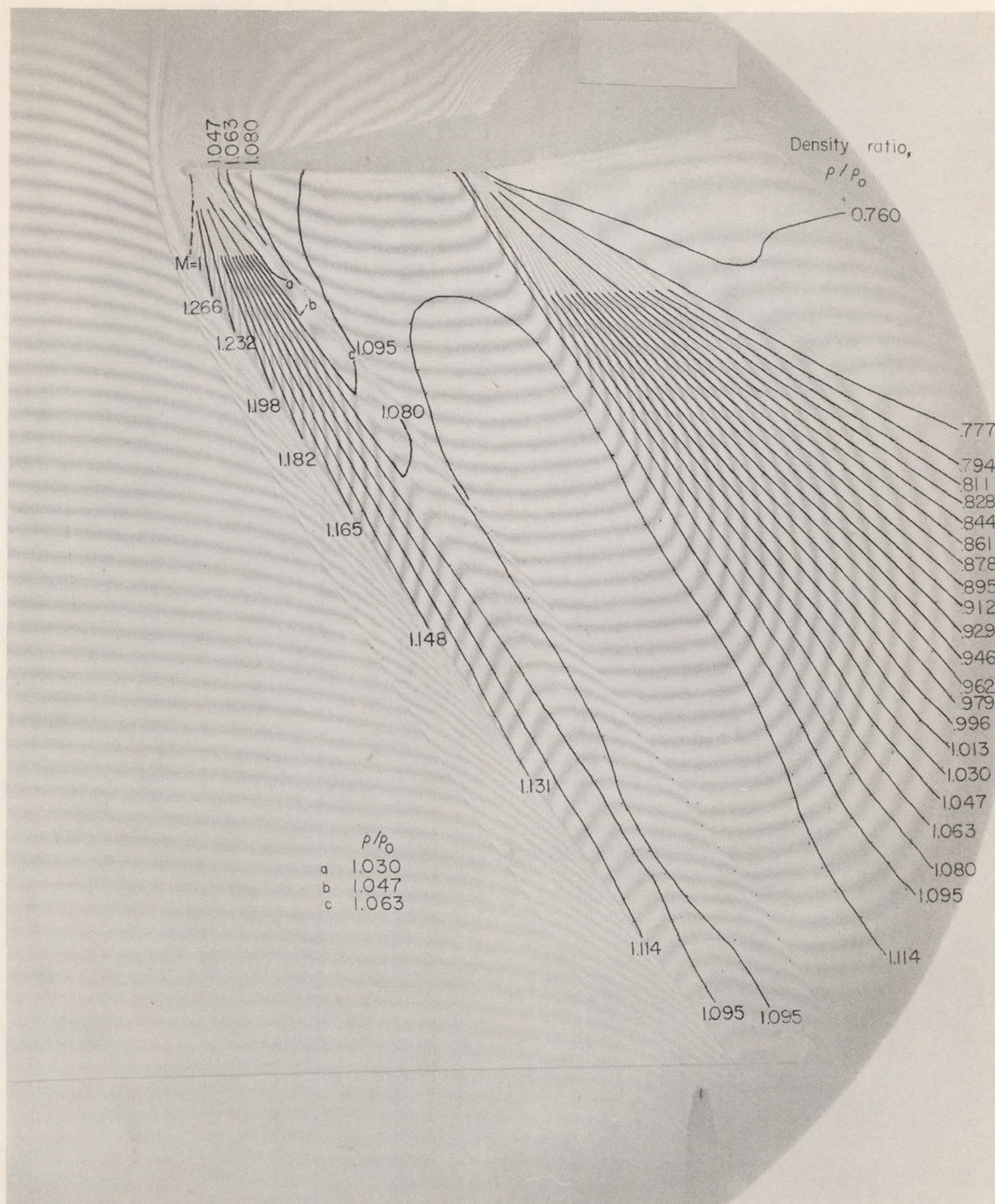
Figure 5.- Continued.



(j) $\alpha = -2.35^\circ$.

L-91723

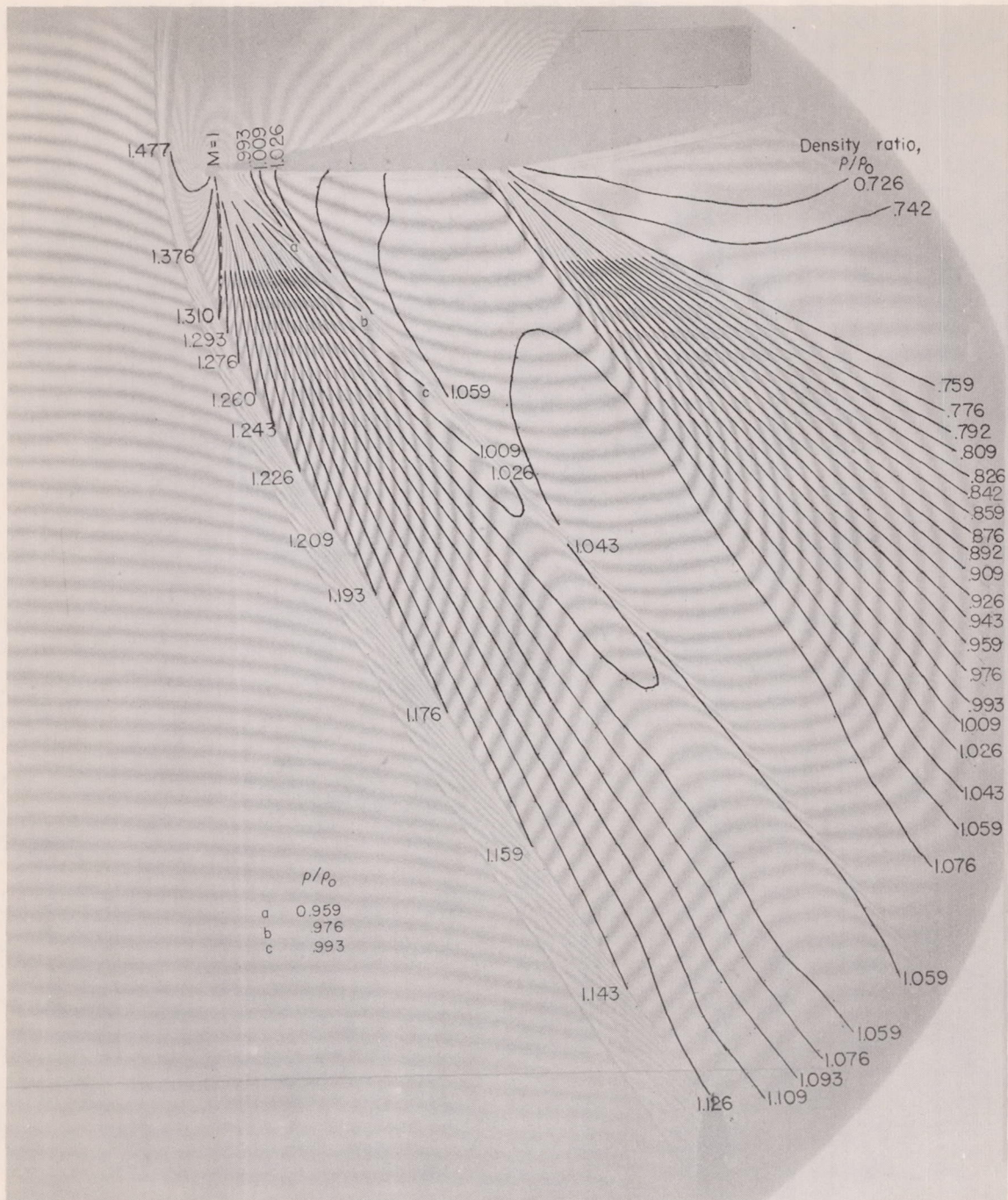
Figure 5.- Continued.



(k) $\alpha = -3.40^\circ$.

L-91724

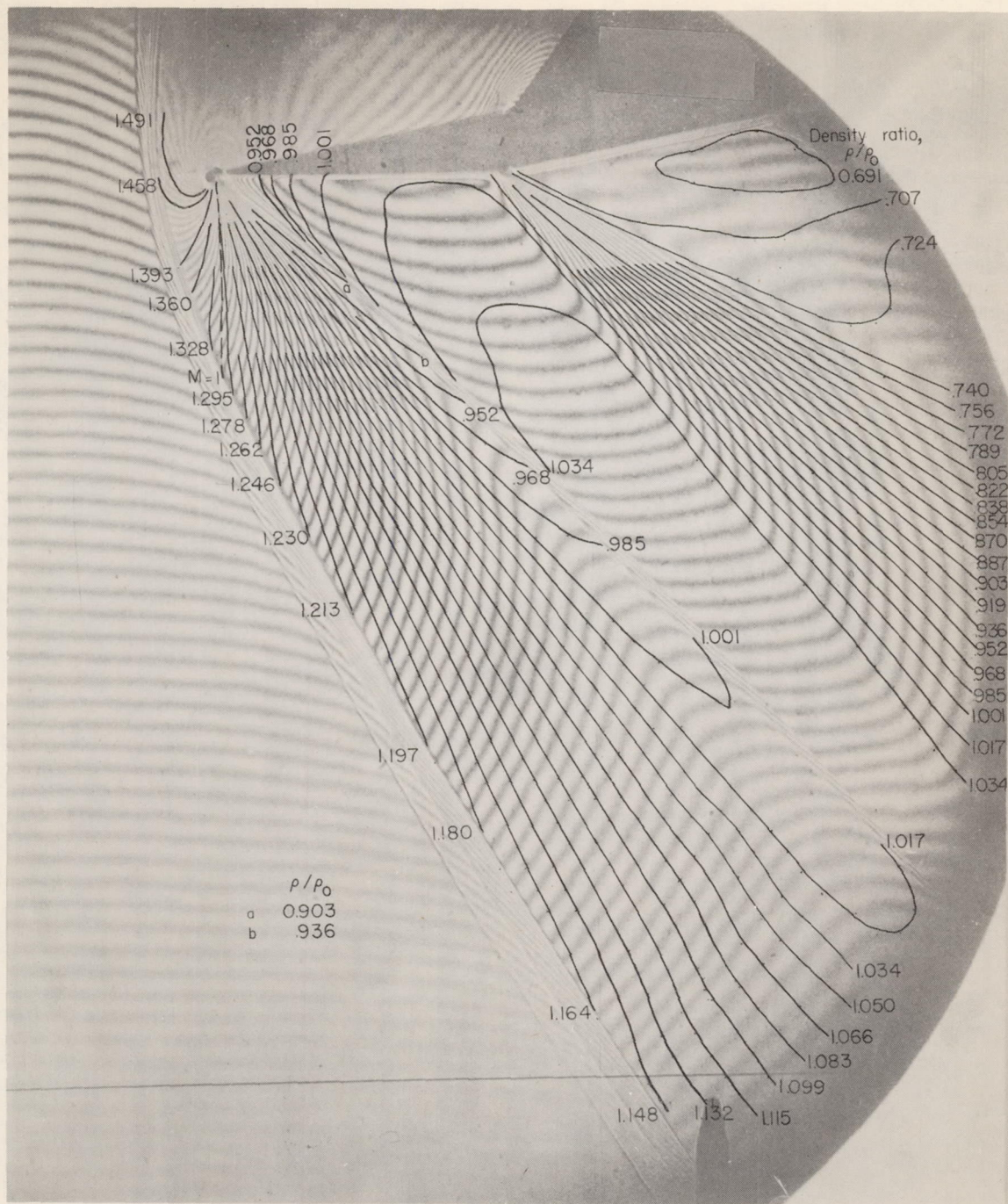
Figure 5.- Continued.



(2) $\alpha = -4.45^\circ$.

L-91725

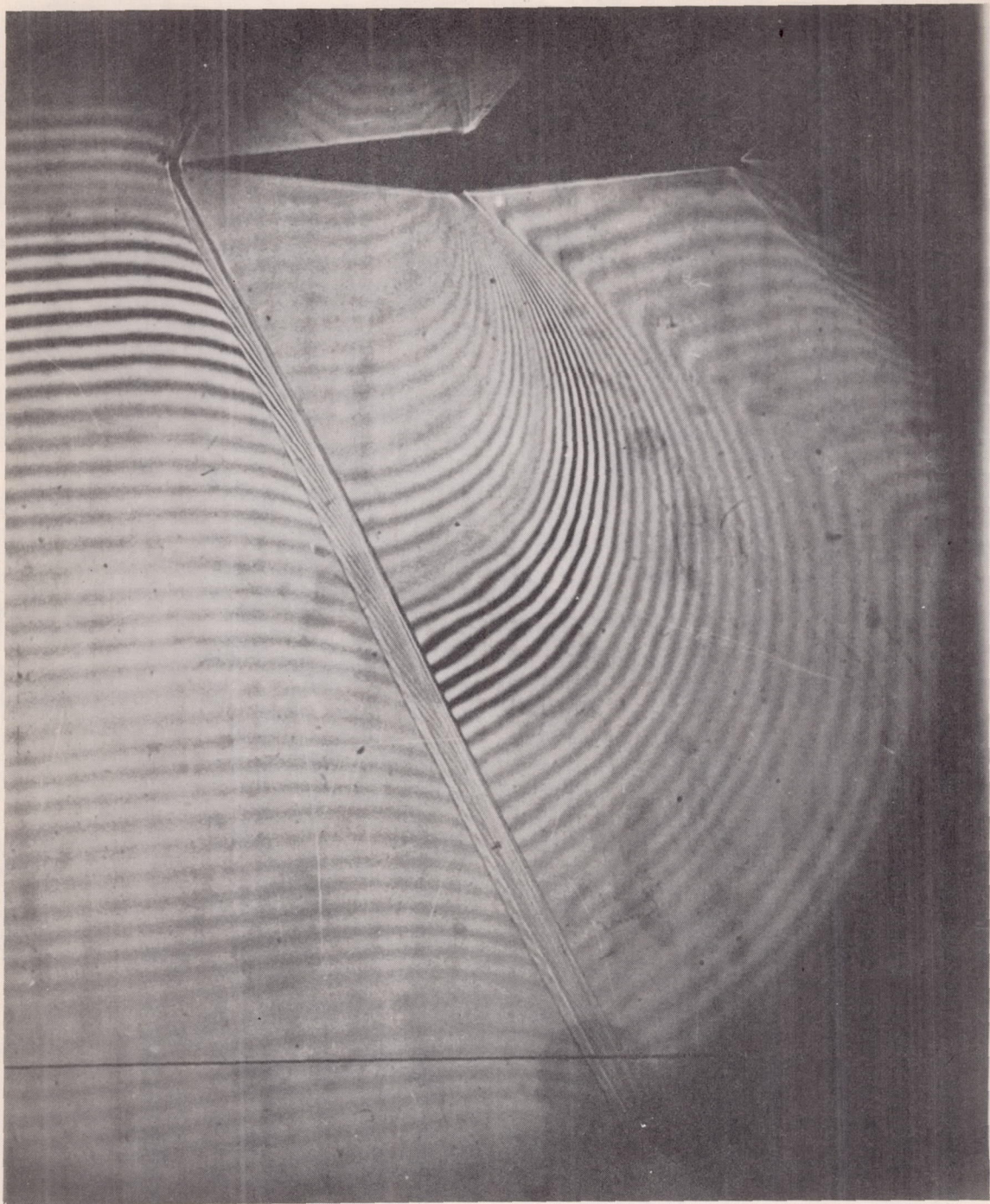
Figure 5.- Continued.



(m) $\alpha = -5.50^\circ$.

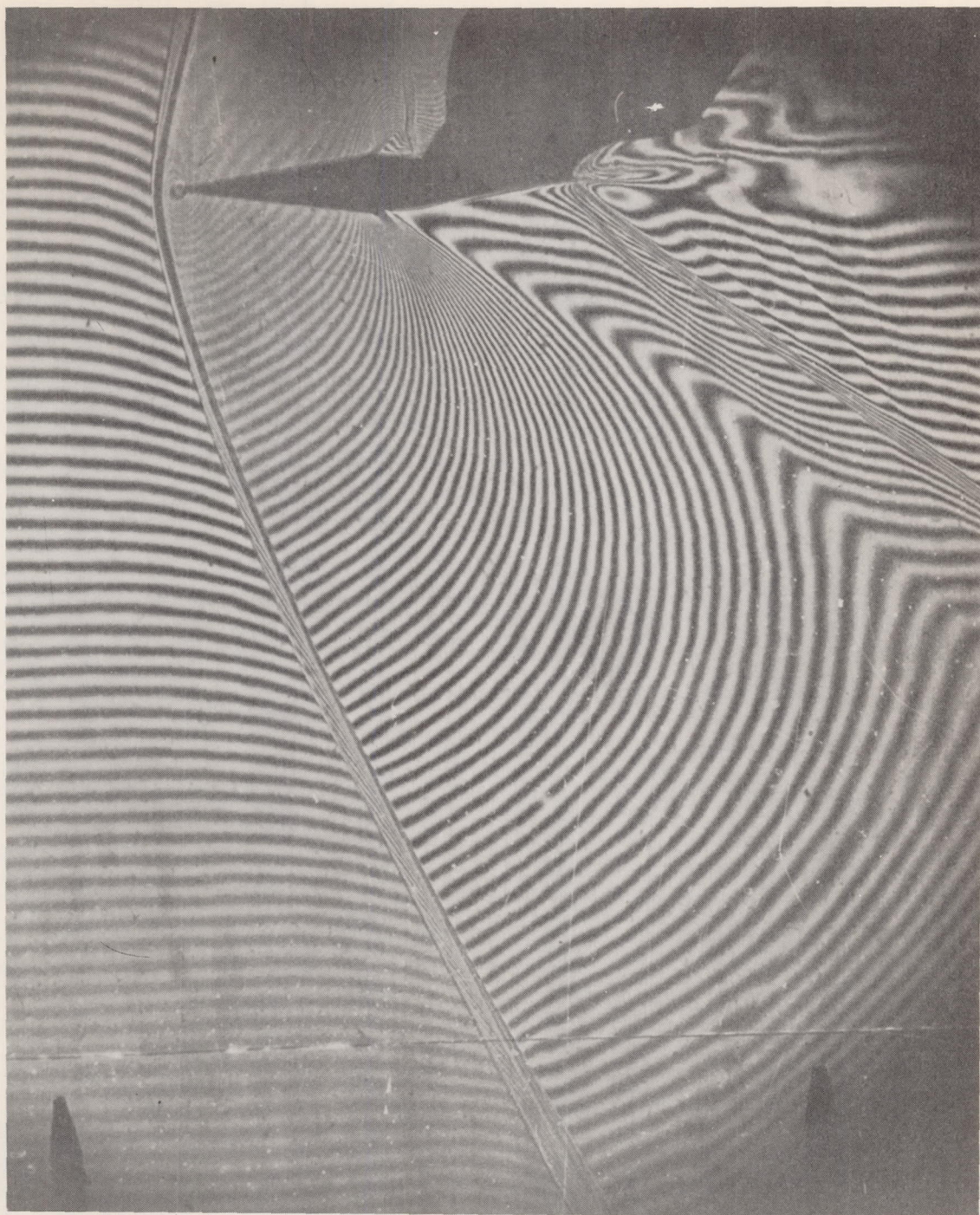
L-91726

Figure 5.- Concluded.



L-91727

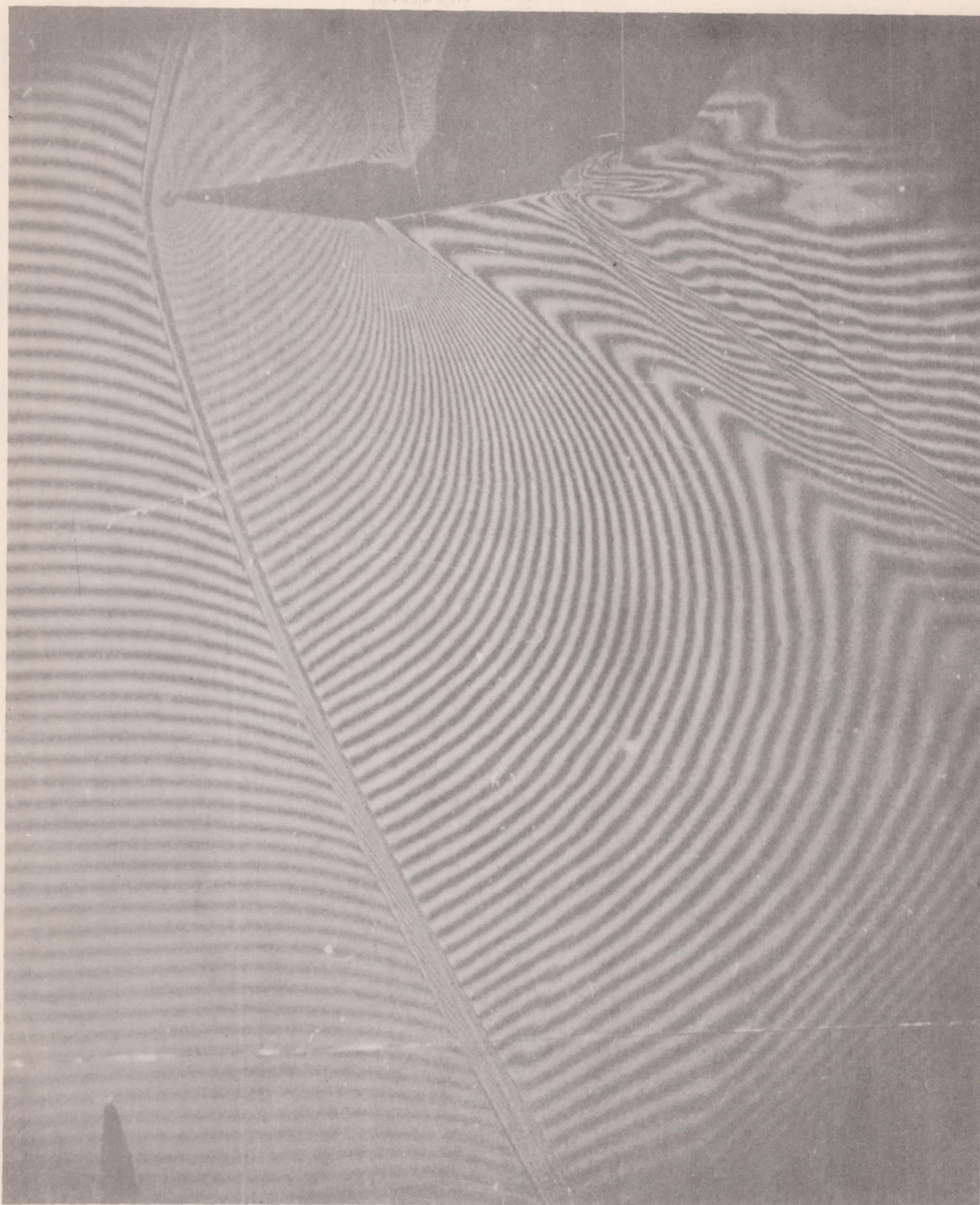
Figure 6.- Typical white-light interferogram of flow past 10-percent-thick double wedge at $M = 1.30$ ($\xi_0 = 1.26$).



(a) $\alpha = 0.40^\circ$.

L-91728

Figure 7.- Interferograms of flow past 14.2-percent-thick double wedge at $M = 1.30$ ($\xi_0 = 1.00$).



(b) $\alpha = 0.95^\circ$.

L-91729

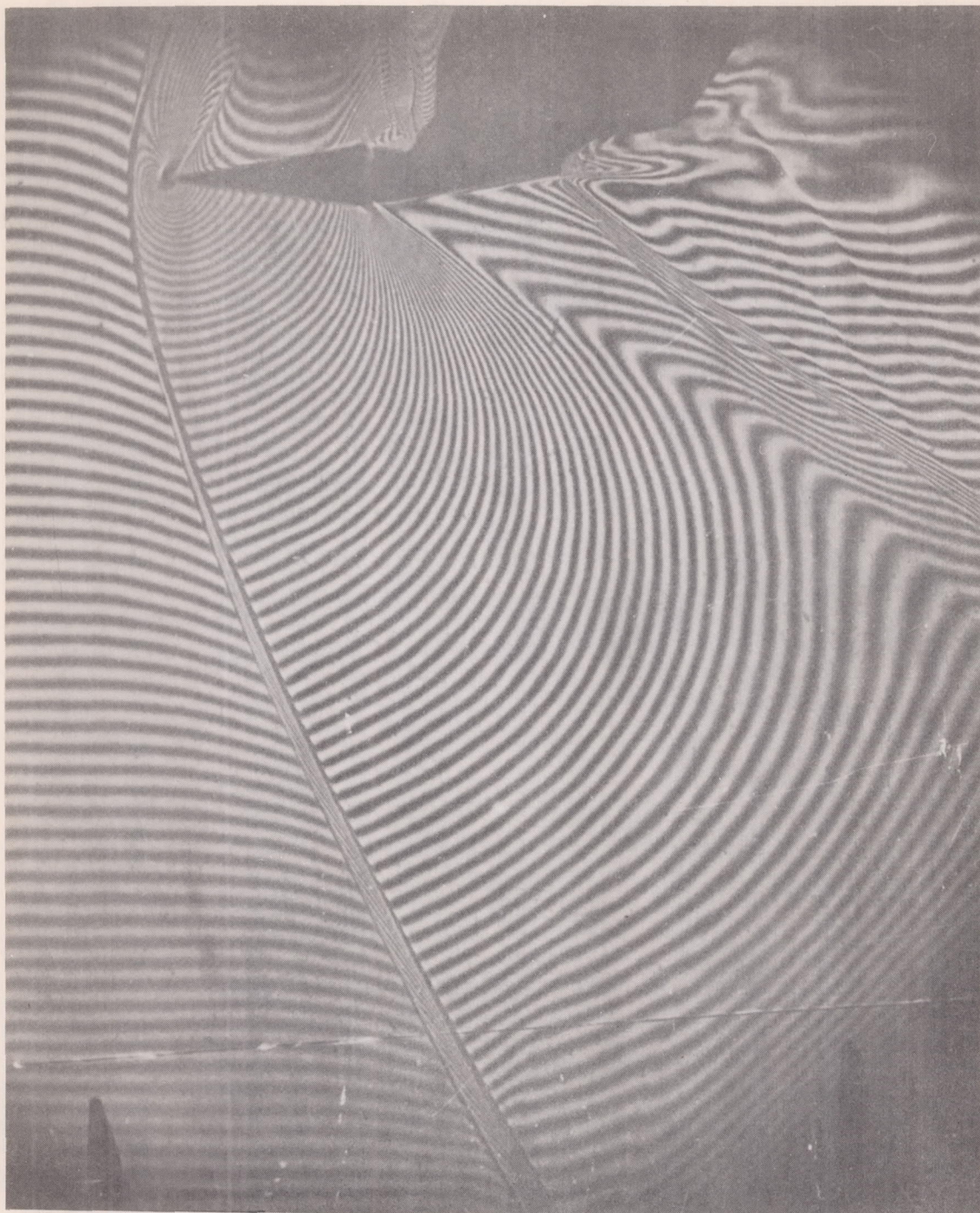
Figure 7.- Continued.



(c) $\alpha = 2.05^\circ$.

L-91730

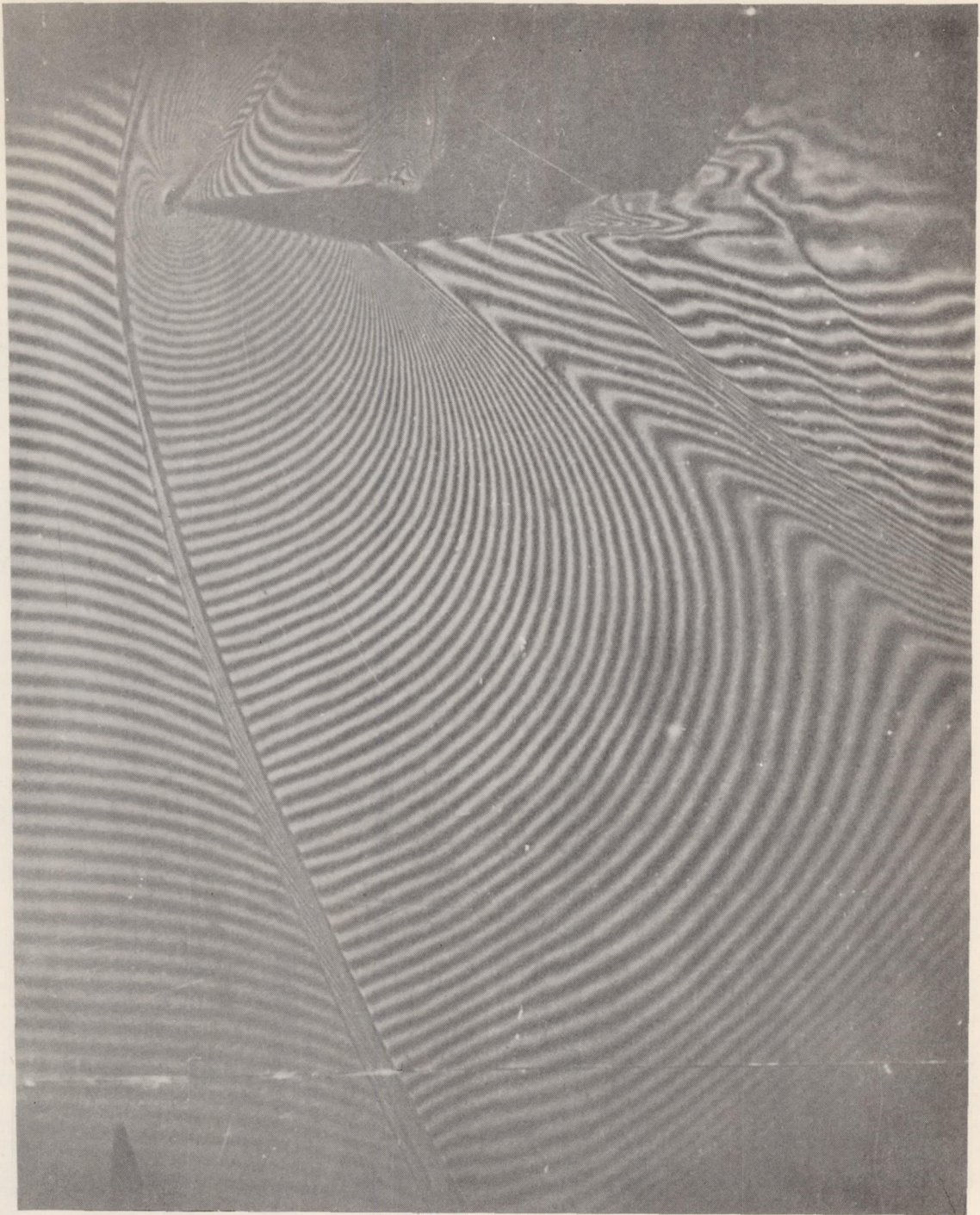
Figure 7.- Continued.



(d) $\alpha = 3.15^\circ$.

L-91731

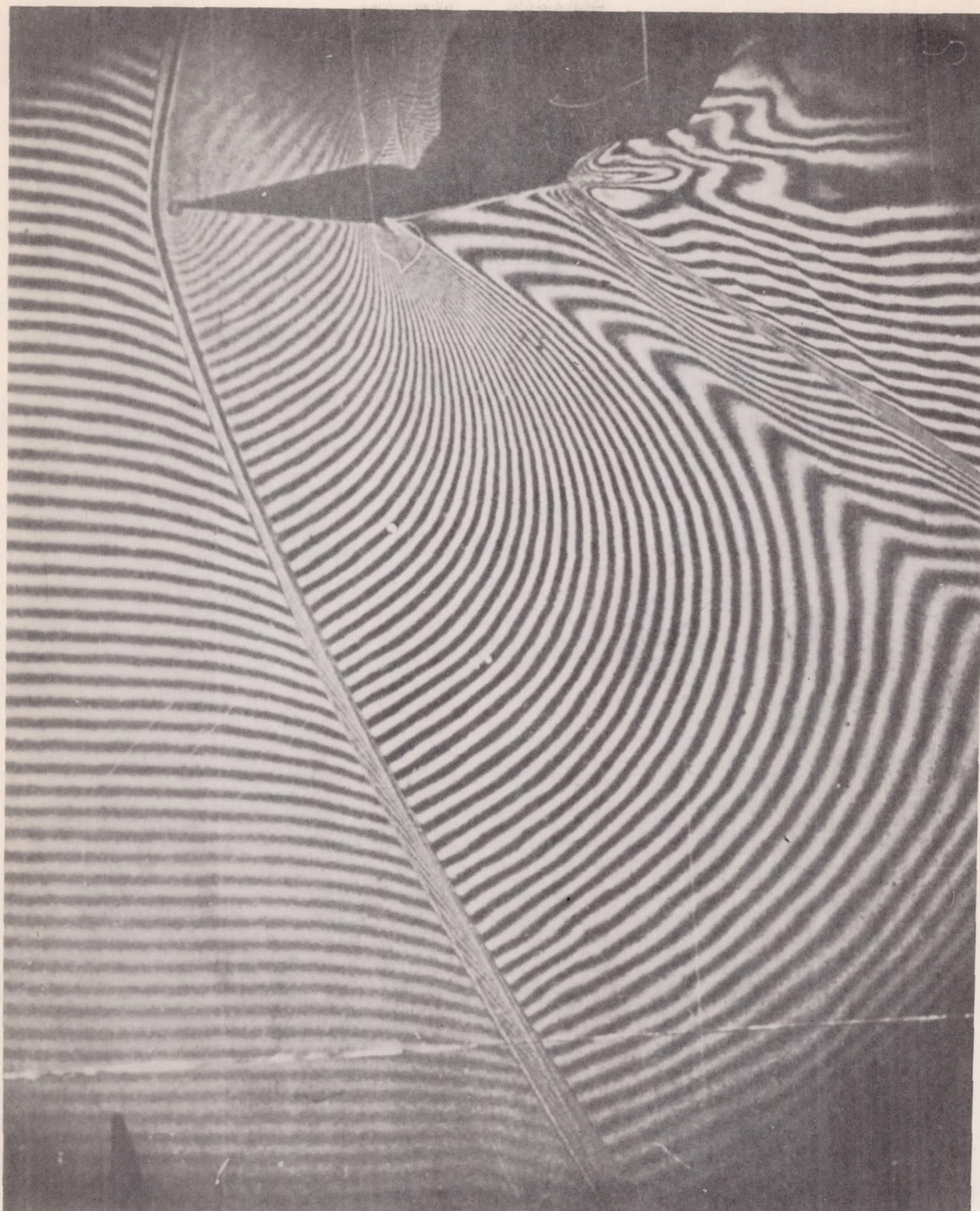
Figure 7.- Continued.



(e) $\alpha = 4.25^\circ$.

L-91732

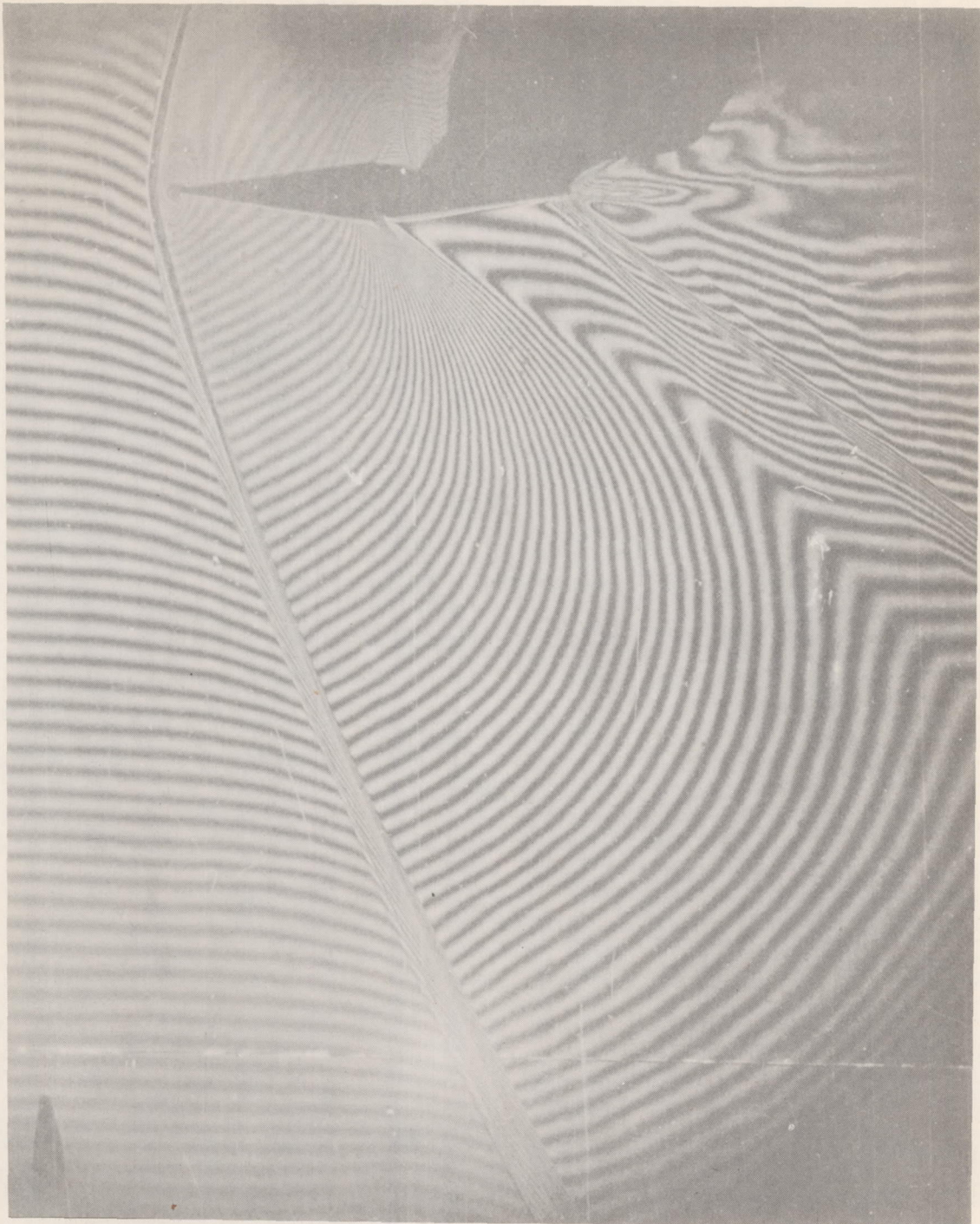
Figure 7.- Continued.



(f) $\alpha = -0.20^\circ$.

L-91733

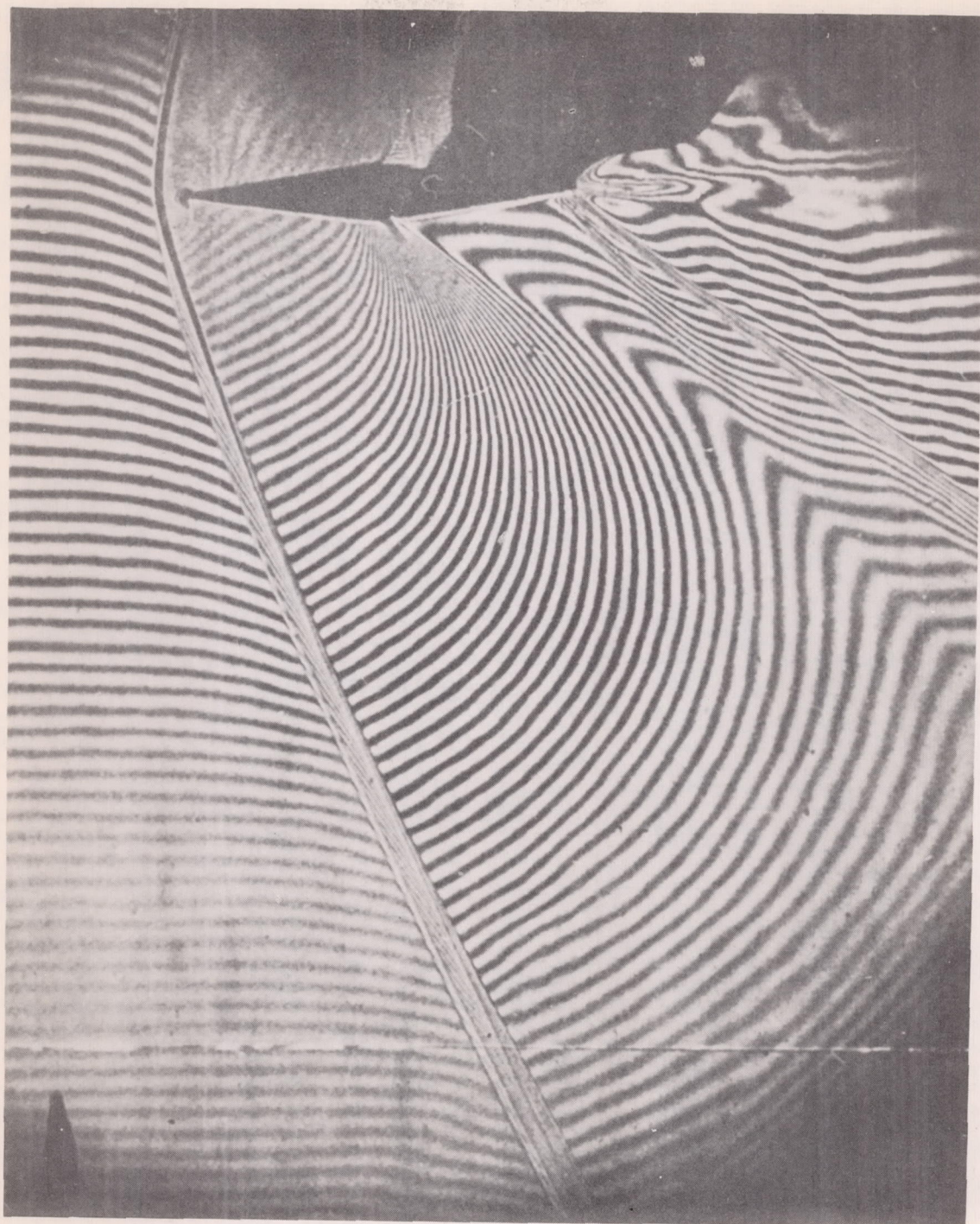
Figure 7.- Continued.



(g) $\alpha = -0.75^\circ$.

L-91734

Figure 7.- Continued.



(h) $\alpha = -1.30^\circ$.

L-91735

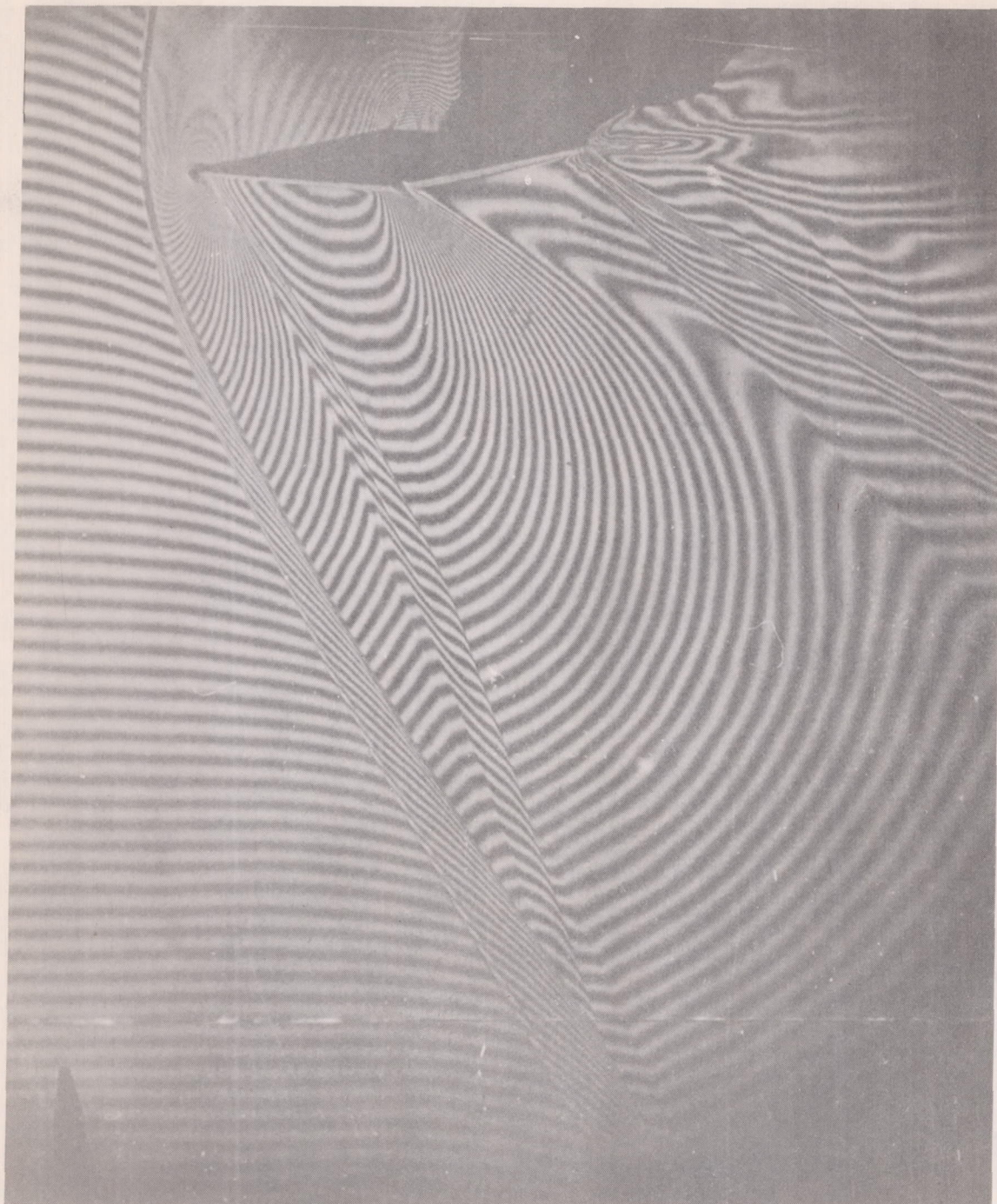
Figure 7.- Continued.



(i) $\alpha = -2.50^\circ$.

L-91736

Figure 7.- Continued.



(j) $\alpha = -3.65^\circ$.

L-91737

Figure 7.- Continued.



(k) $\alpha = -4.80^\circ$.

L-91738

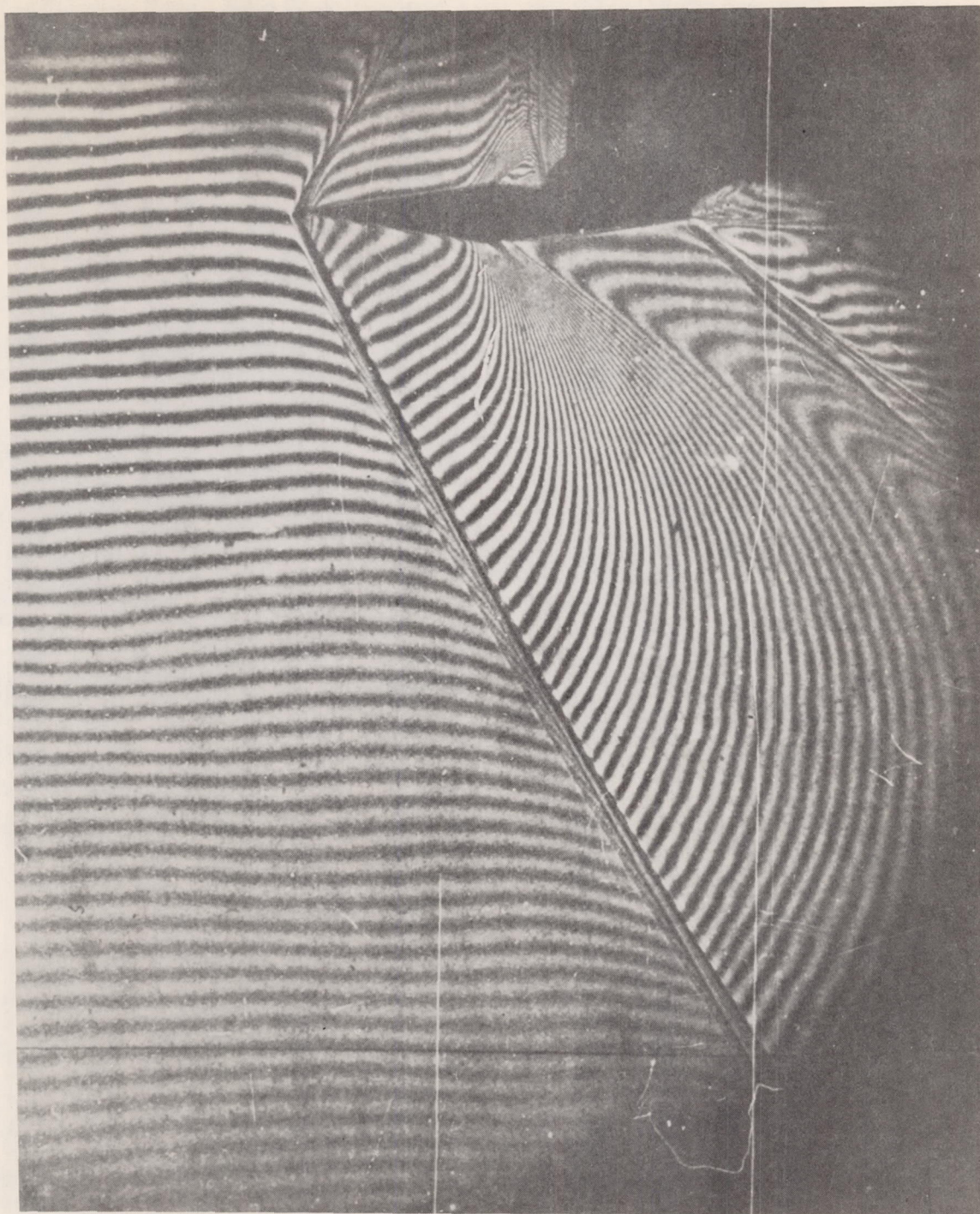
Figure 7.- Concluded.



(a) $\alpha = 0.18^\circ$.

L-91739

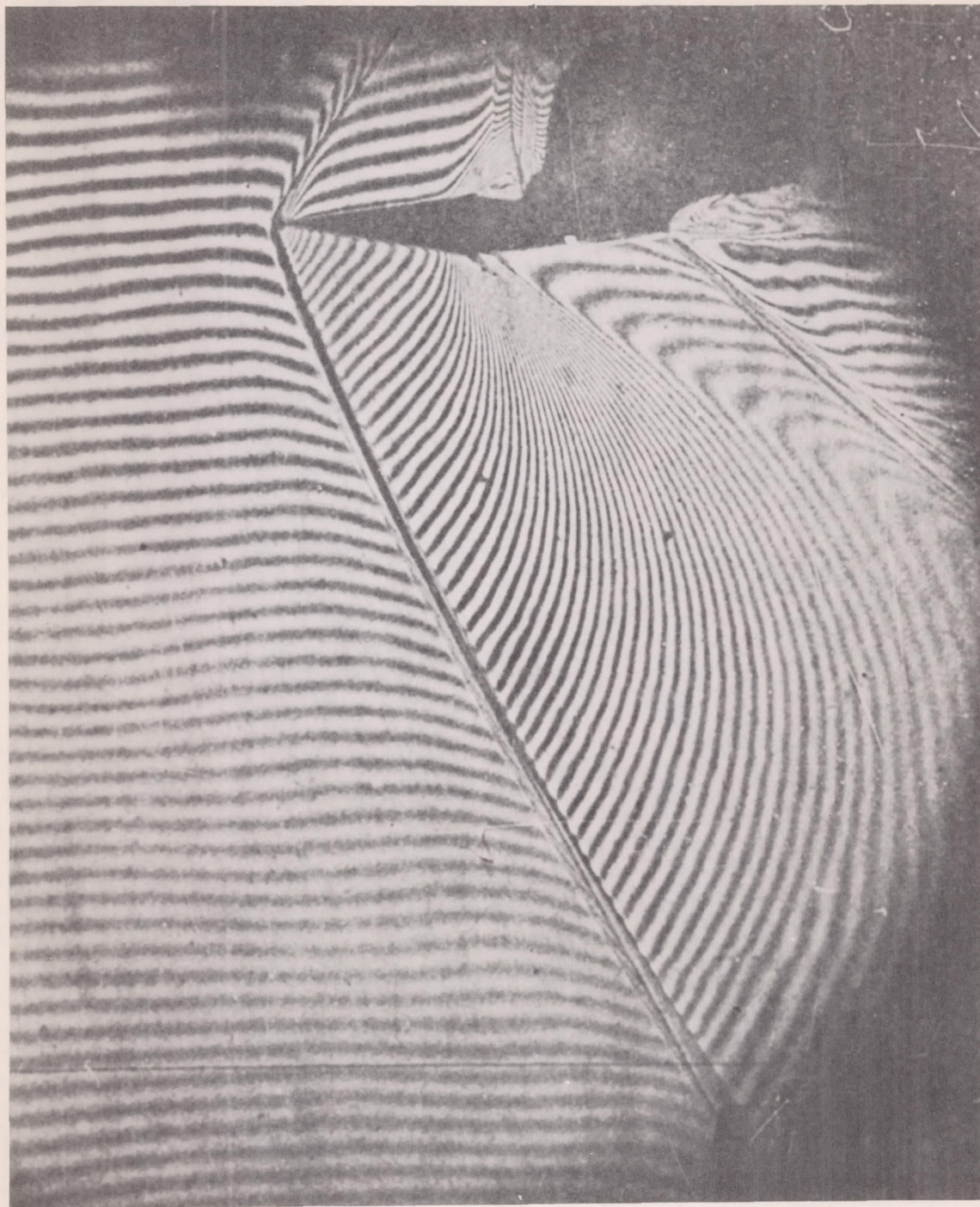
Figure 8.- Interferograms of flow past 14.2-percent-thick double wedge at
 $M = 1.41$ ($\xi_0 = 1.28$).



(b) $\alpha = 0.70^\circ$.

L-91740

Figure 8.- Continued.



(c) $\alpha = 1.80^\circ$.

L-91741

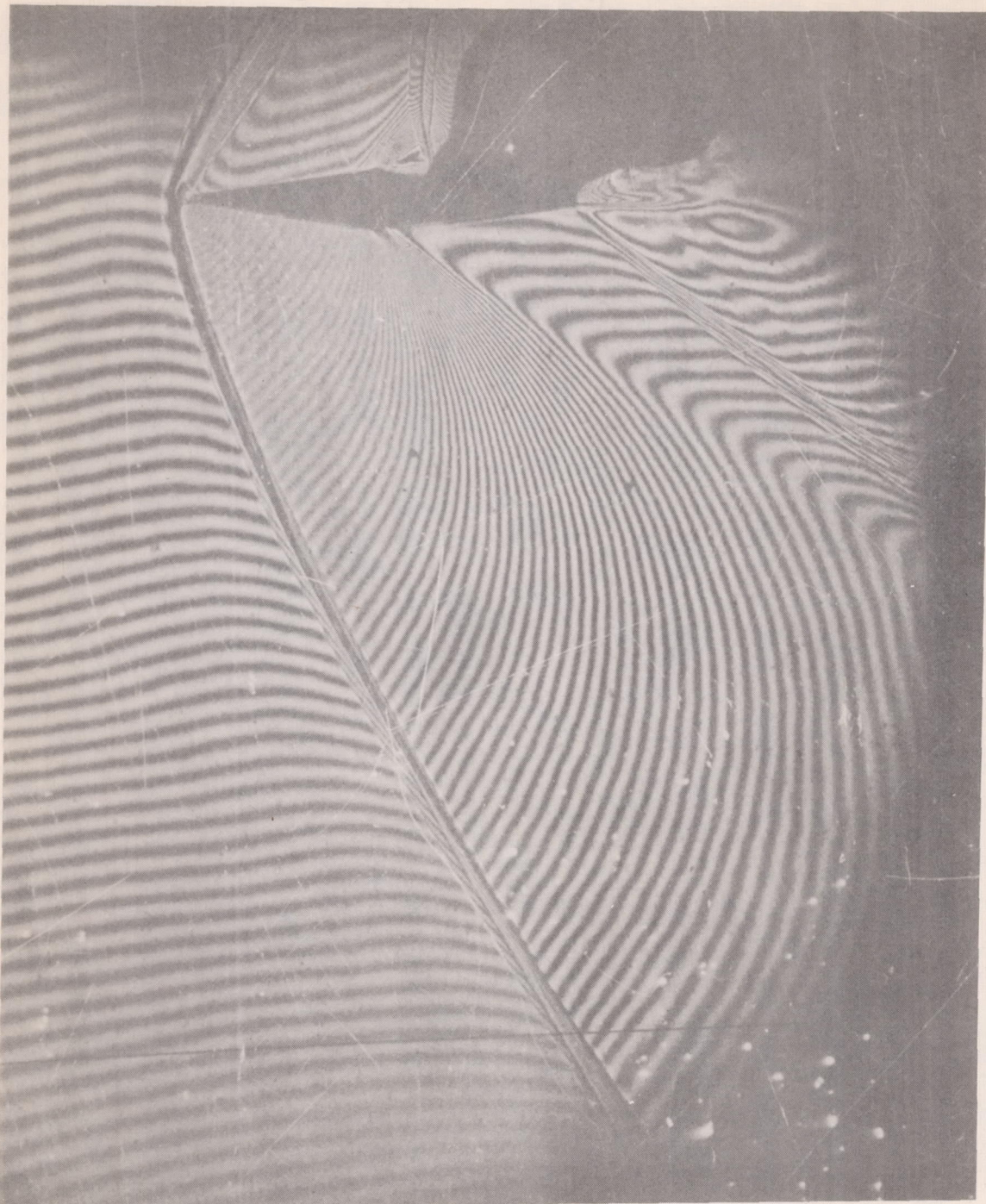
Figure 8.- Continued.



(d) $\alpha = 2.90^\circ$.

L-91742

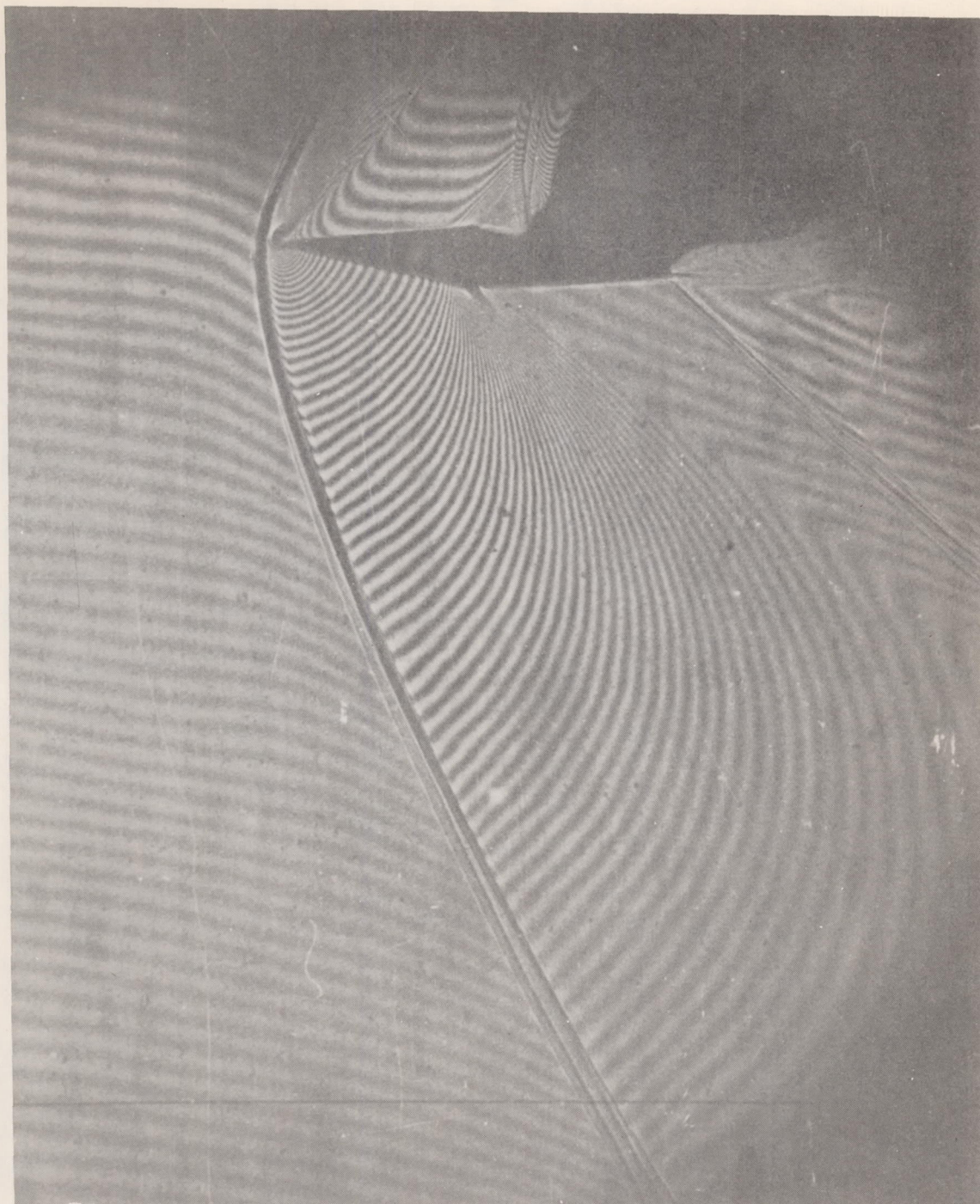
Figure 8.- Continued.



(e) $\alpha = 4.00^\circ$.

L-91743

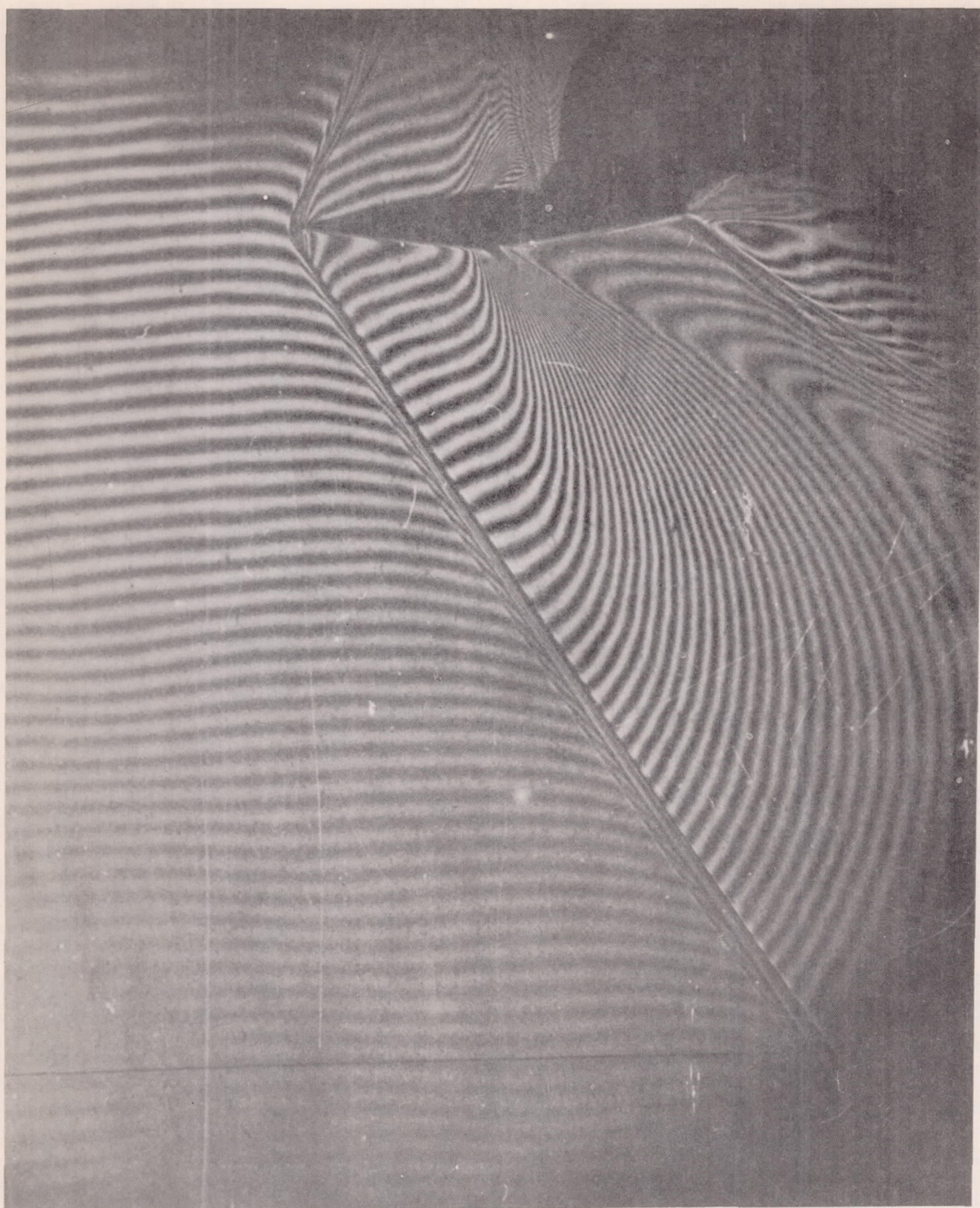
Figure 8.- Continued.



(f) $\alpha = 5.06^\circ$.

L-91744

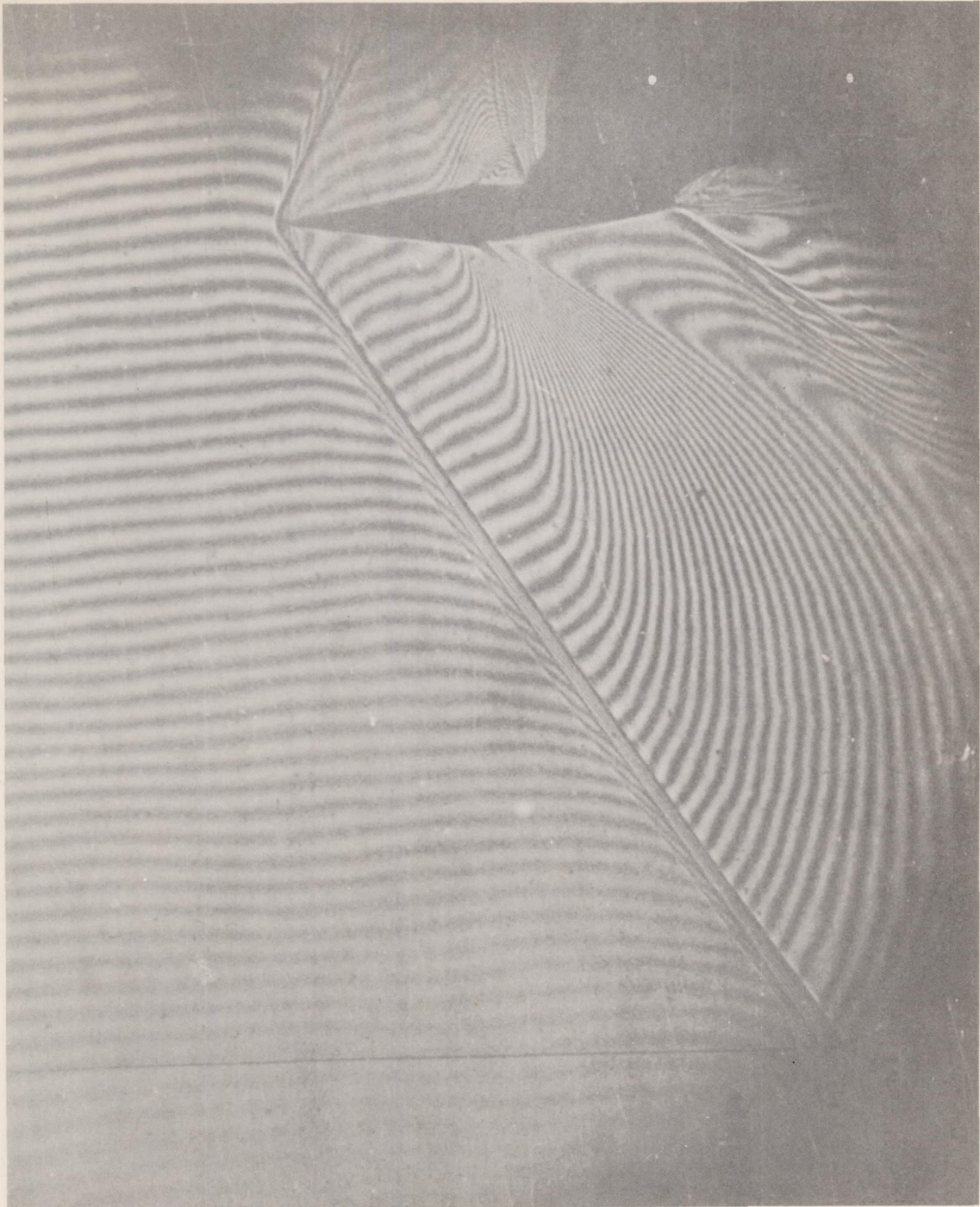
Figure 8.- Continued.



(g) $\alpha = -0.38^\circ$.

L-91745

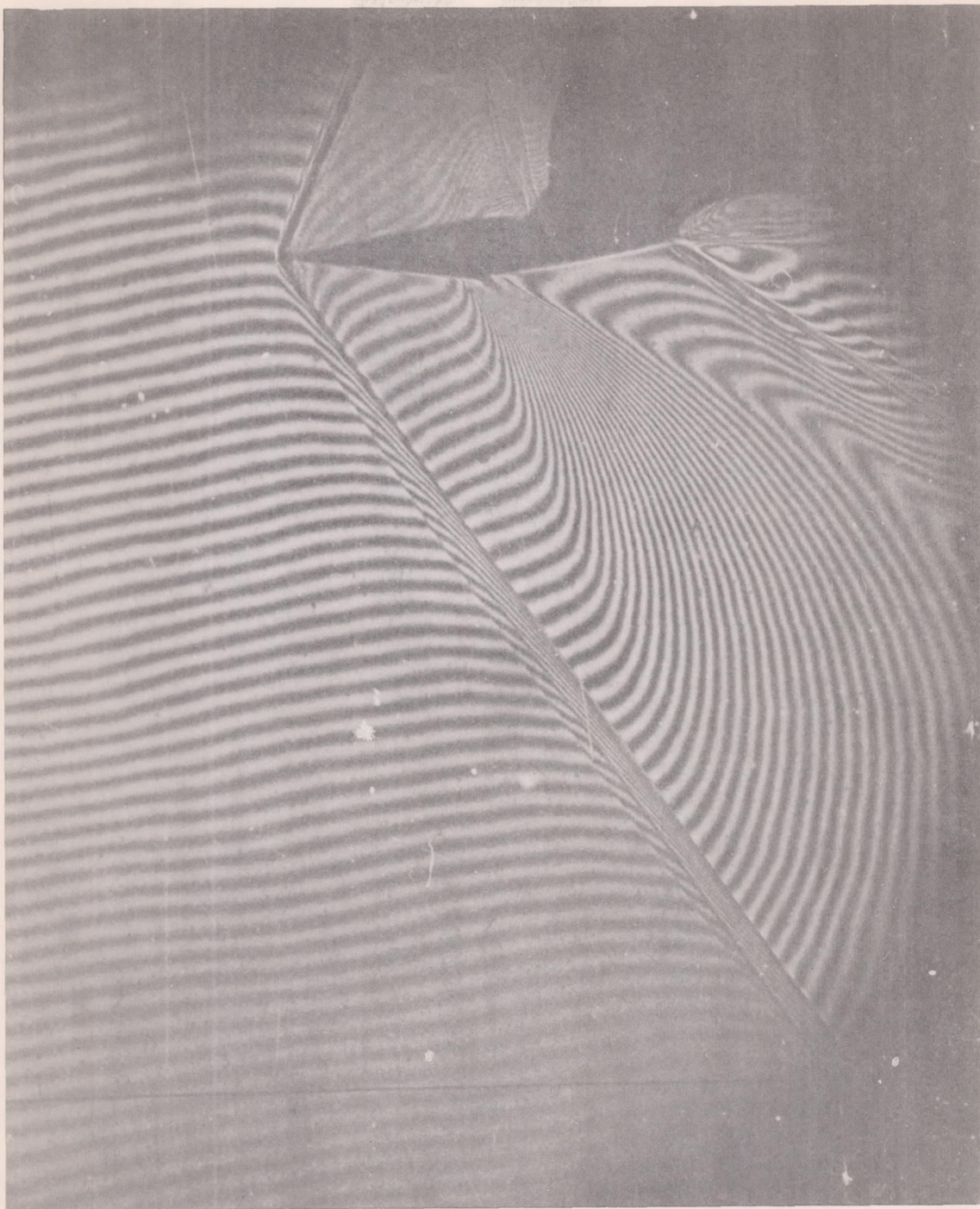
Figure 8.- Continued.



(h) $\alpha = -0.93^\circ$.

L-91746

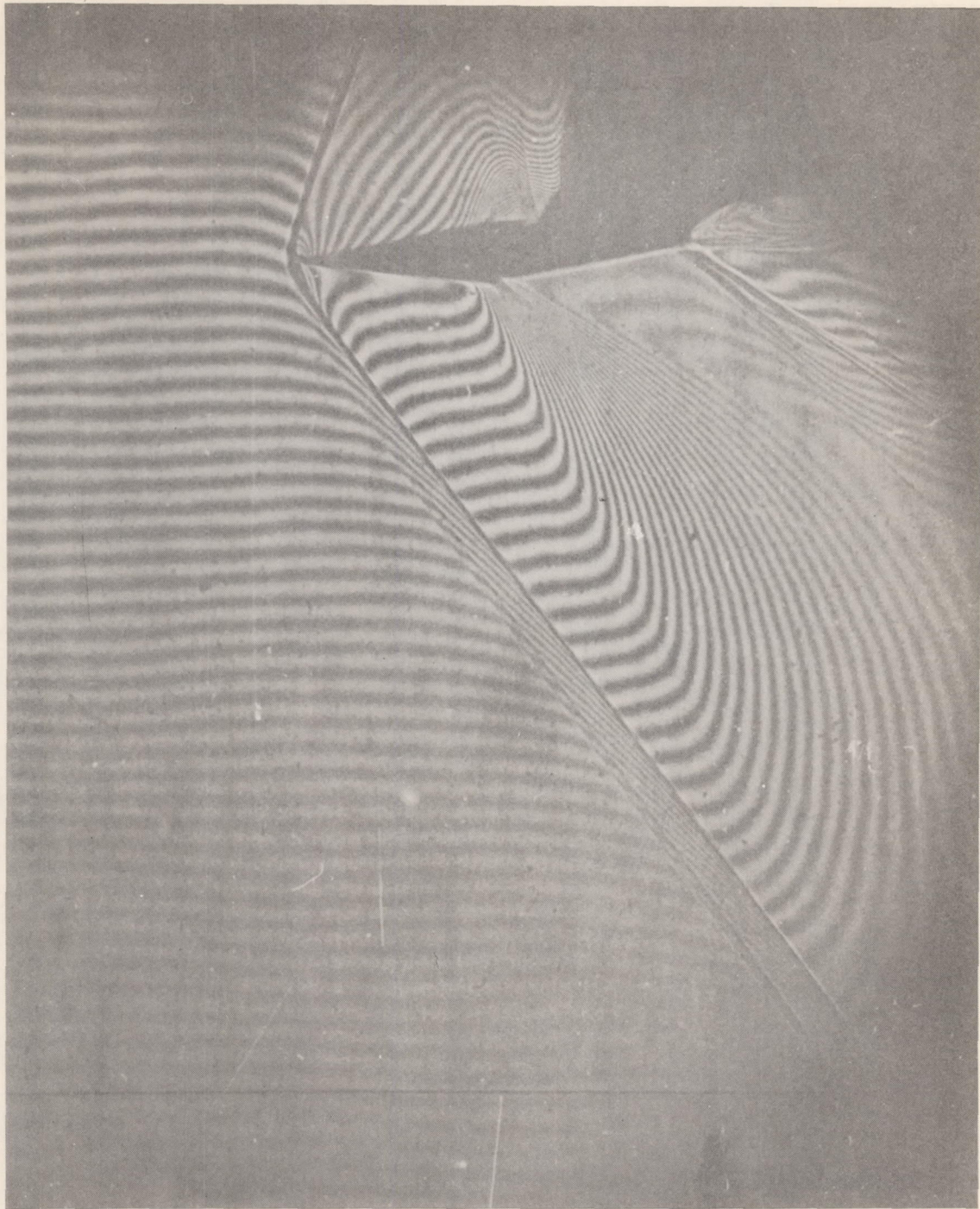
Figure 8.- Continued.



(i) $\alpha = -1.45^\circ$.

L-91747

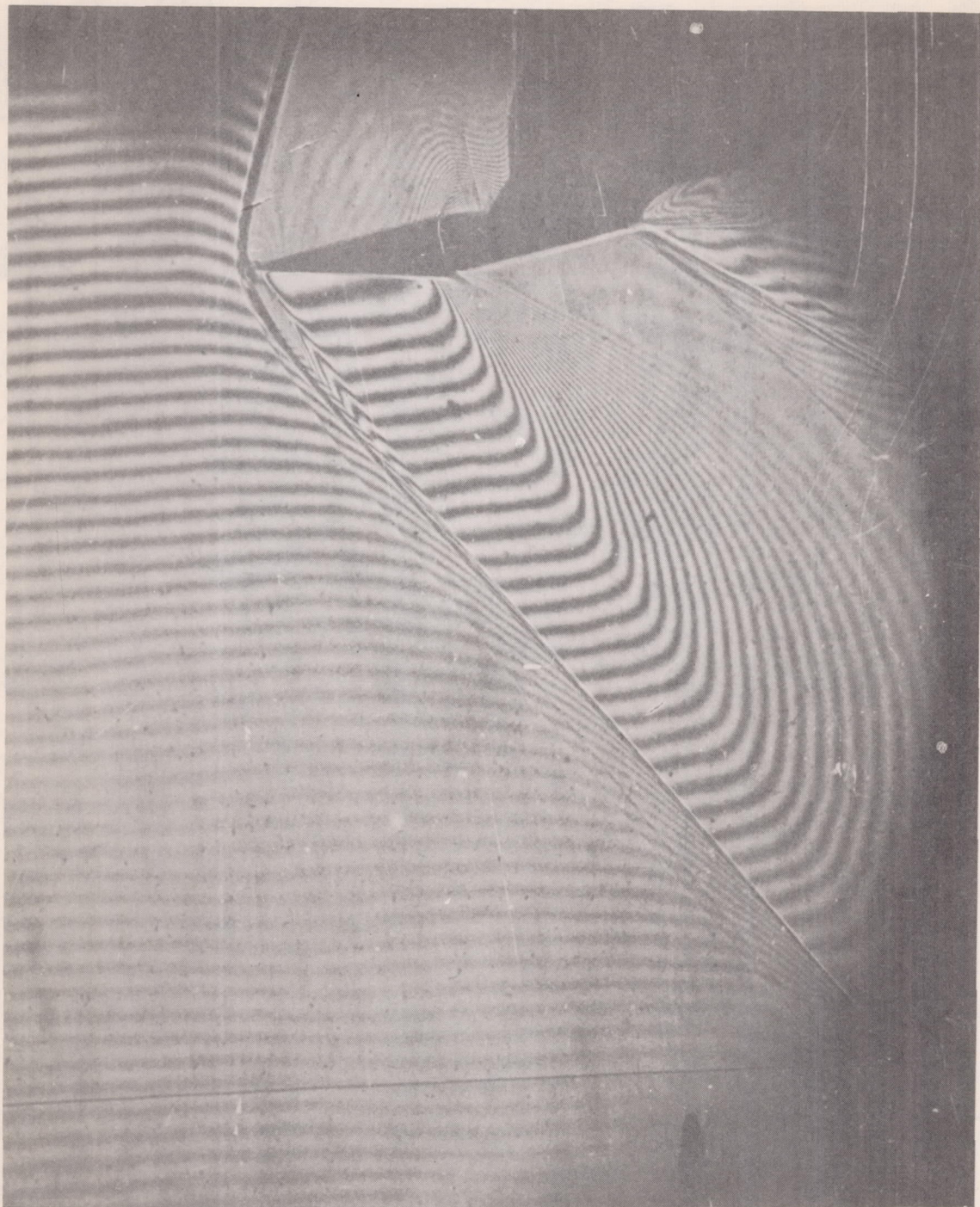
Figure 8.- Continued.



(j) $\alpha = -2.55^\circ$.

L-91748

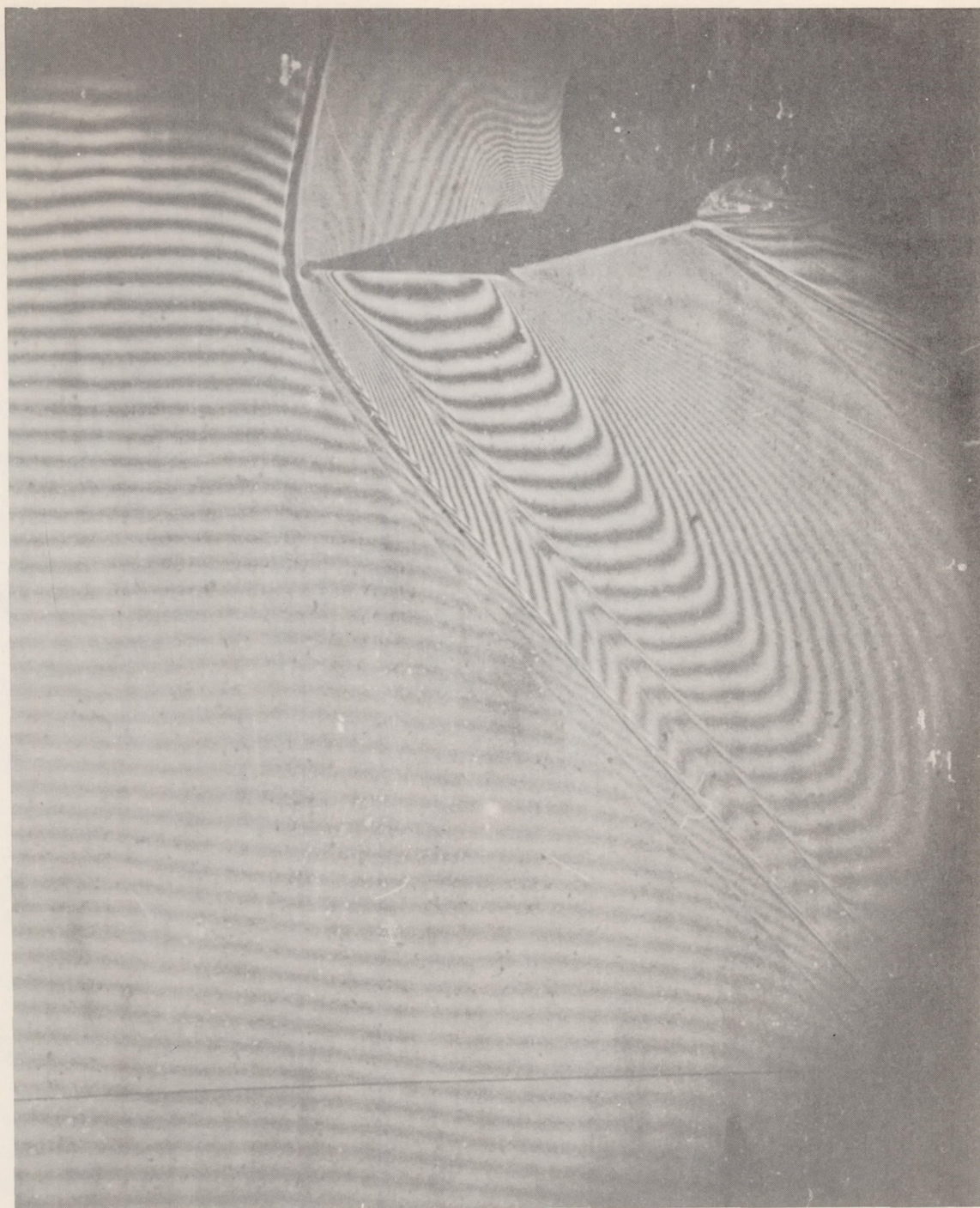
Figure 8.- Continued.



(k) $\alpha = -3.65^\circ$.

L-91749

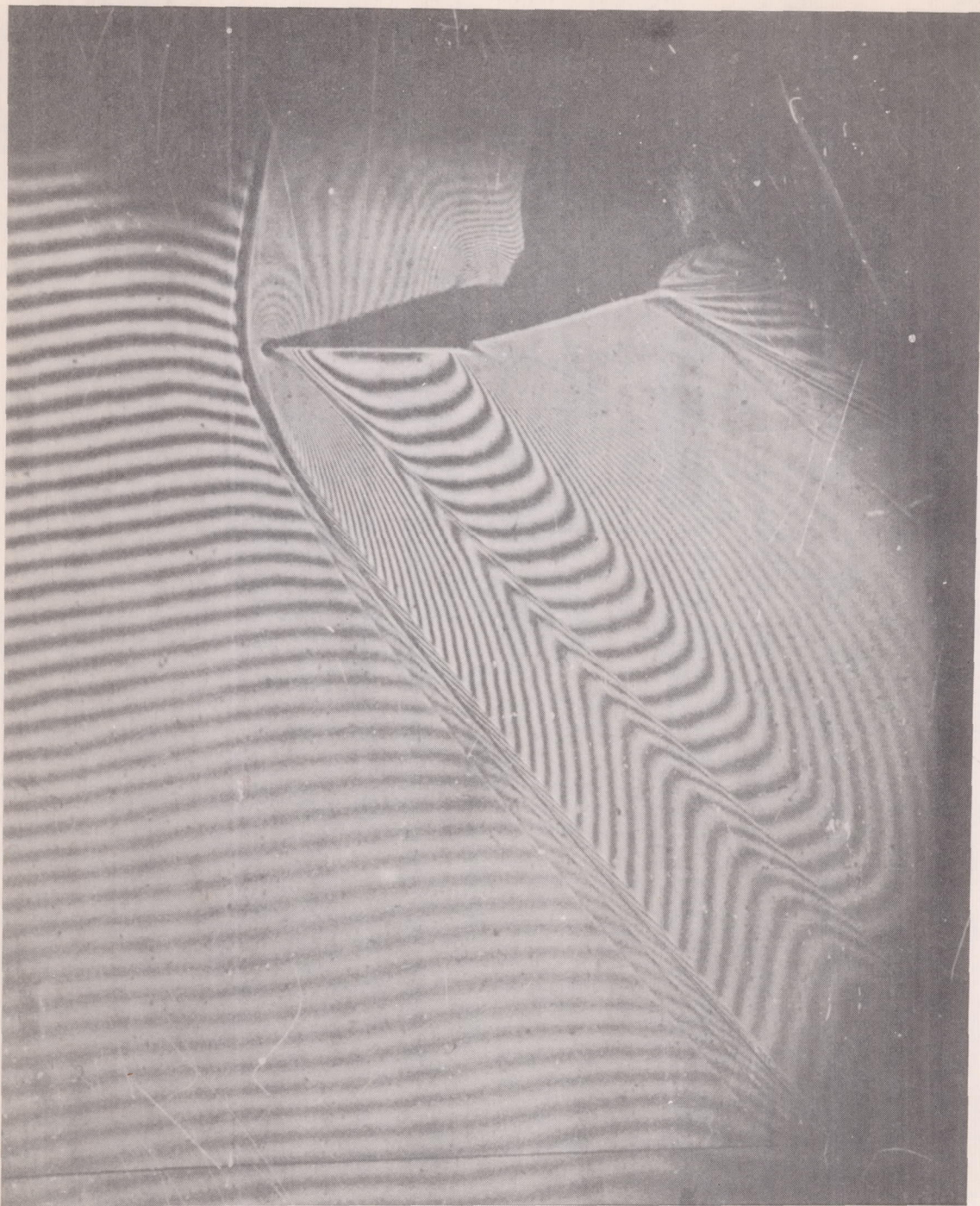
Figure 8.- Continued.



(2) $\alpha = -4.75^\circ$.

L-91750

Figure 8.- Continued.



(m) $\alpha = -5.80^\circ$.

L-91751

Figure 8.- Concluded.

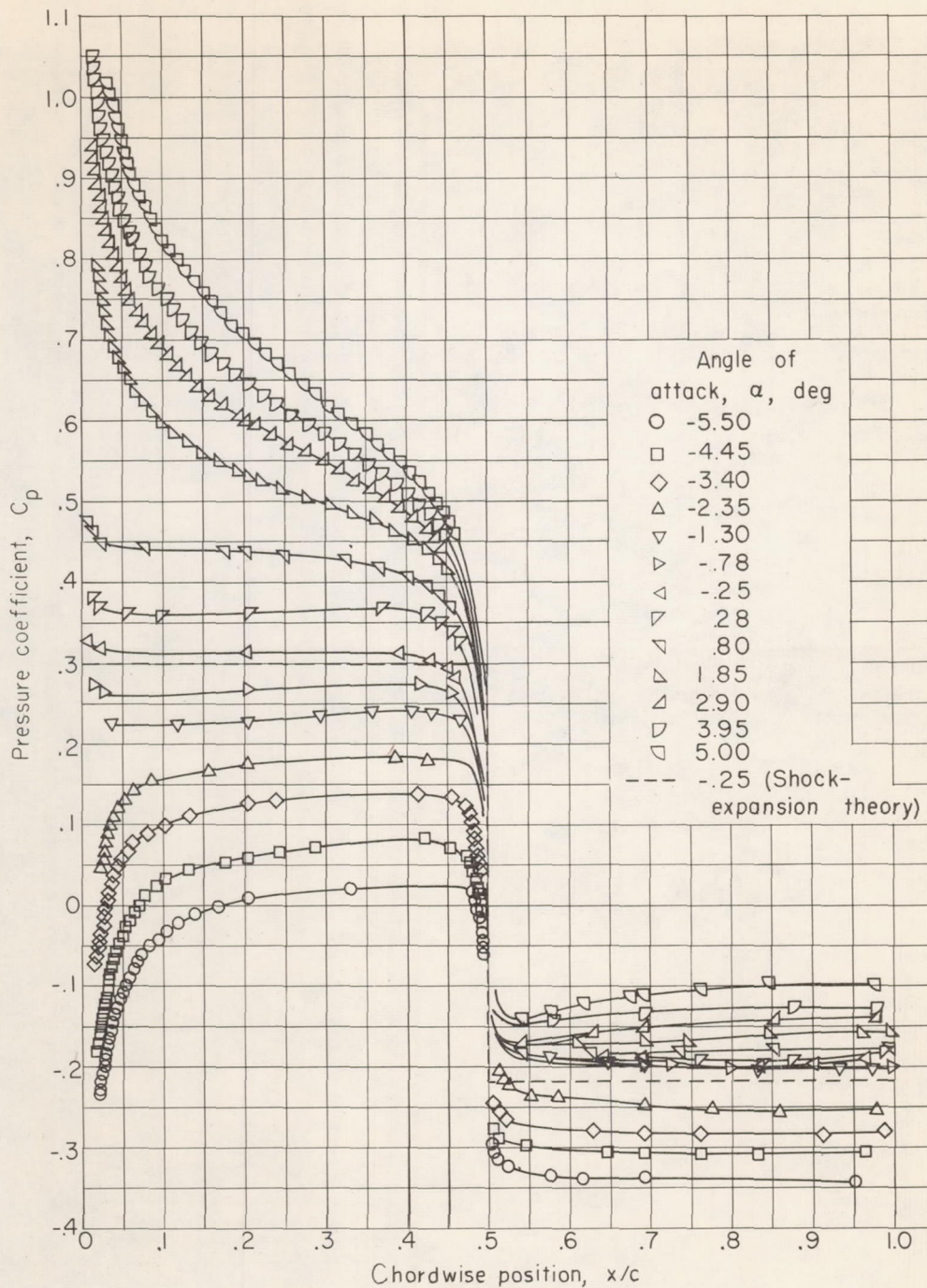
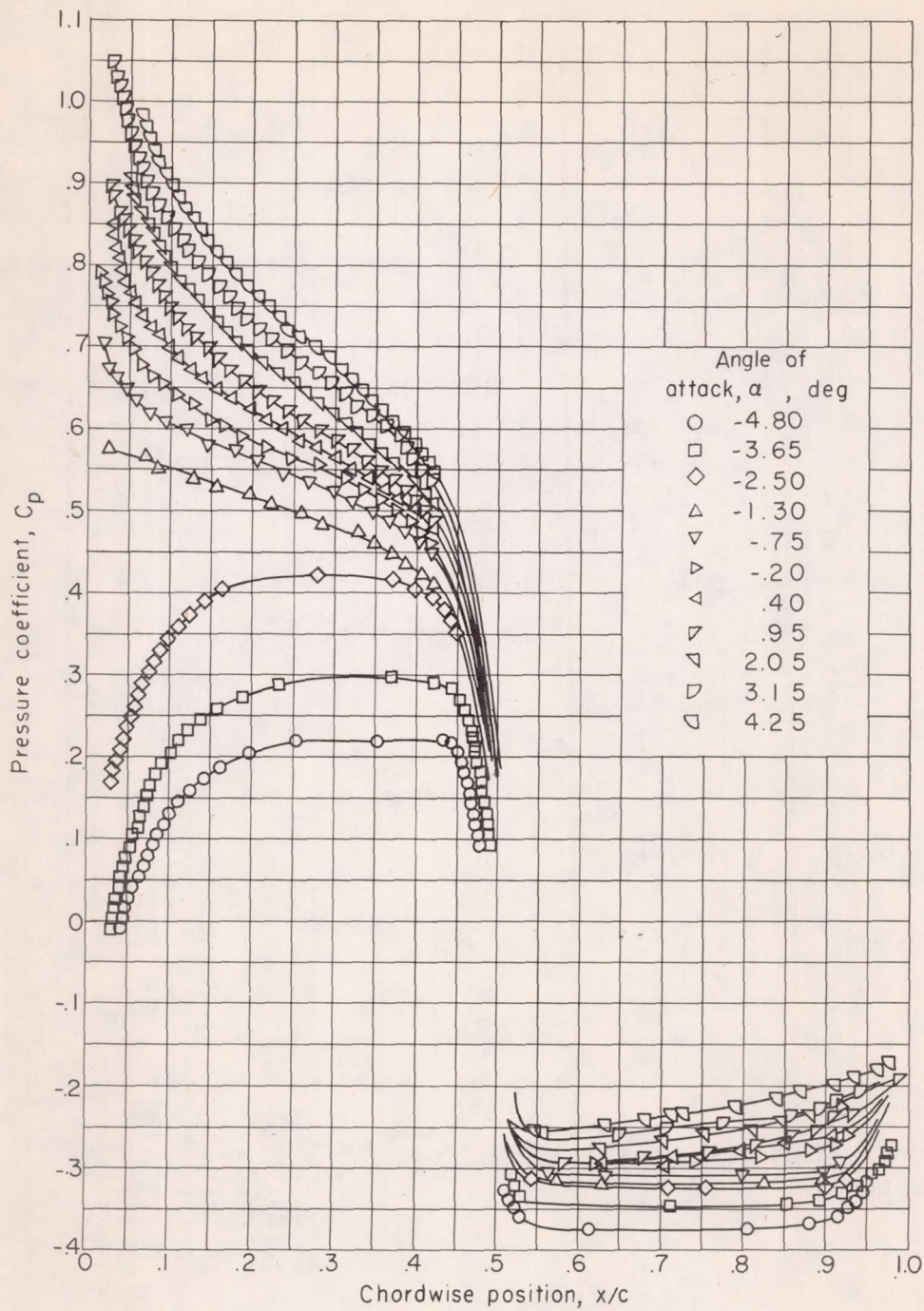
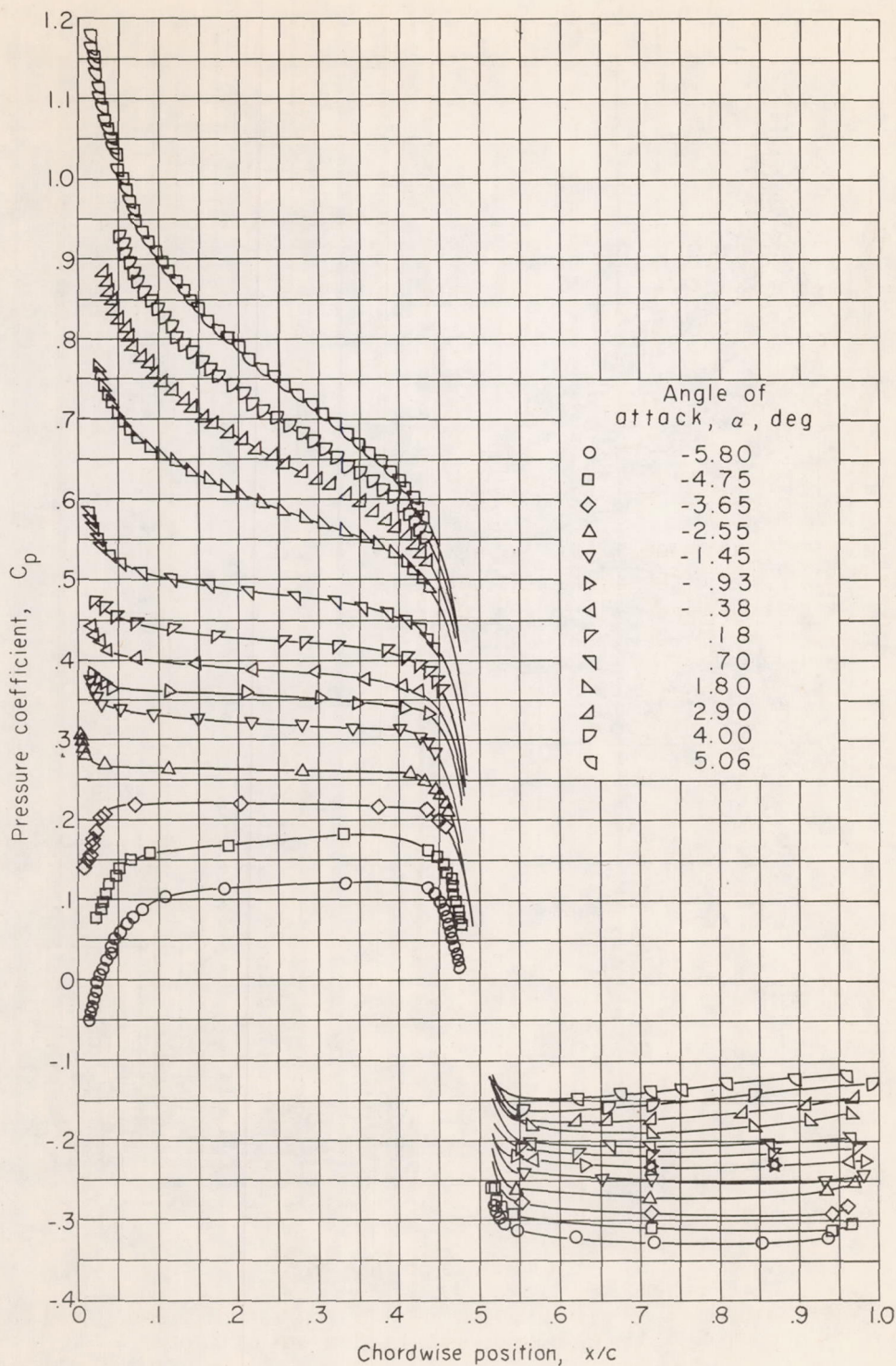
(a) $t/c = 0.10$; $M = 1.30$.

Figure 9.- Surface pressure distributions for positive and negative angles of attack.



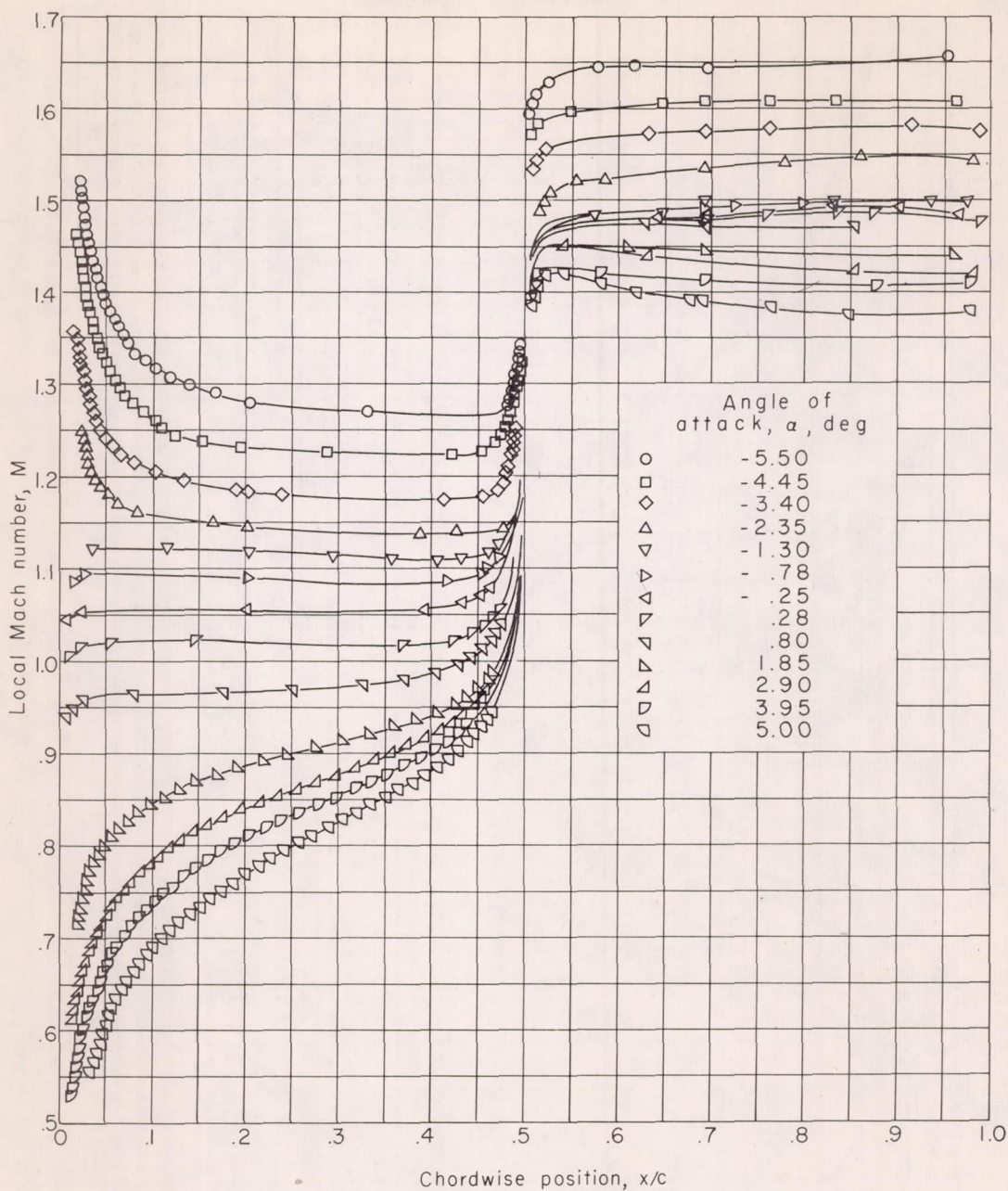
(b) $t/c = 0.142$; $M = 1.30$.

Figure 9.- Continued.



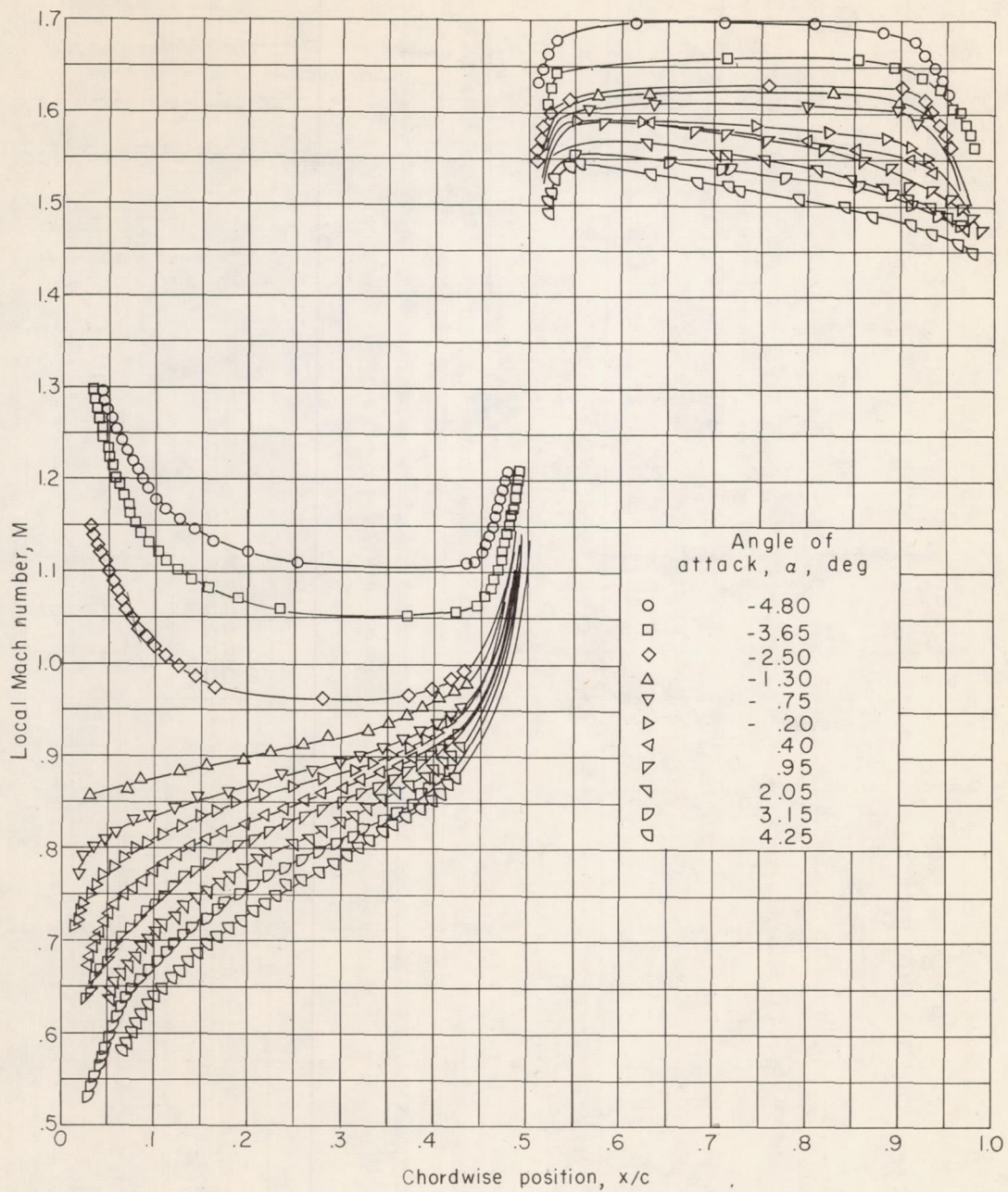
(c) $t/c = 0.142$; $M = 1.41$.

Figure 9.- Concluded.



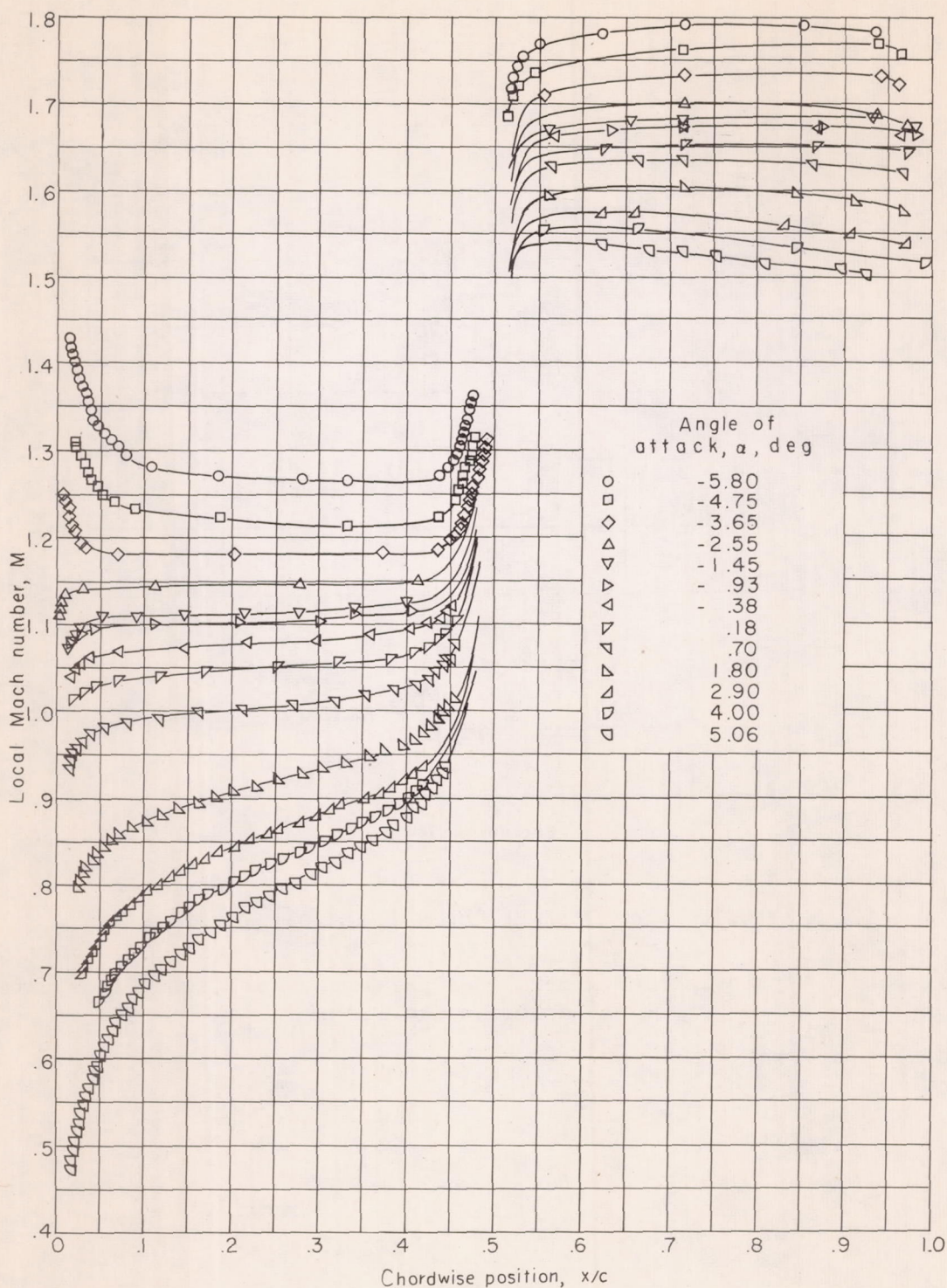
(a) $t/c = 0.10$; $M = 1.30$.

Figure 10.- Variation of local Mach number with chordwise position for positive and negative angles of attack.



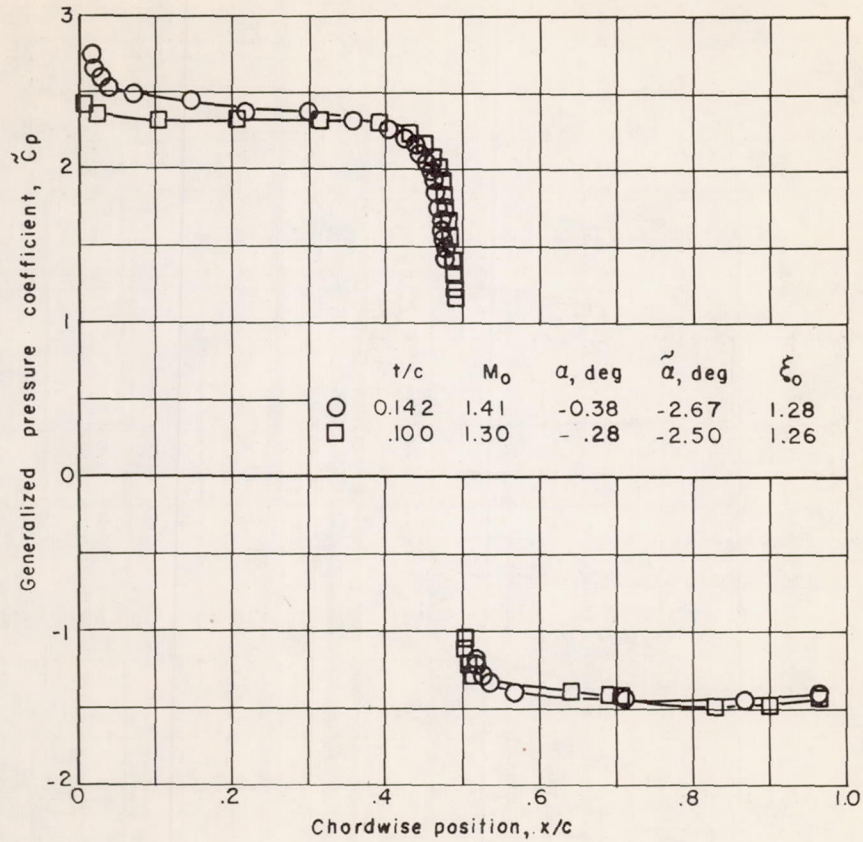
(b) $t/c = 0.142$; $M = 1.30$.

Figure 10.- Continued.



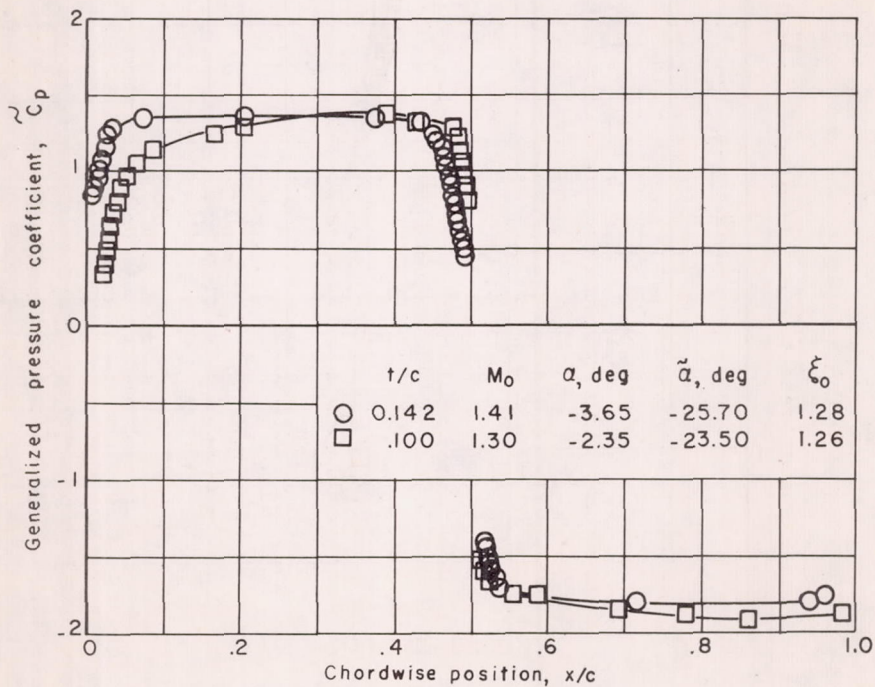
(c) $t/c = 0.142$; $M = 1.41$.

Figure 10.- Concluded.



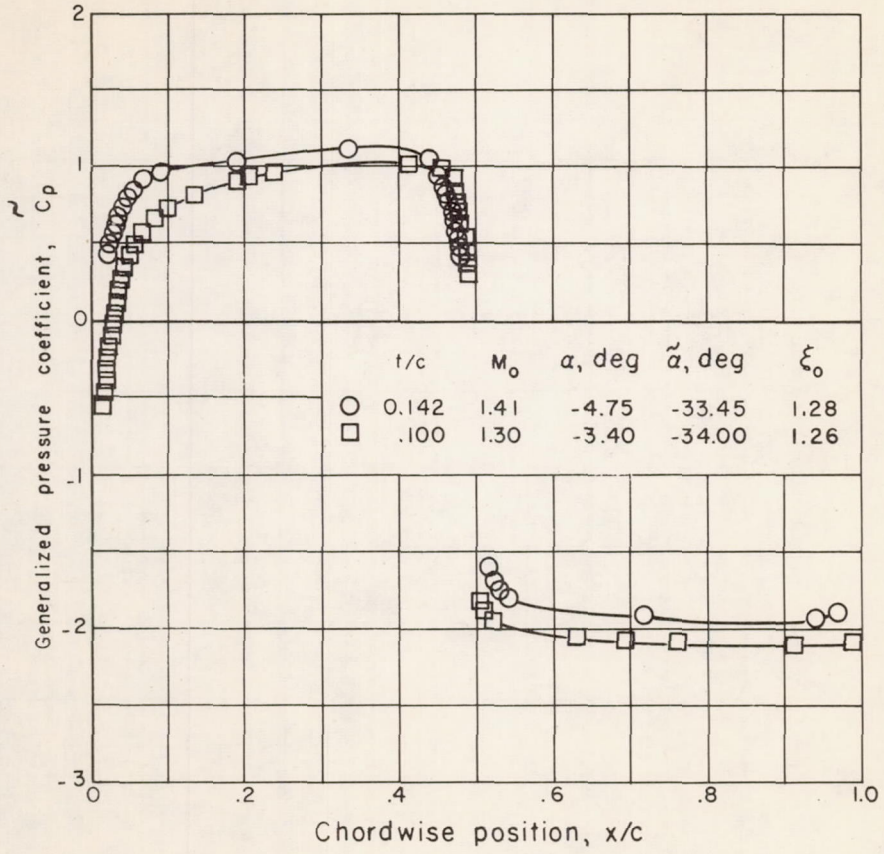
(a) $\alpha = -0.38^\circ$ for $\xi_0 = 1.28$; $\alpha = -0.25^\circ$ for $\xi_0 = 1.26$.

Figure 11.- Comparison of generalized pressure-coefficient distributions between double-wedge airfoils.



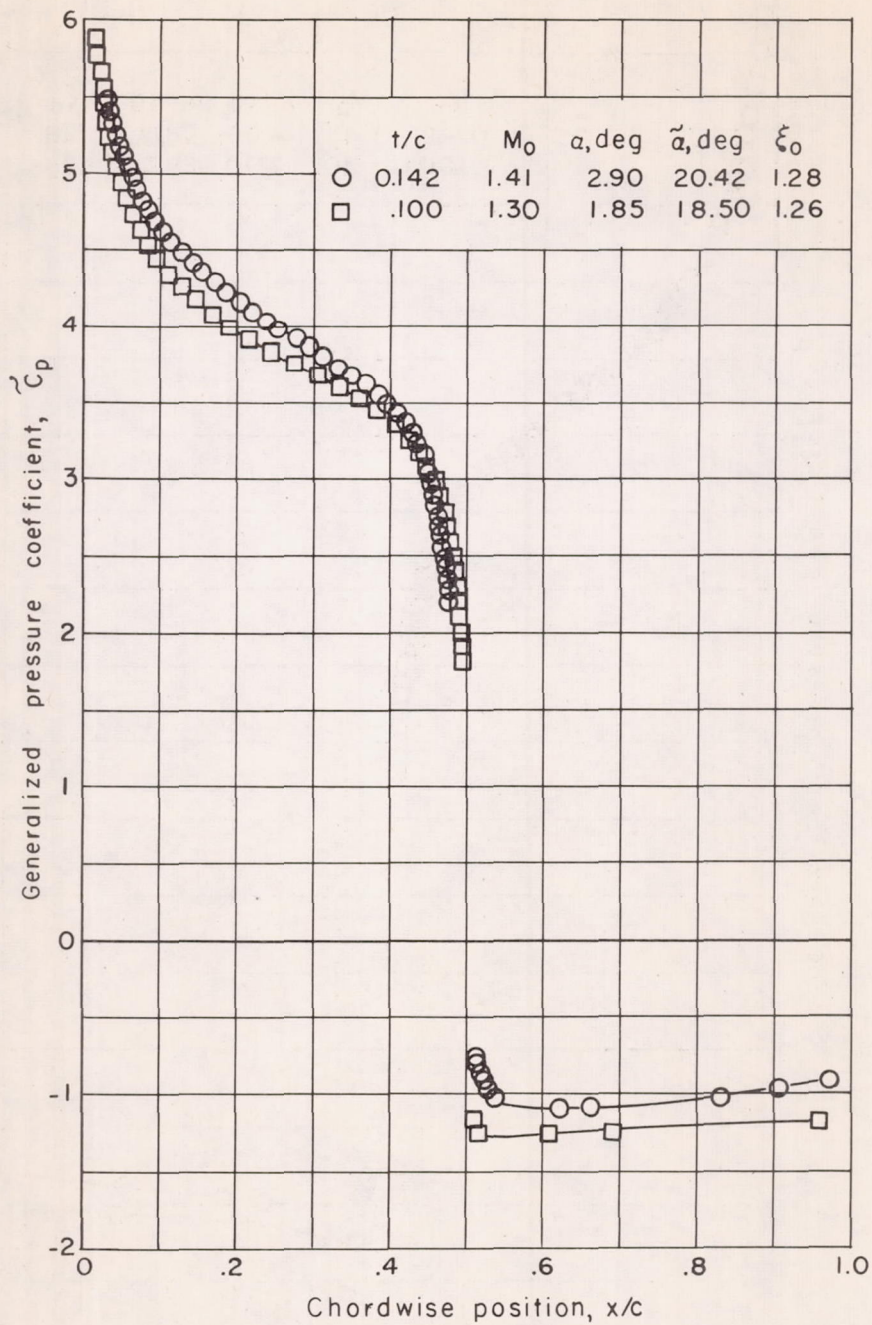
(b) $\alpha = -3.65^\circ$ for $\xi_0 = 1.28$; $\alpha = -2.35^\circ$ for $\xi_0 = 1.26$.

Figure 11.- Continued.



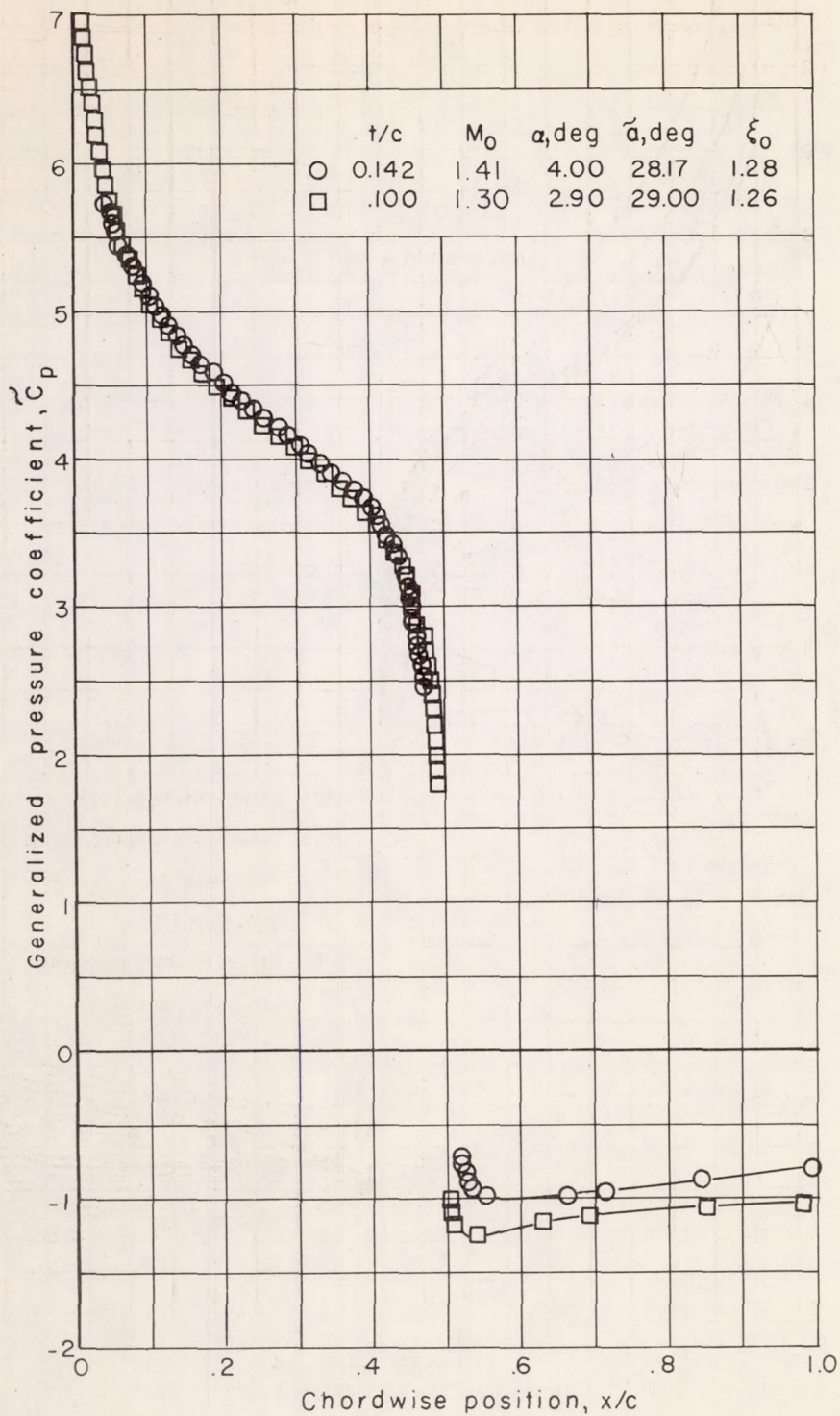
(c) $\alpha = -4.75^\circ$ for $\xi_0 = 1.28$; $\alpha = -3.40^\circ$ for $\xi_0 = 1.26$.

Figure 11.- Continued.



(d) $\alpha = 2.90^\circ$ for $\xi_0 = 1.28$; $\alpha = 1.85^\circ$ for $\xi_0 = 1.26$.

Figure 11.- Continued.



(e) $\alpha = 4.00^\circ$ for $\xi_0 = 1.28$; $\alpha = 2.90^\circ$ for $\xi_0 = 1.26$.

Figure 11.- Concluded.

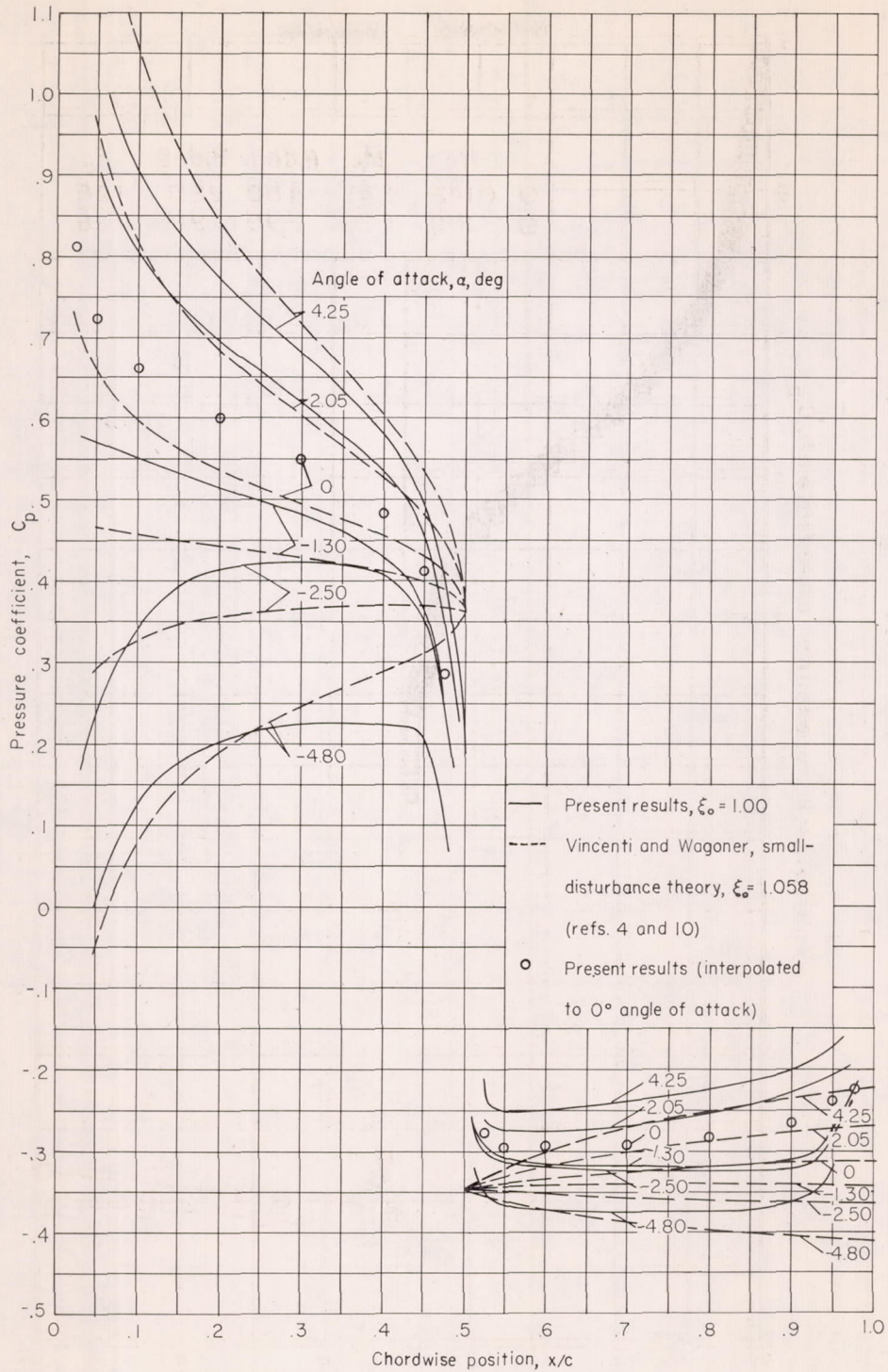


Figure 12.- Comparison of pressure distributions for lower surface of double wedge of $\xi_0 = 1.00$ with small-disturbance theory for positive and negative angles of attack.

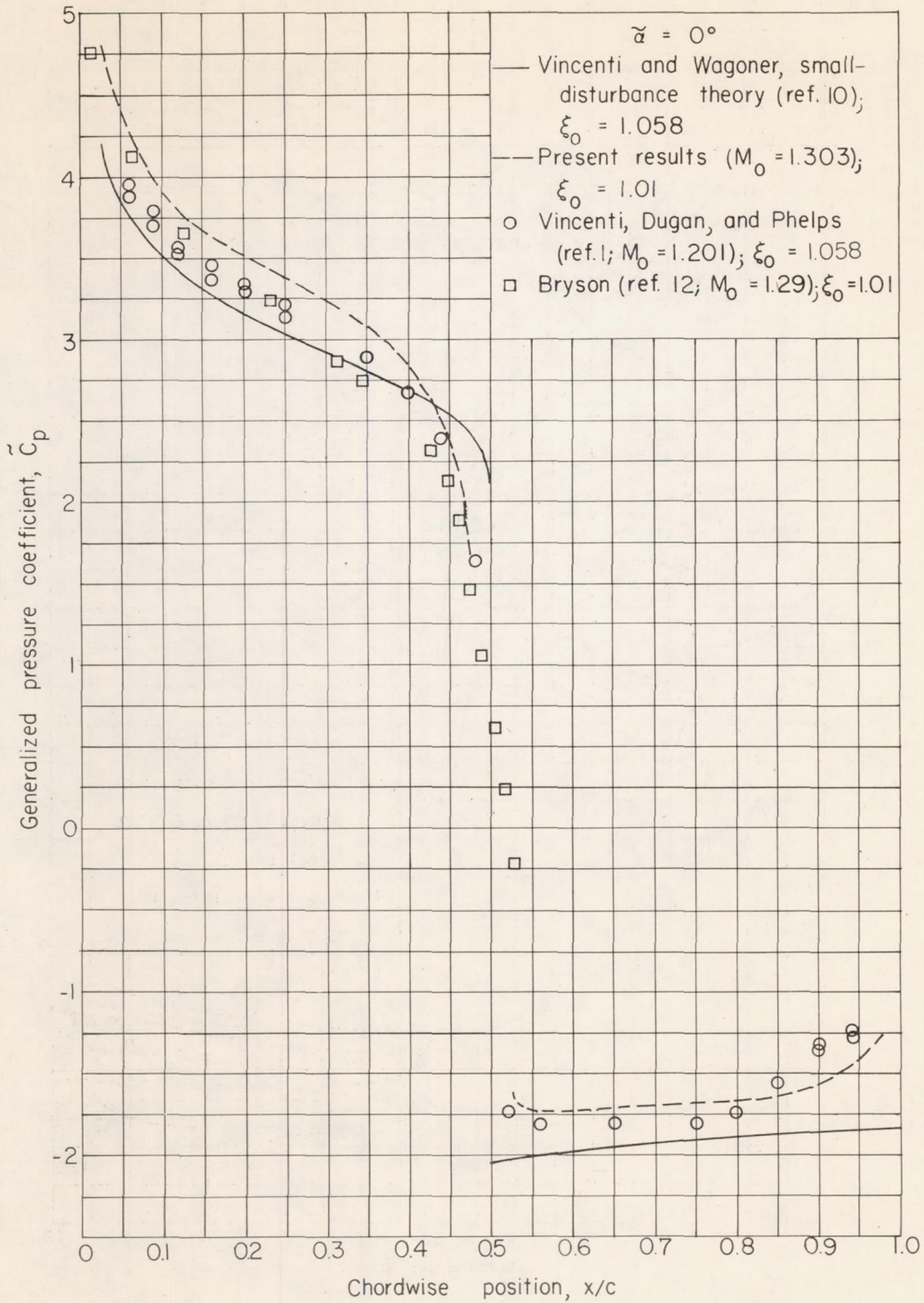
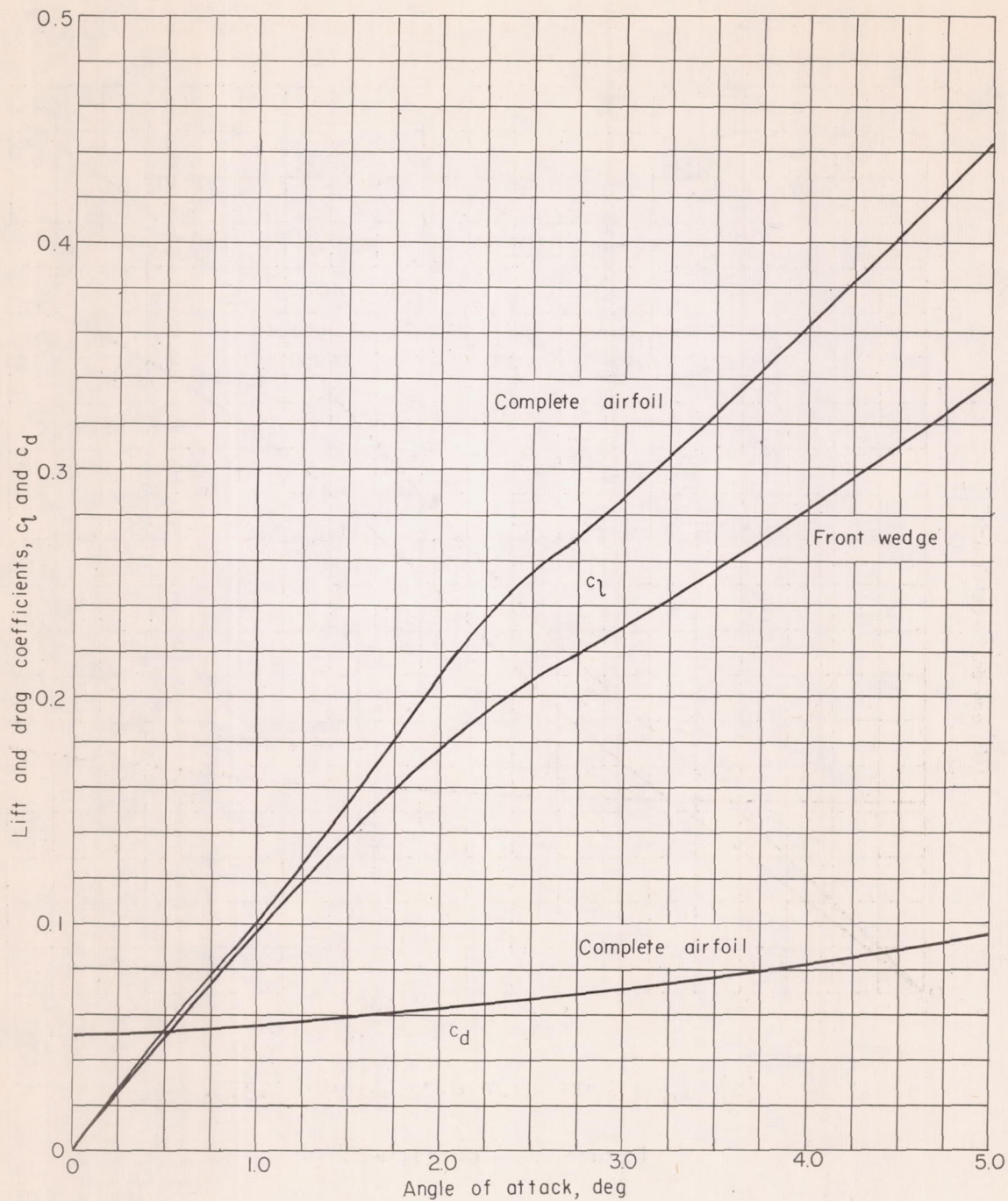
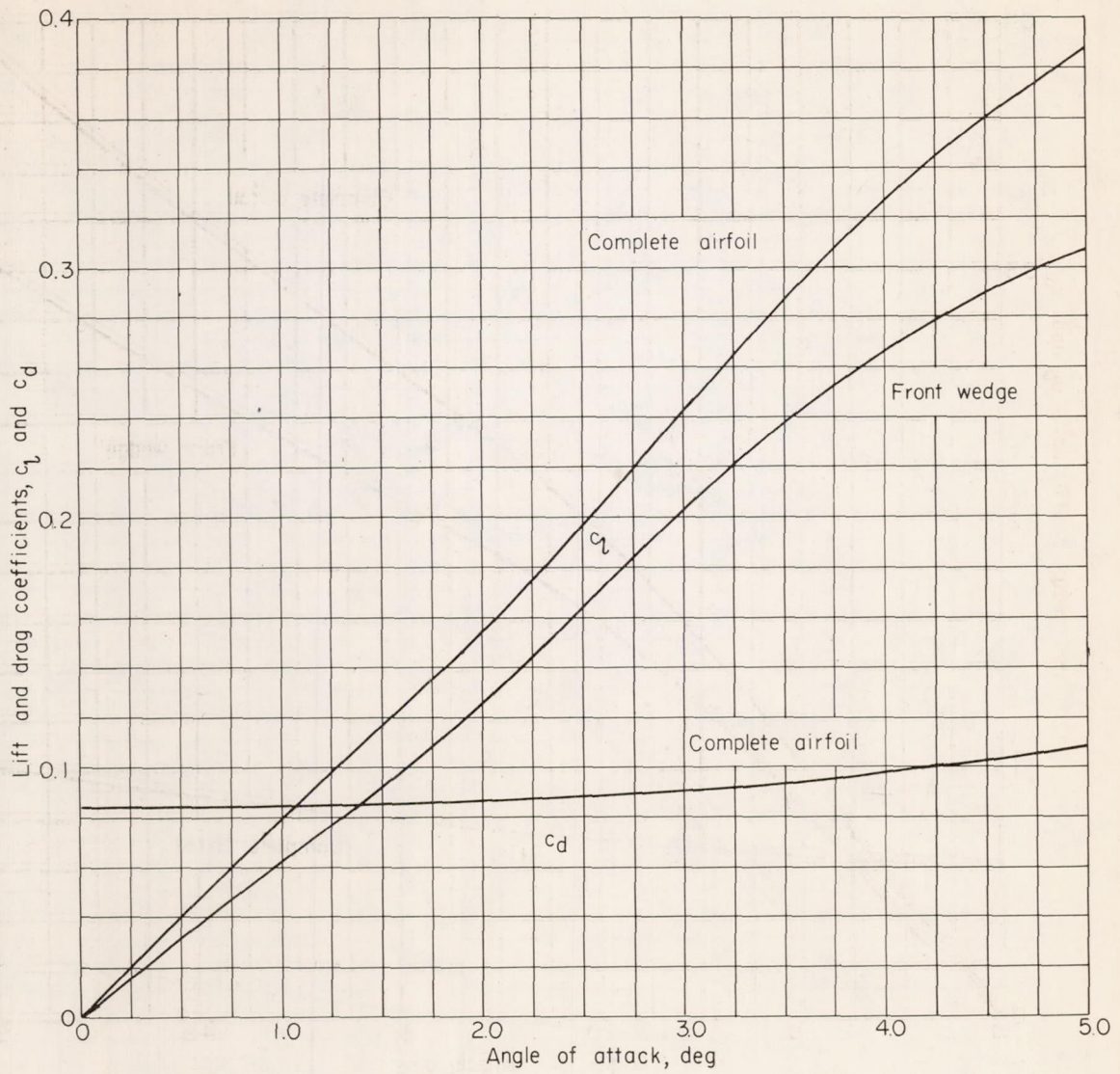


Figure 13.- Comparison of pressure distribution for double wedge of $\xi_0 = 1.00$ with small-disturbance theory and with some experimental data. $\alpha = 0^\circ$.



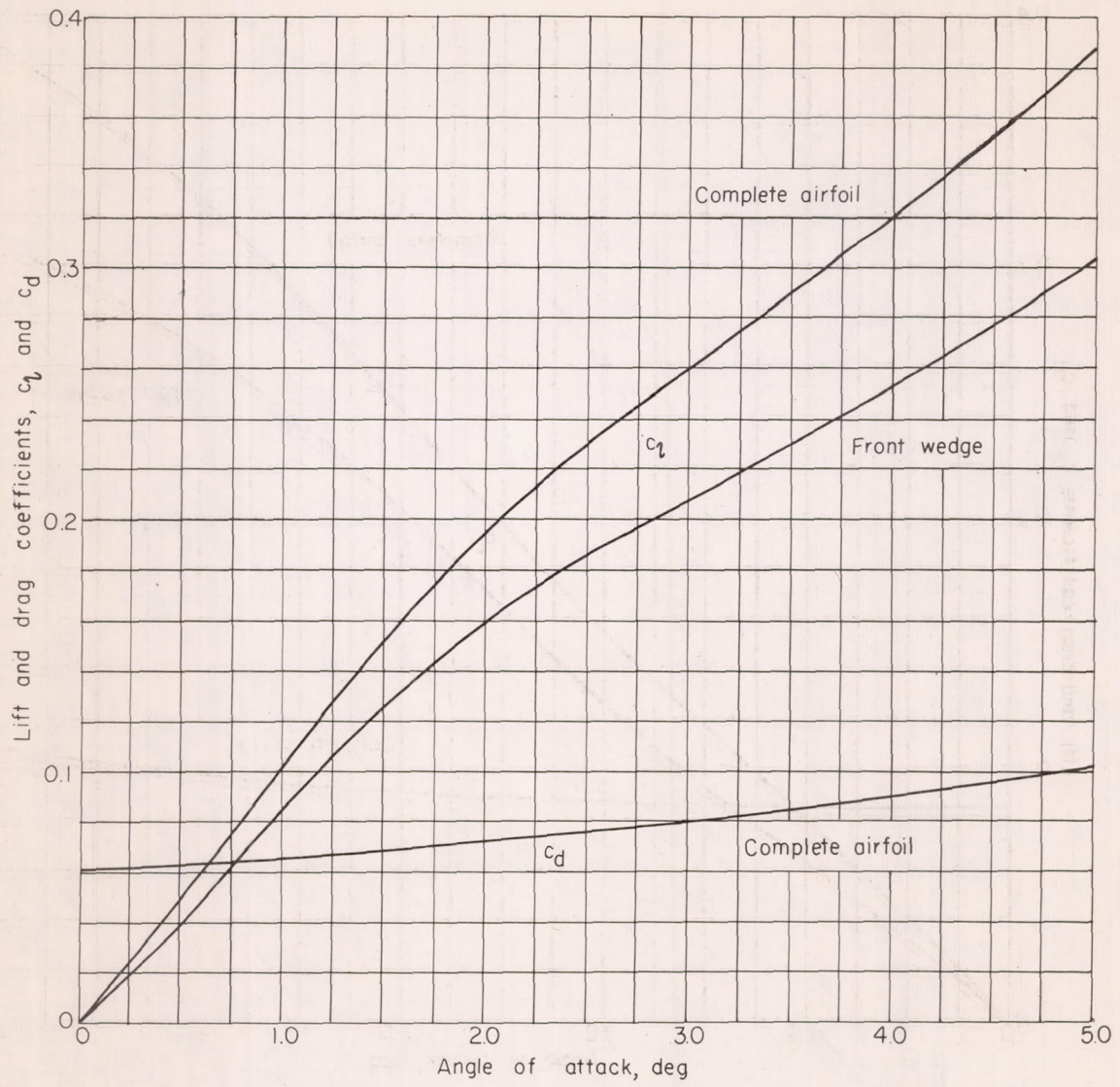
(a) $\xi_0 = 1.26$ ($t/c = 0.10$; $M = 1.30$).

Figure 14.- Variation of lift and drag coefficients with angle of attack.



(b) $\xi_0 = 1.00$ ($t/c = 0.142$; $M = 1.30$).

Figure 14.- Continued.



(c) $\xi_0 = 1.28$ ($t/c = 0.142$; $M = 1.41$).

Figure 14.- Concluded.

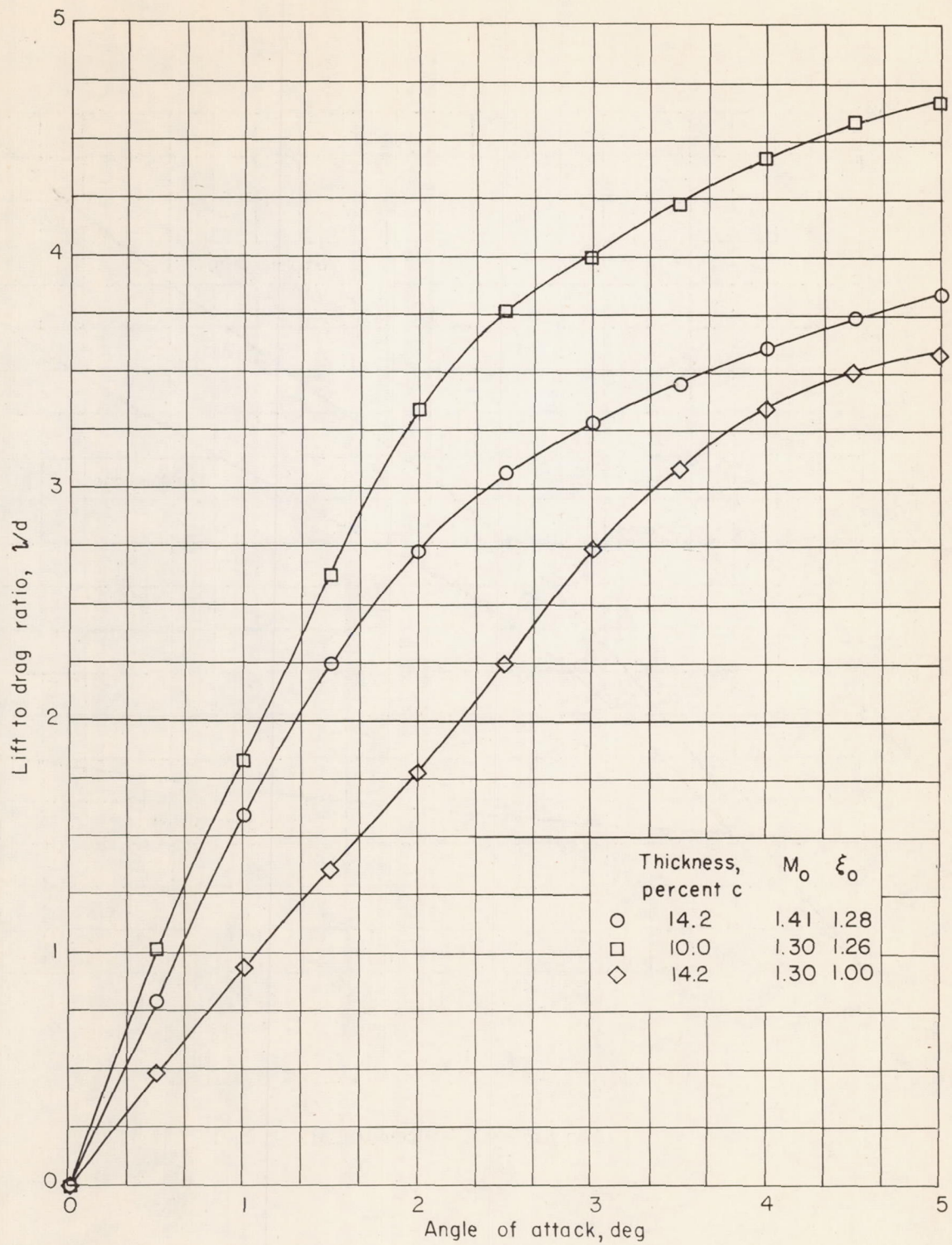


Figure 15.- Variation of lift-drag ratio with angle of attack.

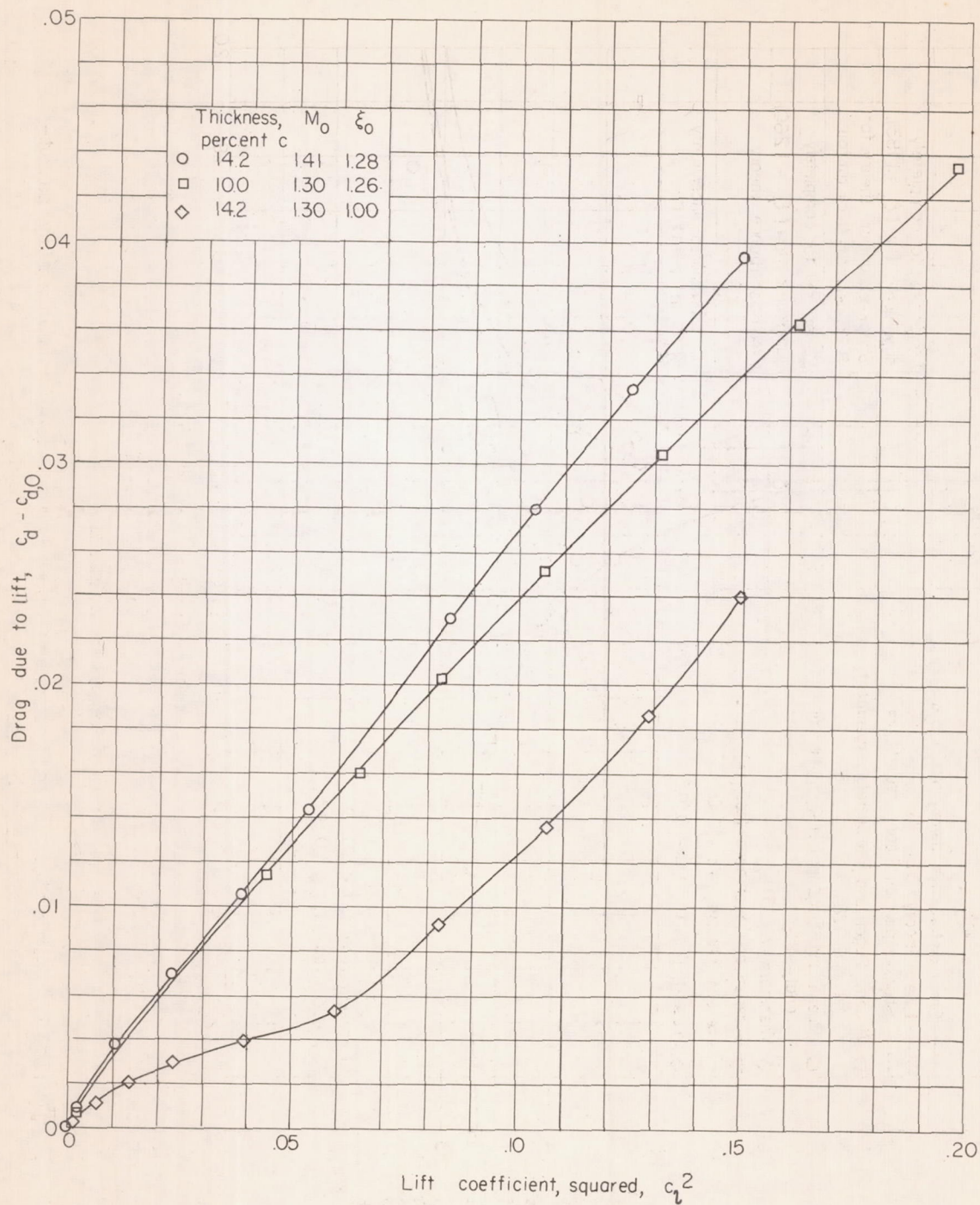
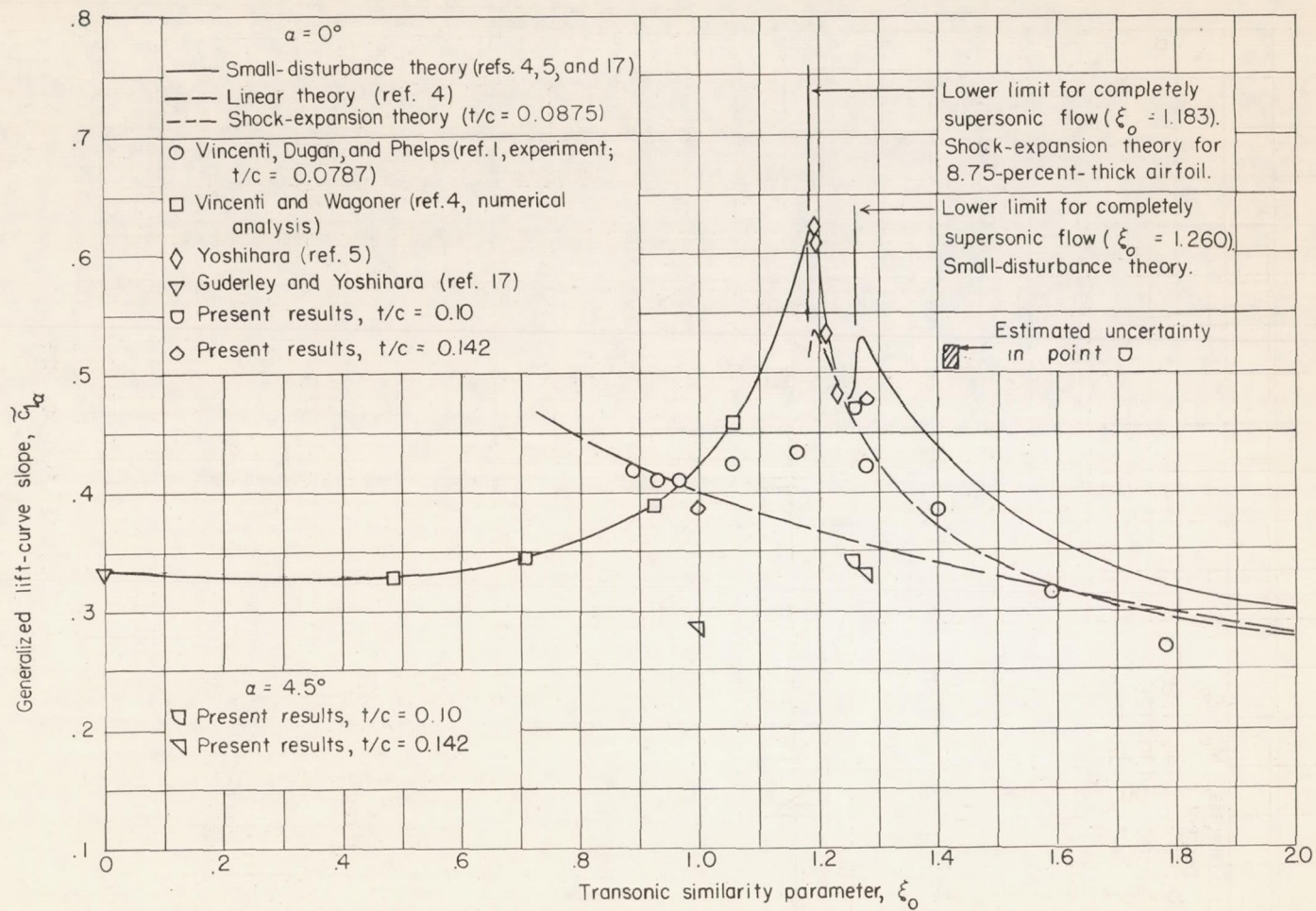
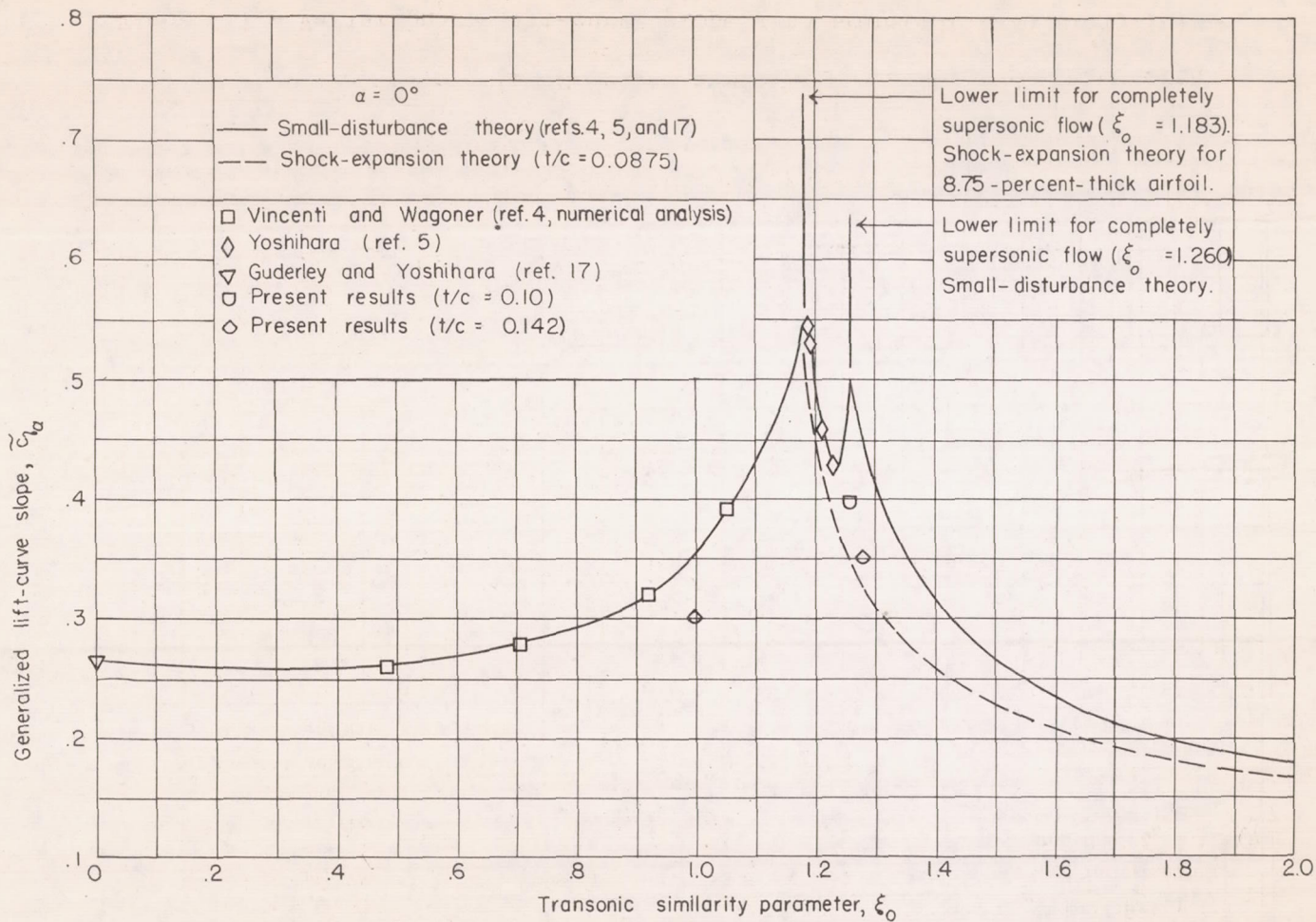


Figure 16.- Variation of drag due to lift with square of lift coefficient.



(a) Complete airfoil.

Figure 17.- Variation of lift-curve slope with transonic similarity parameter for small angles of attack.



(b) Front wedge.

Figure 17.- Concluded.

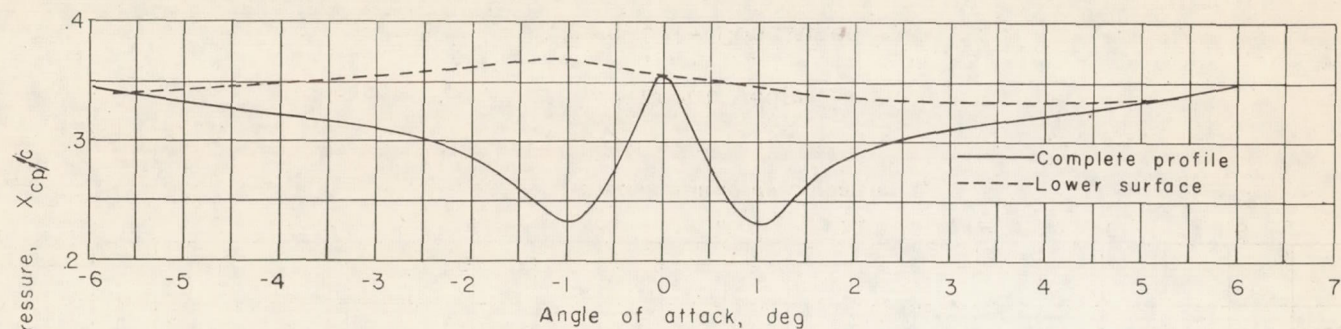
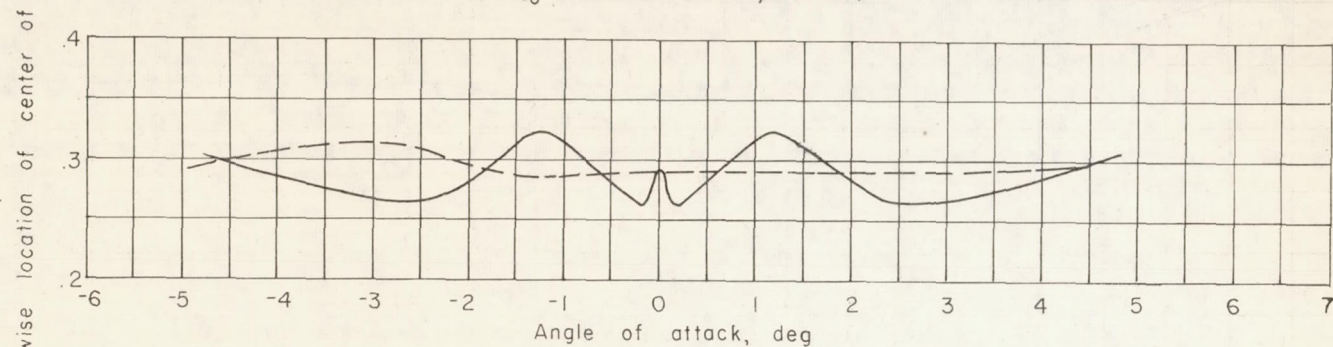
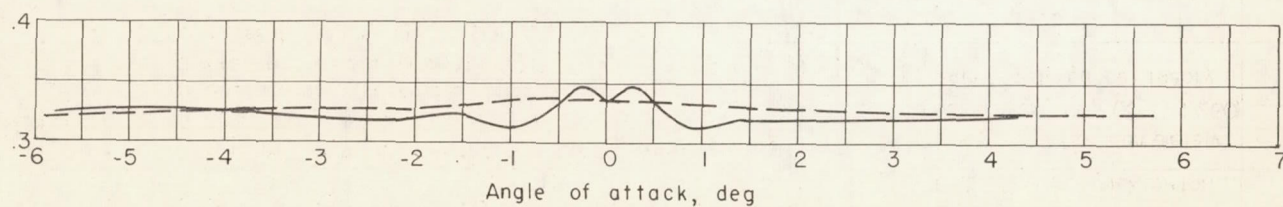
(a) $\xi_0 = 1.00$ ($t/c = 0.142$; $M = 1.30$).(b) $\xi_0 = 1.28$ ($t/c = 0.142$; $M = 1.41$).(c) $\xi_0 = 1.26$ ($t/c = 0.10$; $M = 1.30$).

Figure 18.- Variation of location of aerodynamic center of pressure with angle of attack.

Chordwise location of center of pressure for small angles of attack,

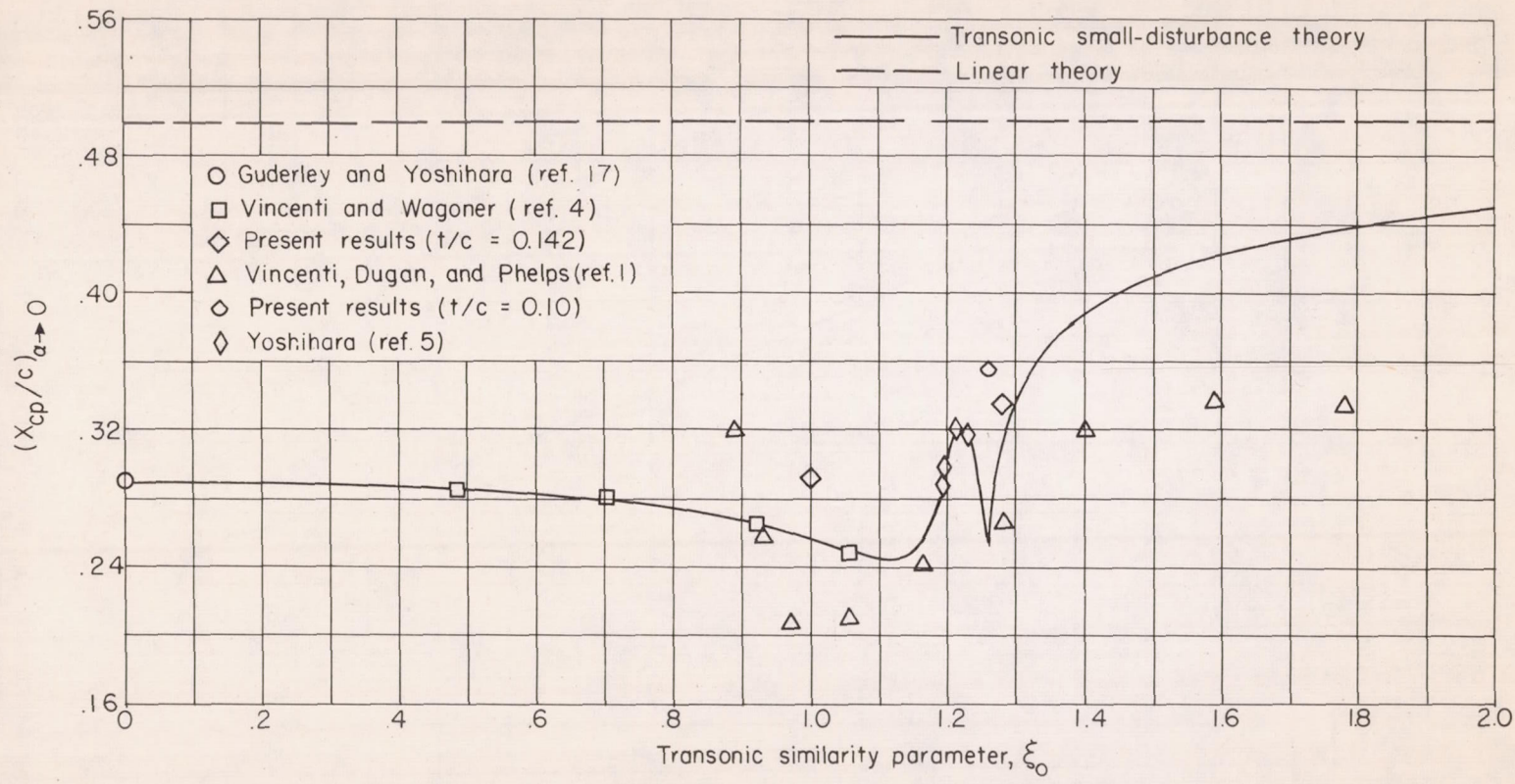


Figure 19.- Variation of location of aerodynamic center of pressure with transonic similarity parameter for small angles of attack.

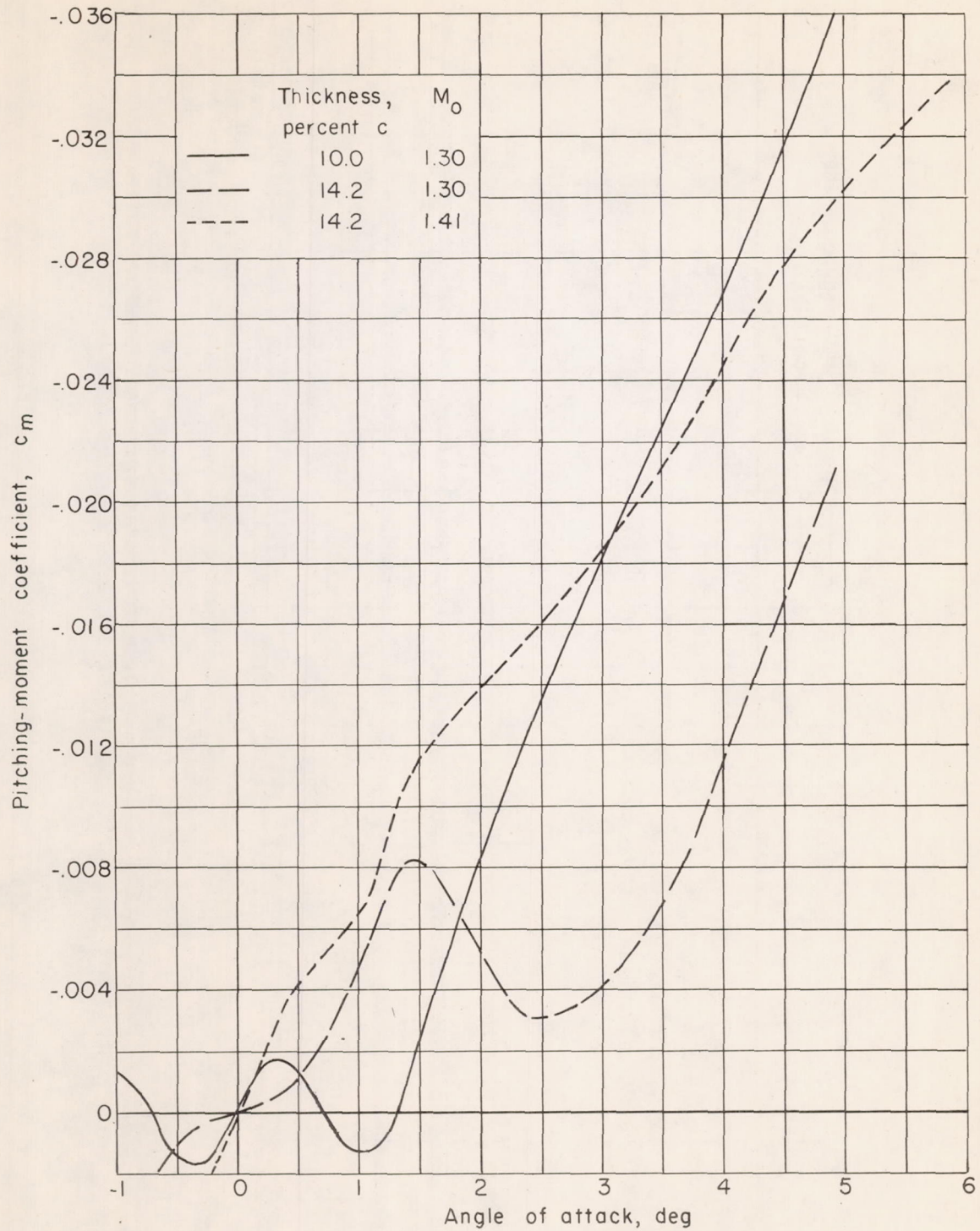


Figure 20.- Variation of pitching-moment coefficient about quarter-chord point with angle of attack.